Compressible Flow Characterization Using Non-Intrusive Acoustic Measurements

Raul Otero Jr.

Dissertation submitted to the faculty of the
Virginia Polytechnic Institute and State University
in partial fulfillment of the requirements for the degree of

Doctor of Philosophy
in
Mechanical Engineering

Wing F. Ng, co-chair
K. Todd Lowe, co-chair
Ricardo A. Burdisso
Walter F. O'Brien
Alfred L. Wicks

September 20, 2017
Blacksburg, Virginia, USA

Keywords: Non-Intrusive, Acoustic, Tomography, Anemometry, Thermometry

Compressible Flow Characterization Using Non-Intrusive Acoustic Measurements

Raul Otero Jr.

ABSTRACT

Non-intrusive acoustic instruments that measure fluid velocity and temperature have been restricted to low subsonic Mach number applications due to increased complexities associated with acoustic refraction, low signal-to-noise ratios, and a limited range of practical applications. In the current work, the use of acoustics for non-intrusive flow monitoring in compressible flows is explored and a novel sonic anemometry and thermometry (SAT) technique is developed. Using multiple arrangements of SAT equipment, a compressible acoustic tomography technique was also developed to resolve flow non-uniformities. Three validation experiments were used to investigate the novel SAT technique performance, and a fourth validation experiment was used to explore compressible flow tomography capabilities.

In the first experiment, an unheated jet was used to verify that the acoustic technique could measure fluid velocities in high subsonic Mach number flows. The application demonstrated velocity root mean square (RMS) errors of 9 m/s in unheated jet flows up to Mach 0.83. Next, a heated jet facility was used to assess the impact of fluid temperature on measurement accuracy. Using jet Mach numbers up to 0.7 and total temperatures up to 700 K, RMS velocity and static temperature errors up to 8.5 m/s (2.4% of maximum jet velocity) and 23.3 K (3.3% of total temperature) were observed. Finally, the acoustic technique was implemented at the exhaust of a JT15D-1A turbofan engine to investigate technique sensitivity to bypass engine conditions. A mass flow rate and thrust estimation approach was developed and RMS errors of 1.1 kg/s and 200 N were observed in conditions up to an exhaust Mach number of 0.48.

Since modern acoustic tomography techniques require an incompressible flow assumption for velocity detection, advancements were made to extend acoustic tomography methods to compressible flow scenarios for the final experiment. The approach was tested in the heated jet operating at Mach 0.48 and 0.72 (total temperature of 675 K, approximately 2.25 times the ambient) and numerical simulations were used to identify technique sensitivity to input variables and system design. This research marks the first time an acoustic method has been used to estimate compressible flow velocities and temperatures.

Compressible Flow Characterization Using Non-Intrusive Acoustic Measurements

Raul Otero Jr.

GENERAL AUDIENCE ABSTRACT

Traditionally, intrusive instruments such as pressure and temperature probes have been used to measure flow conditions. While these instruments are effective and widely used, they generate turbulence and produce blockage which could be undesirable in a variety of applications. In the current work, the use of non-intrusive acoustic measurements for flow velocity and temperature detection in compressible flow (Mach>0.3) environments was investigated. First, a novel acoustic technique was developed for compressible flow applications. The new approach was used to measure jet velocities and temperatures in compressible flow conditions for the first time. Later, this technique was implemented at the exhaust of a turbofan gas turbine engine. The results of this experiment demonstrated that acoustic measurements could be used to estimate engine mass flow rate and thrust in a non-intrusive manner. The final portion of this research focuses on the non-intrusive detection of fluid velocity and temperature gradients. Since existing acoustic techniques require an incompressible flow assumption, a novel approach was identified and used to perform a validation experiment. The experimental findings confirmed that non-intrusive acoustic measurements could be used to measure velocity and temperature gradients in compressible flow environments.

Acknowledgements

I would first like to thank my beautiful wife, Kathleen, for all of her love and support these last few years. It is not easy putting up with a grumpy doctoral student, but you have never stopped encouraging me to push through. To my mother, father, sister, and grandparents, I am so blessed to have you in my life. You are my inspiration. Additionally, I would like to thank my family and friends for keeping me sane through one of the toughest challenges of my life. While there are too many of you to name individually, you are all greatly appreciated!

I would also like to thank my co-advisors, Dr. Wing Ng and Dr. Todd Lowe, as well as the other three members of my committee: Dr. Ricardo Burdisso, Dr. Walter O'Brien, and Dr. Al Wicks. It has truly been an honor to learn from you. Dr. Srinath Ekkad and Dr. Lin Ma, although you were not members of my committee, your support these past few years has been greatly appreciated as well. Finally, I would like to thank Rolls Royce for sponsoring my research project. Specifically, thank you Ed, Vic, Fred, and Loren for asking those tough questions every two weeks!

Raul Otero Jr.

September 2017

Contents

List of Figures

List of Tables

Attributions

Several colleagues and mentors aided in the research and writing contained in this dissertation. A brief description of their contributions is indicated below.

Dr. Wing F. Ng and Dr. K. Todd Lowe were both co-advisors for this research. They provided extensive guidance regarding the research focus of this dissertation and editorially revised every document presented in this work. They also provided advice regarding the post processing and analysis of the experimental data in each manuscript.

Chuyoung Kim was directly involved in the acquisition of the data presented in parts 3, 4, and 5. He provided editorial revisions for parts 3 and 4.

Kevin Silas was directly involved in the acquisition of the data presented in part 5. He provided editorial revisions for the work presented in this section as well.

Dr. Lin Ma provided editorial support for the content presented in part 4.

Part I. Introduction

The primary objective of this work is to outline an acoustic approach for non-intrusive measurements of compressible flows (Mach > 0.3). While techniques such as sonic anemometry and thermometry have been around for several decades [1-5], a thorough review of the literature has revealed that most applications have been restricted to sub-Mach 0.3 fluid conditions. The author hypothesizes that this apparent limitation has largely been a product of technical challenges associated with complex acoustic refraction and reduced measurement signal-to-noise (SNR) ratios.

In recent years, several experiments carried out by Siemens in the exhaust of a ground based gas turbine engine [6,7] have uncovered a need for higher Mach number acoustic methods. While Siemen's results looked promising, their system was confined by assumptions about the fluid's velocity behavior, which are undesirable. In the current work, a new technique is described which significantly reduces the number of assumptions required for sonic anemometry and thermometry, even at high subsonic Mach numbers. Using a novel configuration of sound sources and microphones, two stream-wise displaced propagation path measurements (one measurement set) were used to simultaneously measure single stream fluid velocity and temperature. Flow non-uniformities were also resolved using a novel acoustic tomography approach.

1. Structure and Contents

This dissertation is written in a manuscript format and contains content from four papers that have been published in a journal, under review for journal publication or, in one case, pending submission. Of the four manuscripts, the first has been accepted and published by Measurement Science and Technology [8]. The second manuscript was recently submitted to Measurement Science and Technology as a continuation of the work presented in the first manuscript. The third manuscript was originally presented at the 32nd AIAA Aerodynamic Measurement Technology and Ground Testing Conference, but has since been modified and submitted to the AIAA Journal of Propulsion and Power. The final manuscript is currently pending journal submission. The author of this dissertation was directly involved in the planning, testing, and post-processing for all four experiments described in these manuscripts, in addition to being the lead author of all the works.

In addition to the literary contributions described above, the technology described in this work is currently patent pending. Additional details, not discussed in the manuscripts, are provided in the state of the art section of this document or in the appendix section. The reader will be directed to relevant appendices and texts for each manuscript in its corresponding preface section.

Part II.

Part II begins by providing a general overview of the state of the art of non-intrusive instruments. Some of the benefits and challenges for using optic and acoustic measurement approaches is provided, and the case is made for acoustic methods. Further discussion focuses on the sonic anemometry and thermometry (SAT) measurement approach due to its velocity and temperature measurement capabilities. First, the governing equations are derived using the classical configuration, and relevant literature is outlined. In the final section of Part II, the author focuses on the potential limitations of SAT and considers the practicality of implementing this technique in compressible flows.

Part III.

In the first manuscript [8], a novel acoustic approach for flow velocity and temperature detection is developed and described in detail. In addition to describing the theory, the results of a validation experiment in an unheated laboratory jet operating at conditions up to Mach 0.83 are presented. The experimental data proved that non-intrusive acoustic measurements could be used to detect velocities in flow conditions greater than Mach 0.3.

Part IV.

The second manuscript [9] presents an application of the acoustic technique in a single-stream, heated laboratory jet operating at subsonic flows up to Mach 0.7 and total temperatures of 700 K. The purpose of this experiment was to show that the technique can be used to accurately estimate single-stream jet temperatures at high subsonic Mach numbers. This set of measurements was also used to better understand the effects of fluid velocity and temperature on system accuracy. Overall, the intrusive and non-intrusive measurements showed good agreement, but the effects of the jet's shear layer were more apparent as the jet temperature increased. Overall, the results of this experiment underscored the need for non-uniform flow handling.

Part V.

In the third paper [10], the results of a proof-of-concept experiment in a turbofan gas turbine engine are described. The overarching objective of this experiment was to explore acoustic technique sensitivity to engine operating conditions since this technique is a likely candidate for such an environment. Although velocity and temperature values for the core and bypass streams could not be resolved using two acoustic propagation path measurements, integrated path velocities and temperatures showed a sensitivity to engine fan speed as expected. Furthermore, intrusive probe measurements showed that the normalized exhaust profiles did not vary significantly for several engine power settings. Capitalizing on this observation, a mass flow rate and thrust estimation procedure was established and used to approximate engine performance.

Part VI.

The last manuscript [11] largely focuses on the detection of flow non-uniformities through the use of a novel acoustic tomography approach. By using multiple sets of acoustic sound source and microphone positions at various orientations, a new method for coupled velocity and temperature tomography is developed. The novel approach is of significant interest because it avoids the incompressible fluid assumption required by existing techniques, and enables the detection of fluid non-uniformities in compressible flows. A validation experiment in a heated jet facility operating at conditions up to Mach 0.72 and a total temperatures of 675 K was performed. Overall, the results were consistent with expectations, and the validation experiment demonstrated the merits of this novel approach.

Note that each chapter may contain contents and citation styles that deviate from others due to different publication submission guidelines for the journal in which they are intended to be published.

2. Summary of Major Contributions

The major contributions and accomplishments of this work are described below:

1. First application of sonic anemometry and thermometry in Mach > 0.3 Flows

A novel sonic anemometry and thermometry method was developed for compressible flow measurements and several proof of concept experiments were carried out to assess technique performance. This is the first time an acoustic technique has been used to quantify flow velocities and temperatures in Mach numbers greater than 0.3.

2. **First application of sonic anemometry and thermometry in turbofan engine exhaust**
   The non-intrusive acoustic technique was successfully deployed in a JT15D-1A turbofan engine and a process was established for approximating engine mass flow rate and thrust using two acoustic path measurements. Experimental results showed 1.1 kg/s and 200 N RMS errors in mass flow rate and thrust respectively
3. **First validated method for acoustic tomography in high subsonic Mach number flows**
   A novel acoustic tomography technique was developed for simultaneously measuring fluid velocity and temperature non-uniformities in compressible flows. This technique was implemented in flows up to Mach 0.72 and a total temperature of 675K. This application marks the first time an acoustic tomography technique has been used to measure velocity and temperature non-uniformities in a compressible flow environment.

References

[1] R. Sozzi and M. Favaron, "Sonic anemometry and thermometry: theoretical basis and data prcessing software," *Environmental Software,* vol. 11, no. 4, pp. 259-270, 1996.

[2] J. Kaimal and J. Gaynor, "Another look at sonic thermometry," *Boundary-Layer Meteorology,* vol. 56, no. 4, pp. 401-410, 1991.

[3] B. McKeon, "Velocity, Vorticity, and Mach number," in *Springer Handbook of Experimental Fluid Mechanics*, Springer, 2007, pp. 215-471.

[4] J. C. Wyngaard, "Cup, propeller, vane, and sonic anemometers in turbulence research," *Annual Review of Fluid Mechanics,* vol. 13, no. 1, pp. 399-423, 1981.

[5] A. Cuerva and A. Sanz-Andres, "On sonic anemometer measurement theory," *Journal of Wind Engineering and Industrial Aerodynamics,* vol. 88, no. 1, pp. 25-55, 2000.

[6] U. DeSilva, R. H. Bunce and H. Claussen, "Novel Gas Turbine Exhaust Temperature Measurement System," in *Proceedings of ASME Turbo Expo 2013*, 2013.

[7] U. DeSilva, R. H. Bunce, J. M. Schmitt and H. Claussen, "Gas Turbine Exhaust Temperature Measurement Approach Using Time-Frequency Controlled Sources," in *Proceedings of ASME Turbo Expo 2015*, 2015.

[8] R. Otero Jr, K. T. Lowe and W. F. Ng, "Extension of sonic anemometry to high subsonic Mach number flows," *Measurement Science and Technology,* vol. 28, pp. 1-12, 2017.

[9] R. Otero Jr, K. T. Lowe and W. F. Ng, "Non-intrusive acoustic measurement of flow velocity and temperature in a high subsonic Mach number jet (Submitted)," *Measurement Science and Technology,* 2017.

[10] R. Otero Jr, K. T. Lowe, W. F. Ng, L. Ma and C. Y. Kim, "Non-Intrusive Gas Turbine Engine Exhaust Characterization using Acoustic Measurements," in *32nd AIAA Aerodynamic Measurement Technology and Ground Testing Conference*, 2016.

[11] R. Otero Jr, K. T. Lowe, W. F. Ng and K. A. Silas, "Coupled velocity and temperature tomography in high subsonic Mach number flows (pending submission)," *TBD,* 2017.

Part II. State of the Art

In fluid mechanics, scientists and engineers are interested in the measurement of fluid conditions under various circumstances. Traditionally, these measurements have been collected using intrusive instruments such as Pitot probes and thermocouples, but there are a number of situations where intrusive devices are undesirable. In gas turbine engine applications, for example, the obstruction of flow produced by an intrusive instrument would result in increased turbulence production and an unacceptable reduction in efficiency. Oftentimes, intrusive instruments require cooling and their performance is degraded by operation in harsh flows as well. In such applications, non-intrusive approaches are much more appealing. Figure 2.1 outlines some of the existing types of non-intrusive measurement techniques found in the literature.

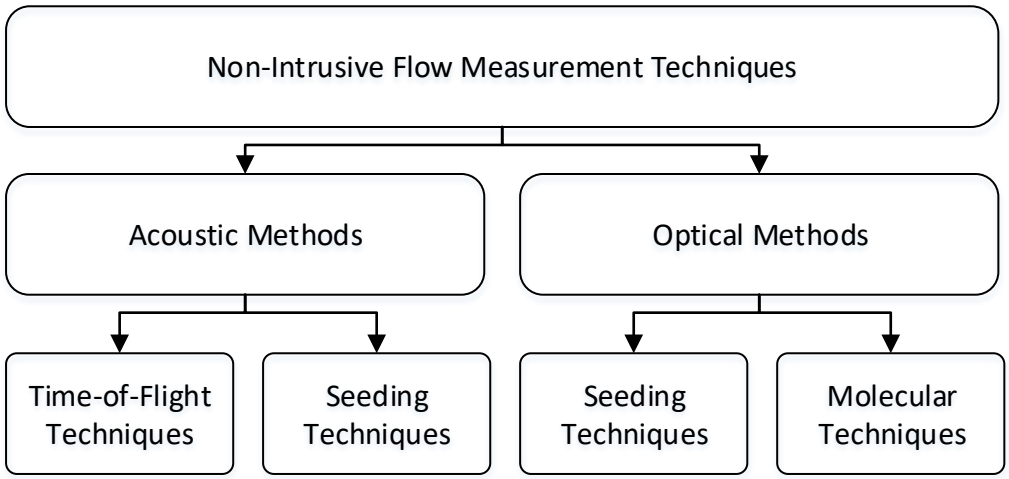

Figure 2.1. *Types of non-intrusive flow measurement techniques*

A list of several existing non-intrusive techniques and relevant references is provided in Table 2.1 below. The reader is encouraged to review the references provided for more information on each measurement technique.

Table 1.1. *List of non-intrusive techniques and relevant references*

(Type) Technique Name	Abbreviation	V	T	χ	Relevant References
(M) Laser Absorption Spectroscopy	LAS	✓	✓	✓	[1–6]
(M) Laser Induced Fluorescence	LIF	✓	✓	✓	[7–9]
(S) Laser Doppler Anemometry	LDA (LDV)	✓			[10–12]
(S) Doppler Global Velocimetry	DGV	✓			[13–17]
(S) Particle Image Velocimetry	PIV	✓			[18,19]
(S) Acoustic Doppler Velocimetry	ADV	✓			[20–22]
(T) Sonic Anemometry & Thermometry	SAT	✓	✓		[23–25]

When selecting a non-intrusive technique for fluid measurements, the advantages and disadvantages of each technique must be carefully weighed. First, the experimentalist must choose between acoustic and optical methods. Optical methods offer the ability to detect fluid conditions very accurately using a wide range of techniques, but they require optical access and are generally sensitive to optical fouling, vibrations, and misalignment which could augment the amount of maintenance required. Acoustic techniques require less equipment maintenance and are more robust to vibrations and misalignment, but wave propagation behavior is much more sensitive to temperature and velocity gradients in the flow field.

Throughout this research, the author considers the use of a non-intrusive acoustic instrument for commercial gas turbine engine applications. Although optical methods have been used to measure fluid conditions in gas turbine engine environments before, the aforementioned drawbacks make commercial implementation very difficult. Engine manufacturers are specifically concerned that such an in-flight instrument would require too much maintenance. Only two techniques are available for non-intrusive flow detection using acoustics – sonic anemometry and thermometry (SAT) and acoustic Doppler velocimetry (ADV). Since SAT enables the detection of both velocity and temperature, it is chosen over ADV in the current work.

1. Sonic Anemometry & Thermometry

Sonic anemometry and thermometry uses a unique configuration of sound sources and microphones to resolve fluid velocity and temperature simultaneously[25]. Before discussing

technique capabilities and limitations, the approach is described below. Consider the arrangement of acoustic equipment shown in Figure 2.2.

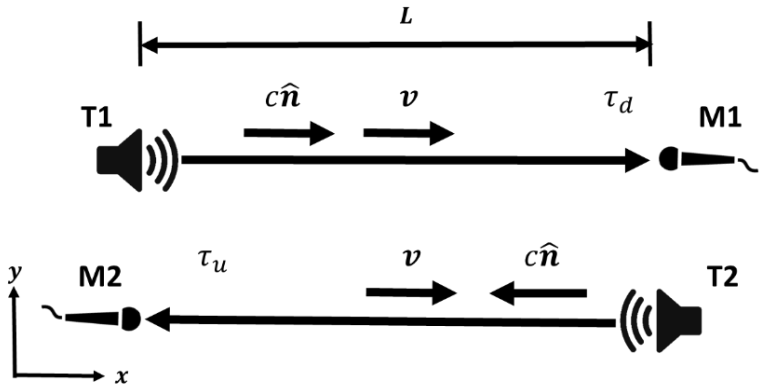

Figure 2.2. *Classical arrangement of sonic anemometry and thermometry equipment*

Using a geometrical (ray) acoustics approach, the acoustic propagation time can be described using the group velocity expression shown below[26].

$$\tau = \int_0^L \frac{ds}{(c\hat{\boldsymbol{n}} + \boldsymbol{v}) \cdot \mathbf{t}} \tag{1}$$

The SAT method is capable of dissociating the effects of fluid velocity and temperature on propagation speed by taking advantage of fluid convection[27]. When the acoustic wave travels in the downstream direction, medium convection produces a shorter propagation time than when the wave travels in the upstream direction. First, an acoustic time-of-flight (TOF) expression for each path is obtained.

$$\tau_d = \int_0^L \frac{ds}{(c\hat{\boldsymbol{n}} + \boldsymbol{v}) \cdot \mathbf{t_1}} = \frac{L}{c + v} \tag{2}$$

$$\tau_u = \int_0^L \frac{ds}{(c\hat{\boldsymbol{n}} + \boldsymbol{v}) \cdot \mathbf{t_2}} = \frac{L}{c - v} \tag{3}$$

Combining the two expressions, an equation for fluid velocity and thermodynamic speed of sound can be derived.

$$v = \frac{L}{2}\left(\frac{1}{\tau_d} - \frac{1}{\tau_u}\right) \tag{4}$$

$$c = \frac{L}{\tau_d} - \frac{L}{2}\left(\frac{1}{\tau_d} - \frac{1}{\tau_u}\right) = \frac{L}{\tau_u} + \frac{L}{2}\left(\frac{1}{\tau_d} - \frac{1}{\tau_u}\right) \tag{5}$$

If the fluid's molecular composition is known, the temperature can be obtained as well. For an ideal gas, for example, equation (6) can be used.

$$T_s = \frac{c^2}{\gamma \bar{R}/MW} \tag{6}$$

In Figure 2.2, the acoustic equipment was placed parallel with the flow field to facilitate this discussion. Often, the equipment is positioned at an angle relative to the Flow-field to prevent fluid obstruction[23,25,27].

In the literature, there is a wide range of documented applications of this technique, dating back to the 1950s[25,28]. Several applications of this work include atmospheric [24,29,30], pipe flow [31,32,28], wind tunnel [33], and boundary layer applications([23,27]) to name a few. Generally, the SAT instrument operates using either a continuous wave sound source[29] or a pulsed ultrasonic signal[34], and can be used to measure up to three component velocities if multiple orientations of the SAT configurations are used[25]. SAT devices are widely used in the field because they lack moving parts and offer great measurement accuracy. These sensors are mostly limited by their line-of-sight averaging requirements and signal-to-noise ratios[27,31]. Typical velocity accuracies are on the order of $\pm$ 0.02-0.05 m/s for a range of $\pm$30 m/s [25]. The temperature accuracy is generally $\pm$0.1 to 2.0°C[25]. Kaijo-Denki devices have been used in the past to measure wind velocities up to 60 m/s and obtained a velocity accuracy within $\pm$1% of measured values[35]. An experiment performed by Mylvaganam et al. in pipe flows yielded 3% uncertainties up to 70 m/s[31]. Throughout this experiment, measurements were collected in flows

up to 100 m/s, but increased acoustic absorption and reduced signal-to-noise ratios prevented flow velocity estimation.

Among all the literature reviewed, the highest reported Mach number application of SAT observed was approximately Mach 0.2[31] (if flow temperature is assumed 300 K). In the next section, we consider the characteristics that could prevent SAT measurements from being collected in compressible flows (Mach>0.3).

2. Compressible Flow SAT Challenges

Fundamentally, acoustic waves are sensitive to fluid properties, medium convection, and stratification. For the SAT technique to work, the acoustic wave must be loud enough to reach each microphone. The SAT measurement itself is prone to two types of errors, signal detection and fluid non-uniformities. In compressible flows, signal attenuation and increased flow noise could result in insufficient signal-to-noise ratios (SNR) which may lead to an inability to properly estimate acoustic propagation times. Additionally, if the fluid contains any stratification of temperature or fluid velocity, the acoustic wave may no longer travel in a straight line between sound source and receiver. In fact, the acoustic signal may not even reach the microphone if it is placed in a refractive shadow zone. An inability to approximate acoustic refraction could result in an over or under estimation of fluid conditions. In the following sub-sections, these topics are explored in more detail.

2.1. Signal to Noise Ratio Reduction

In 1973, Ingard and Singhal [36] performed a pipe flow experiment to investigate the behavior of acoustic waves travelling in an upstream and downstream direction. An acoustic sound source was placed in a rectangular duct and the wave frequency was tuned to match the plane wave mode of the duct. Two microphones were placed at equidistant locations from the sound source in a downstream and upstream position to measure the acoustic signal and Mach 0-0.5 flows were used to carry out the experiment. The measurement results showed that sound pressure was generally higher in the upstream direction than the downstream direction. In fact, the ratio of upstream to downstream pressure grew larger as the Mach number increased! In the mathematical analysis portion of Ingard and Singhal's investigation, the authors derived an expression to

describe the acoustic relationship between the two measurements in laminar and turbulent flows. The laminar and turbulent flow relationships are denoted in Figure 2.3 below:

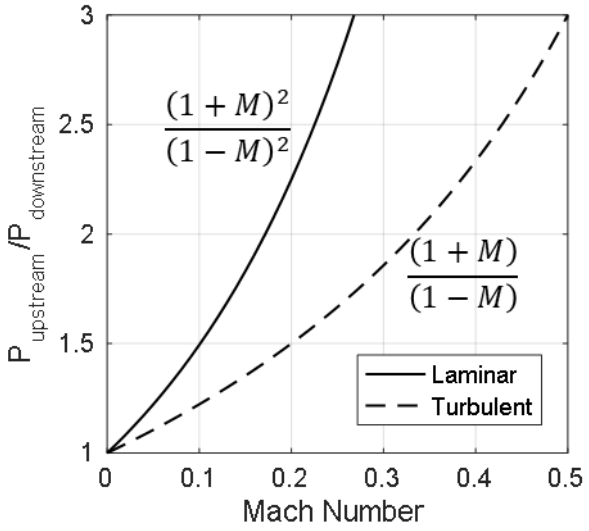

Figure 2.3. *Upstream vs. Downstream acoustic propagation pressure in laminar and turbulent flows (source mounted transverse to moving fluid).*

Although Ingard and Singhal's results where characteristic to the plane wave in a duct application, the pressure ratio for a SAT configuration is expected to grow similarly. Overall, these observations represent a significant obstacle for SAT applications in compressible flows since both upstream and downstream measurements are required.

In addition to a reduction in signal strength associated with propagation direction, the noise generated by a moving fluid plays an important role on SNR as well. In the current work, the impact of jet noise is of significant interest. A comparison of heated and cold-air jet measurements conducted in various operating environments have been previously used to estimate the sound power level of a jet using equation (7) [37]:

$$W = \frac{10^{-4}\rho_{amb}v^8 A}{2c_{amb}^5} \tag{7}$$

Qualitatively, it is evident that increased flow velocities could have a detrimental effect on SAT measurement SNR in higher Mach number flows. Additionally, as the temperature of the jet increases, the velocity at a given Mach number becomes even greater, further amplifying the

problem. For SAT measurements to be performed in compressible flows, the acoustic signal must be able to overcome the noise level of the jet. Although this may be accomplished through the selection of a relatively quiet operating frequency, it still poses a significant challenge to technique success.

2.2. Acoustic Propagation in Inhomogeneous Moving Media

The final challenge that must be overcome to successfully implement SAT in compressible flows is associated with fluid inhomogeneity. In the classical SAT formulas, the end result is one velocity and one temperature value. As the Mach number of a flow increases, pressure fluctuations could harm the acoustic equipment if it is placed in the flow field. As a result, the acoustic equipment will need to be mounted at a safe distance from the flow field. If the equipment is no longer in the flow, the acoustic wave will inevitably refract as it propagates through the medium. When the conditions of the stagnant (ambient) field are known, it may still be possible to identify fluid velocity and temperature in a non-intrusive manner, but such a measurement would require appropriate modelling of acoustic refraction in the presence of a shear layer. For more information on the theory of acoustic propagation, the reader is encouraged to review the work of Ostashev and Wilson[26] (See chapters 2,3, and 10).

In the literature, a lot of the work on sound propagation through a turbulent jet shear layer was performed by Amiet [38–40] and verified by several experimental measurements [41,42]. Amiet's major contribution to this work was the simplifying lip-line model which can be used to estimate acoustic refraction through a turbulent shear layer. The procedure he proposed, proved relatively independent of the shear layer thickness in numerous wind tunnel experiments and could be applied in both planar and cylindrical shear layers with 1D stratification[43]. The caveat to using this technique for single-stream jet SAT is that the fluid characteristics (velocity and thermodynamic speed of sound) must be known in the ambient section. In the presence of multiple stratifications, a different approach is required.

Previously, acoustic tomography methods have been used to solve for fluid flow non-uniformities as well. Fundamentally, tomography is an iterative approach that uses integrated path measurements, collected at different orientations, to estimate a field function such as a temperature or velocity distribution[44–50]. In many applications, acoustic tomography has been used to identify fluid temperatures and the effects of fluid velocity have been neglected. This approach

offers reduced modelling requirements and a significant improvement in computational time, but sacrifices accuracy as the Mach number increases. Coupled velocity and temperature techniques have been implemented in the past [33,46,47,51], but they have generally been restricted to low Mach number applications because of the non-linear acoustic time-of-flight relationship. Since existing tomography techniques require linearization, a $|\boldsymbol{v}| \ll c$ assumption is often used to identify a solenoidal ($\nabla \cdot v = 0$) velocity field. The resulting formulation, however, makes information about an irrotational velocity field difficult to obtain. For more information, the reader is encouraged to review the work of Jovanović et al. [52].

Throughout the author's literature review, the highest fluid velocity estimated using acoustic tomography was only 4 m/s [33]. If an ambient temperature of 300 K is assumed, that is approximately Mach 0.01! To resolve temperature and velocity non-uniformities in much higher Mach numbers, it is clear that a new approach is needed which avoids the incompressible flow assumption previously mentioned. Among some of the complications associated with this task are the need for proper modelling of acoustic propagation at higher Mach numbers, the identification of a coupled (velocity and temperature) acoustic tomography convergence procedure, and an optimized design for satisfactory system performance. In the chapters to follow, each of these items are addressed using theory and experiments, resulting in new methods for high subsonic Mach number acoustics-based measurements for flows of interest to aerospace propulsion applications.

3. References

[1] Docquier, N., and Candel, S., 2002, "Combustion control and sensors: a review," Prog. Energy Combust. Sci., 28(2), pp. 107–150.

[2] Arroyo, M. P., Langlois, S., and Hanson, R. K., 1994, "Diode-laser absorption technique for simultaneous measurements of multiple gasdynamic parameters in high-speed flows containing water vapor," Appl. Opt., 33(15), pp. 3296–3307.

[3] Philippe, L. C., and Hanson, R. K., 1991, "Laser-absorption mass flux sensor for high-speed airflows," Opt. Lett., 16(24), pp. 2002–2004.

[4] Miller, M. F., Kessler, W. J., and Allen, M. G., 1996, "Diode laser-based air mass flux sensor for subsonic aeropropulsion inlets," Appl. Opt., 35(24), pp. 4905–4912.

[5] Allen, M. G., 1998, "Diode laser absorption sensors for gas-dynamic and combustion flows," Meas. Sci. Technol., 9(4), pp. 545–562.

[6] Lyle, K. H., Jeffries, J. B., Hanson, R. K., and Winter, M., 2007, "Diode-Laser Sensor for Air-Mass Flux 2: Nonuniform Flow Modeling and Aeroengine Tests," AIAA J., 45(9), pp. 2213–2223.

[7] Crosley, D. R., and Smith, G. P., 1983, "Laser-Induced Fluorescence Spectroscopy For Combustion Diagnostics," Opt. Eng., 22(5), p. 225545.

[8] Kinsey, J. L., 1977, "LASER-INDUCED FLUORESCENCE," Annu. Rev. Phys. Chem., 28(1), pp. 349–372.

[9] Seitzman, J. M., Kychakoff, G., and Hanson, R. K., 1985, "Instantaneous temperature field measurements using planar laser-induced fluorescence," Opt. Lett., 10(9), p. 439.

[10] Abbiss, J. B., Chubb, T. W., and Pike, E. R., 1974, "Laser Doppler anemometry," Opt. Laser Technol., 6(6), pp. 249–261.

[11] Nezu, I., and Rodi, W., 1986, "Open-channel Flow Measurements with a Laser Doppler Anemometer," J. Hydraul. Eng., 112(5), pp. 335–355.

[12] Tropea, C., 1995, "Laser Doppler anemometry: recent developments and future challenges," Meas. Sci. Technol., 6(6), pp. 605–619.

[13] Meyers, J. F., 1995, "Development of Doppler global velocimetry as a flow diagnostics tool," Meas. Sci. Technol., 6(6), pp. 769–783.

[14] Meyers, J. F., and Komine, H., 1991, "Doppler global velocimetry: a new way to look at velocity," ASME 4th International Conference on Laser Anemometry, Cleveland, pp. 289–296.

[15] Ecker, T., Brooks, D. R., Lowe, K. T., and Ng, W. F., 2014, "Development and application of a point Doppler velocimeter featuring two-beam multiplexing for time-resolved measurements of high-speed flow," Exp. Fluids, 55(9), p. 1819.

[16] Cadel, D. R., and Lowe, K. T., 2015, "Cross-correlation Doppler global velocimetry (CC-DGV)," Opt. Lasers Eng., 71, pp. 51–61.

[17] Ainsworth, R. W., Thorpe, S. J., and Manners, R. J., 1997, "A new approach to flow-field measurement—A view of Doppler global velocimetry techniques," Int. J. Heat Fluid Flow, 18(1), pp. 116–130.

[18] Raffel, M., Willert, C. E., and Kompenhans, J., 1998, Particle Image Velocimetry: A Practical Guide - Markus Raffel, Christian E. Willert, Steven Wereley, Jürgen Kompenhans - Google Books, Springer.

[19] Adrian, R. J., 2005, “Twenty years of particle image velocimetry,” Exp. Fluids, 39(2), pp. 159–169.

[20] Voulgaris, G., Trowbridge, J. H., Voulgaris, G., and Trowbridge, J. H., 1998, “Evaluation of the Acoustic Doppler Velocimeter (ADV) for Turbulence Measurements*,” J. Atmos. Ocean. Technol., 15(1), pp. 272–289.

[21] Fox, M. D., and Gardiner, W. M., 1988, “Three-dimensional Doppler velocimetry of flow jets,” IEEE Trans. Biomed. Eng., 35(10), pp. 834–841.

[22] Jones, S. A., 1993, “Fundamental sources of error and spectral broadening in Doppler ultrasound signals.,” Crit. Rev. Biomed. Eng., 21(5), pp. 399–483.

[23] Kaimal, J. C., and Gaynor, J. E., 1991, “Another look at sonic thermometry,” Boundary-Layer Meteorol., 56(4), pp. 401–410.

[24] Sozzi, R., and Favaron, M., 1996, “Sonic anemometry and thermometry: Theoretical basis and data-processing software,” Environ. Softw., 11(4), pp. 259–270.

[25] McKeon, B., 2007, “Velocity, Vorticity, and Mach Number,” Springer Handbook of Experimental Fluid Mechanics, Springer Science+Business Media, pp. 215–471.

[26] Ostashev, V. E., and Wilson, D. K., 2015, Acoustics in moving inhomogeneous media, CRC Press.

[27] Cuerva, A., and Sanz-Andrés, A., 2000, “On sonic anemometer measurement theory,” J. Wind Eng. Ind. Aerodyn., 88(1), pp. 25–55.

[28] Lynnworth, L. C., and Liu, Y., 2006, “Ultrasonic flowmeters: Half-century progress report, 1955–2005,” Ultrasonics, 44, pp. e1371–e1378.

[29] Kaimal, J. C., and Businger, J. A., 1962, “A Continuous Wave Sonic Anemometer-Thermometer,” J. Appl. Meteorol., 2, pp. 156–164.

[30] Cuerva, A., Sanz-Andrés, A., and Lorenz, R. D., 2003, “Sonic anemometry of planetary atmospheres,” J. Geophys. Res., 108(E4), pp. 295–302.

[31] Mylvaganam, K. S., 1989, “High-Rangeability Ultrasonic Gas Flowmeter for Monitoring Flare Gas,” IEEE Trans. Ultrason. Ferroelectr. Freq. Control, 36(2), pp. 144–149.

[32] Johnson, S. A., Greenleaf, J. F., Hansen, C. R., Samoya, W. F., Tanaka, M., Lent, A., Christensen, D. A., and Woolley, R. L., 1977, “Reconstructing Three-Dimensional Fluid Velocity Fields From Acoustic Transmission Measurments,” Acoustical Holography, L.W. Kessler, ed., Springer US, pp. 307–326.

[33] Barth, M., and Raabe, A., 2011, "Acoustic tomographic imaging of temperature and flow fields in air," Meas. Sci. Technol. Meas. Sci. Technol, 22(22), pp. 35102–13.

[34] Franklin, D. L., Baker, D. W., and Rushmer, R. F., 1962, "Pulsed Ultrasonic Transit Time Flowmeter," Ire Trans. Biomed. Electron., 9(1), pp. 44–49.

[35] Kato, N., Ohkuma, T., Kim, J. R., Marukawa, H., and Niihori, Y., 1992, "Full scale measurements of wind velocity in two urban areas using an ultrasonic anemometer," J. Wind Eng. Ind. Aerodyn., pp. 67–78.

[36] Ingard, U., and Singhal, V. K., 1973, "Upstream and Downstream Sound Radiation into a Moving Fluid," J. Acoust. Soc. Am., 54(5), pp. 1343–1346.

[37] Lighthill, M. J., 1963, "Jet Noise," AIAA J., 1(7), pp. 1507–1517.

[38] Amiet, R. K., 1975, "Correction of Open Jet Wind Tunnel Measurements for Shear Layer Refraction," 2nd AIAA Aeroacoustics Conference, American Institute of Aeronautics and Astronautics, Hampton.

[39] Amiet, R. K. K., 1978, "Refraction of sound by a shear layer," J. Sound Vib., 58(4), pp. 467–482.

[40] Schlinker, R. H., and Amiet, R. K., 1980, Refraction and scattering of sound by a shear layer, East Hartford.

[41] Candel, S. M., Guedel, A., and Julienne, A., 1976, "Radiation, refraction and scattering of acoustic waves in a free shear flow," 3rd AIAA Aero-Acoustics Conference, American Institute of Aeronautics and Astronautics, Palo Alto.

[42] Ahuja, K. K., Tanna, H. K., and Tester, B. J., 1981, "An experimental study of transmission, reflection and scattering of sound in a free jet flight simulation facility and comparison with theory," J. Sound Vib., 75(1), pp. 51–85.

[43] Sulaiman, Z., 2011, "Effect of Open-Jet Shear Layers on Aeroacoustic Wind Tunnel Measurements," Delft University of Technology.

[44] Verhoeven, D., 1993, "Limited-data computed tomography algorithms for the physical sciences.," Appl. Opt., 32(20), pp. 3736–54.

[45] Herman, G. T., and Lent, A., 1976, "Iterative reconstruction algorithms," Comput. Biol. Med., 6(4), pp. 273–294.

[46] Beckord, P., Hofelmann, G., Luck, H. O., and Franken, D., 1998, "Temperature and velocity flow fields measurements using ultrasonic computer tomography," Heat Mass Transf., 33(1998), pp. 395–403.

[47] Jovanovic, I., Sbaiz, L., and Vetterli, M., 2006, "Acoustic Tomography Method for Measuring Temperature and Wind Velocity," IEEE International Conference on Acoustics, Speech, and Signal Processing, p. 4.

[48] Wiens, T., and Behrens, P., 2009, "Turbulent Flow Sensing using Acoustic Tomography," Proceedings of Innovations in practical Noise Control, Ottawa, p. 6.

[49] DeSilva, U., Bunce, R. H., Schmitt, J. M., and Claussen, H., 2015, "Gas Turbine Exhaust Temperature Measurement Approach Using Time-Frequency Controlled Sources," Proceedings of ASME Turbo Expo 2015, ASME, Montreal, pp. 1–7.

[50] DeSilva, U., Bunce, R. H., and Claussen, H., 2013, "Novel Gas Turbine Exhaust Temperature Measurement System," Proceedings of ASME Turbo Expo 2013, ASME, San Antonio, pp. 1–8.

[51] Komiya, K.-I., and Teerawatanachai, S., 1993, "Ultrasonic tomography for visualizing the velocity profile of air flow," Flow Meas. Instrum., 4(2), pp. 61–65.

[52] Jovanović, I., Sbaiz, L., Vetterli, M., Jovanović, I., Sbaiz, L., and Vetterli, M., 2009, "Acoustic Tomography for Scalar and Vector Fields: Theory and Application to Temperature and Wind Estimation," J. Atmos. Ocean. Technol., 26(8), pp. 1475–1492.

Part III. Unheated Laboratory Jet Experiment

Preface

The text presented in Part III was published in the journal of Measurement Science & Technology in 2017. *Otero, R., Lowe, K. T., & Ng, W. F. (2017). Extension of sonic anemometry to high subsonic Mach number flows. Measurement Science and Technology, 28(3), DOI:10.1088/1361-6501/aa54ed.* Note that the appendices referred to in the text are a part of the manuscript and are included at the end of the manuscript, not the end of this dissertation.

The major takeaways of this manuscript are:

- Acoustic measurements can be used to measure compressible velocities and temperatures
- Upstream and downstream measurements are not required to perform SAT

Extension of Sonic Anemometry to High Subsonic Mach Number Flows

R Otero[1], K T Lowe[2] and W F Ng[3]

[1]Graduate Research Assistant, Department of Mechanical Engineering,
Virginia Tech, Blacksburg, VA, USA,

[2]Assistant Professor, Department of Aerospace and Ocean Engineering,
Virginia Tech, Blacksburg, VA, USA.

[3]Chris C. Kraft Endowed Professor, Department of Mechanical Engineering,
Virginia Tech, Blacksburg, VA, USA.

E-mail: raul1991@vt.edu

Abstract. In the literature, the application of sonic anemometry has been limited to low subsonic Mach number, near-incompressible flow conditions. To the best of the authors' knowledge, this paper represents the first time a sonic anemometry approach has been used to characterize flow velocity beyond Mach 0.3. Using a high speed jet, flow velocity was measured using a modified sonic anemometry technique in flow conditions up to Mach 0.83. A numerical study was conducted to identify the effects of microphone placement on the accuracy of the measured velocity. Based on estimated error strictly due to uncertainty in time-of-acoustic flight, a random error of $\pm$4 m/s was identified for the configuration used in this experiment. Comparison with measurements from a Pitot probe indicated a velocity RMS error of $\pm$9 m/s. The discrepancy in error is attributed to a systematic error which may be calibrated out in future work. Overall, the experimental results from this preliminary study support the use of acoustics for high subsonic flow characterization.

Keywords: Sonic Anemometry (SA), Compressible Flows, Acoustic Velocity Measurement, Non-Intrusive Flow Measurement, Time of Flight Techniques

Nomenclature

ADV	Acoustic Doppler Velocimetry
c	Thermodynamic Speed of sound
c_{amb}	Thermodynamic speed of sound in an ambient medium
c_{jet}	Thermodynamic speed of sound in a jet medium
D_{xn}	Stream-wise distance between transmitter and nth microphone
D_y	Distance between transmitter and microphones in direction perpendicular to flow direction
D_{yn}	Distance between transmitter and nth microphone in direction perpendicular to flow direction
$D_{y,jet}$	Jet section thickness in y-direction
f	Frequency of acoustic wave
f_m	Modulation frequency
f_c	Carrier frequency
k_x	Wavenumber component in stream-wise direction
L	Distance between sound transmitter and microphone
MSA	Modified Sonic Anemometry
M	Mach number
$M1$	Microphone 1
$M2$	Microphone 2
$\hat{\boldsymbol{n}}$	Unit vector normal to the acoustic wave front
P	Pressure
R	Ideal gas constant of air
SA	Sonic Anemometry
SNR	Signal to noise ratio
s	Propagation length along Γ_n (nth ray path)
TOF	Time of acoustic flight
$T1$	Transmitter 1
T	Temperature

$\boldsymbol{t_n}$	Unit vector tangent to the ray path (Γ_n)
u_{v_x}	Uncertainty in estimation of velocity in *x*-direction
$u_{\delta\tau}$	Uncertainty in estimation of time of acoustic flight difference for two paths
u_θ	Uncertainty in equipment physical angle estimation relative to transmitter stream-wise plane.
u_M	Uncertainty in estimation of Mach number
v	Flow velocity
v_{amb}	Flow velocity in an ambient medium
v_{jet}	Flow velocity in a jet medium
x	Stream-wise displacement of acoustic ray
x_n	Stream-wise displacement of acoustic ray for nth microphone
y	Displacement of acoustic ray in direction perpendicular to flow direction
β_{amb}	Ray angle relative to positive *x*-direction for the ambient medium absent flow velocity
β_{jet}	Ray angle relative to positive *x*-direction for the jet medium absent flow velocity
γ	Specific heat ratio
Γ_n	nth Ray path
$\delta\tau$	Difference in acoustic time-of-flight between path 2 and path 1
θ_{M1}	Microphone 1 angle relative plane located at transmitter stream-wise position
θ_{M2}	Microphone 2 angle relative plane located at transmitter stream-wise position
λ_x	Wavelength along a flow boundary
λ_{cxn}	Contribution to wavelength along a flow boundary by the flow's speed of sound (c_n)
λ_{vxn}	Contribution to wavelength along a flow boundary by the flow's velocity (v_n) parallel to the boundary
ρ	Density
σ_v	Standard deviation of velocity measurement
σ_t	Standard deviation of time-of-flight measurement
τ_n	Acoustic time-of-flight for the nth path
τ_d	Acoustic time-of-flight in the downstream direction

τ_u	Acoustic time-of-flight in the upstream direction
$\tau_{n,amb}$	Acoustic time-of-flight for the nth path in the ambient medium
$\tau_{n,jet}$	Acoustic time-of-flight for the nth path in the jet medium
ω	Acoustic angular frequency

1. Introduction

In the field of fluid mechanics, engineers have long sought a velocity measurement technique that avoids the complications associated with intrusive probes. Generally, intrusive probes create flow distortion, pressure losses, and increased turbulence that result in unrepresentative flow measurements. Non-intrusive laser based techniques such as Laser Doppler velocimetry and particle image velocimetry have been effective and widely used, but they are often prone to miss-alignment, expensive to implement, and often require particle seeding. In applications where particle seeding is unacceptable, such as gas turbine engine health monitoring, a robust, seedless technique that can handle vibrations and is relatively inexpensive to implement is desirable. Throughout this article, a non-intrusive acoustic alternative that uses distance and acoustic propagation time measurements is presented. The results of flow velocity measurements up to Mach 0.83 will be presented and assessed for high subsonic Mach number measurement feasibility.

When conducting high subsonic acoustic measurements, flow noise (Lighthill, 1963) and shear layer effects (Schlinker & Amiet 1980, Ostashev & Wilson 2015) must be carefully considered. In the following sections, a modification to the classical sonic anemometry technique is proposed in order to improve signal-to-noise ratio (SNR) and overcome certain limitations associated with acoustic propagation. First, an overview of the literature is used to identify classical measurement configurations and procedures, while highlighting existing limitations. Next, a modified sonic anemometry (MSA) approach is presented along with a numerical analysis of measurement error for the current experimental configuration. Finally, intrusive and non-intrusive flow measurements are used to approximate actual measurement error for the current application.

1.1. Principles of Sonic Anemometry

In practice, two fundamental acoustic techniques exist for non-intrusively measuring flow velocities. These two techniques are Acoustic Doppler Velocimetry (ADV) and sonic anemometry (SA). The major difference between these two techniques is that ADV measures a Doppler shift in frequency produced by scattered acoustic signals (Voulgaris & Trowbridge 1998, Fox & Gardiner 1988), while SA uses simultaneous acoustic time-of-flight (TOF) measurements (Cuerva & Sanz-Andres 2000, Wyngaard 1981) instead. Since the ADV measurement requires particulate seeding, and SNR is largely a function of particle size and concentration (Rehmel 2007, Kaus, Lohrmann, & Cabrera 1994), this type of measurement would be counter-productive if the objective is to minimize flow distortion and maximize SNR. For this reason, focus throughout this paper is directed towards a SA based approach.

Instead of using a Doppler shift measurement, SA capitalizes on the integral ray equation for TOF which is a function of the acoustic path (Γ_n) and the group velocity ($c\hat{\boldsymbol{n}} + \boldsymbol{v}$) (Ostashev & Wilson 2015, Jovanovic et al. 2006, Kiminki 2005),

$$\tau_n = \int_{\Gamma} \frac{ds}{(c\hat{\boldsymbol{n}} + \boldsymbol{v}) \cdot \mathbf{t_n}} \tag{1}$$

The classical SA technique consists of two acoustic path measurements that are collected using two transmitter and microphone pairs (Cuerva & Sanz-Andres 2000, 2003). The first measurement follows a downstream acoustic path ($\boldsymbol{v} \cdot \hat{\boldsymbol{n}} > 0$), and the second follows an upstream propagation path ($\boldsymbol{v} \cdot \hat{\boldsymbol{n}} < 0$). For simplicity, consider a medium that moves parallel to a downstream and upstream ray path as shown in Figure 3.1 below:

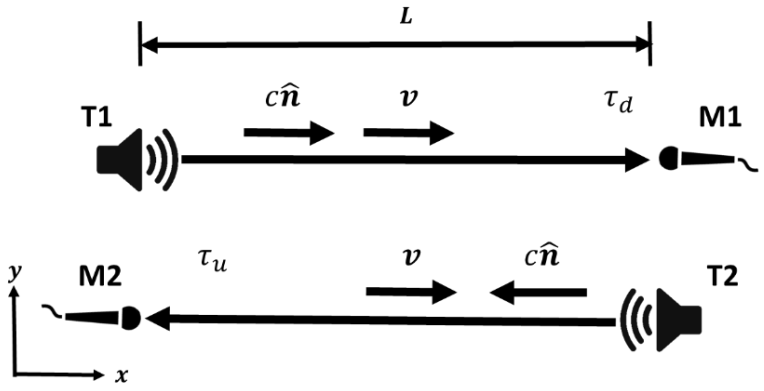

Figure 3.4. *Example configuration for classical sonic anemometry measurement.*

Due to the convective effect that is evident in the denominator of equation (1), the downstream TOF will be lower than the upstream TOF (Banfield & Dissly 2005). Measuring TOF and maintaining a constant length and angle between upstream and downstream pairs, flow velocity can be determined "relatively independently of the flow properties" (Cuerva & Sanz-Andres 2000). These flow properties include thermodynamic speed of sound ($\sqrt{\gamma RT_s}$), pressure, density, & temperature. For an equal path length between each transmitter and microphone pair, equation (1) can be used to obtain flow velocity in the following manner (Cuerva & Sanz-Andres 2000, 2003, Wang, Yernaux, & Deltour 1999, Sozzi & Favaron 1996, Wyngaard 1981):

In downstream direction,

$$\tau_d = \int_0^L \frac{ds}{(c\hat{\boldsymbol{n}} + \boldsymbol{v}) \cdot \mathbf{t_1}} = \frac{L}{c + v}$$

In upstream direction,

$$\tau_u = \int_0^L \frac{ds}{(c\hat{\boldsymbol{n}} + \boldsymbol{v}) \cdot \mathbf{t_2}} = \frac{L}{c - v}$$

For equal thermodynamic speed of sound along both paths,

$$\frac{L}{\tau_d} - v = c = \frac{L}{\tau_u} + v$$

Rearranging,

$$v = \frac{L}{2}\left(\frac{1}{\tau_d} - \frac{1}{\tau_u}\right) \tag{2}$$

1.2. Sonic Anemometry Limitations

The classical SA technique poses several challenges that make immediate implementation in high subsonic Mach number flows difficult. Prior to the current work, the SA technique has generally been used for low Mach number applications. A survey of the literature reveals that applications are generally restricted to velocities less than 100 m/s, while reported uncertainties are widely varied (McKeon et al 2007; Kato et al 1992; Mylvaganam 1989; Tack & Lambert 1965). One study reports a typical sonic anemometer velocity range is $\pm$30 m/s with accuracies in the range of $\pm$0.02-0.05 m/s (McKeon et al 2007). On the other hand, Kaijo-Denki type DA310 devices have been used to measure wind velocities up to 60 m/s with an accuracy of $\pm$ 1 % of the measurement values (Kato et al 1992). In an experimental setting, Mylvaganam et al. performed an investigation in gaseous flows from 0 to 100 m/s, but were only able to report velocity measurements up to 70 m/s with a 3% uncertainty reported across the measurement span (Mylvaganam 1989). Assuming 20°C ambient conditions, the 100 m/s limitation of the aforementioned SA device corresponds to a Mach number of approximately 0.3.

This Mach number limitation is largely due to low measurement SNR. Although the classical SA approach results in minimized TOF uncertainties by maximizing the velocity dependent inverse TOF difference shown in equation (2), SNR may be significantly reduced due to v^8 scaling of flow noise (Lighthill, 1963) and acoustic impedance differences (Ostashev & Wilson 2015). Additionally, the direction of acoustic propagation has a profound effect on signal strength (Ingard 1973, Ostashev & Wilson 2015). Even though certain directivity angles result in higher acoustic pressures than others, there are no inhibiting factors for flows less than Mach 1, other than SNR, that would prevent the SA technique from measuring higher Mach velocities in uniform flows. In a non-uniform configuration, new limitations are introduced due to Snell's law. A critical angle of reflection binds the measurement domain to a specific range of ray propagation angles, and the acoustic paths are no longer a straight line. Traditional SA measurements can

overcome the critical angle reflection problem by changing the orientation of acoustic equipment, but solving for jet velocity in a non-uniform flow configuration is non-trivial.
In the following section, a modified approach and configuration that allows for uniform and non-uniform flow measurements is proposed. The new configuration provides flexibility in the arrangement of acoustic equipment, which facilitates optimization for measurement SNR.

2. Fundamentals of MSA Technique

From equation (1), it is evident that the TOF is a function of the propagation distance (and direction), speed of sound, and flow velocity. In a medium of stream-wise constant flow velocity and thermodynamic speed of sound, it is unnecessary to orient the components so that similar upstream and downstream acoustic ray path measurements can be collected. Instead, a wide range of configurations may be used to optimize SNR and avoid critical angle reflection when gradients are present.

Table 3.2. *MSA flow conditions*

Case 1	Uniform flow	Consists of a constant flow and thermodynamic speed of sound propagation medium
Case 2	Non-uniform flow	Consists of a flow and no-flow section of stream-wise constant flow velocity and thermodynamic speed of sound (properties are known in no flow section)

In the following sections, the modified approach will be outlined for the two flow conditions listed in Table 3.1.

2.1. Uniform Velocity Solution

Figure 3.2 depicts the arrangement of acoustic components for case 1 (the uniform medium described in the introduction to Section 2).

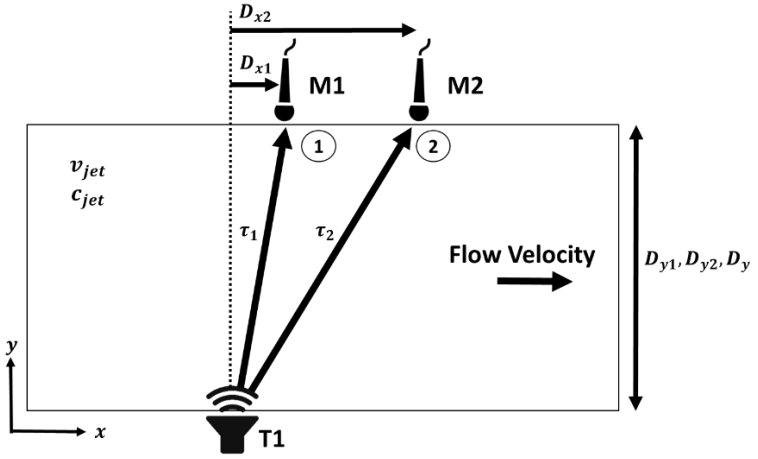

Figure 3.5. *Application of MSA in a homogenous flow medium.*

In order to implement the MSA technique, at least one sound transmitter and two microphones must be used. The transmitter (T1) is positioned on one side of the flow field, and the two microphones (M1 and M2) are positioned on the other, displaced in the stream-wise direction. In a similar manner to the classical SA technique, flow velocity can be determined by measuring the relative displacement of components, and collecting simultaneous TOF measurements along two acoustic propagation paths (see Appendix A for derivation). The equation for uniform flow velocity in the *x*-direction becomes:

$$v_x = \frac{\left[\left(\frac{D_{x2}}{\tau_2}\right)^2 + \left(\frac{D_{y2}}{\tau_2}\right)^2 - \left(\frac{D_{x1}}{\tau_1}\right)^2 - \left(\frac{D_{y1}}{\tau_1}\right)^2\right]}{\left(\frac{2D_{x2}}{\tau_2} - \frac{2D_{x1}}{\tau_1}\right)} \tag{3}$$

As shown in equation (3), the effects of flow properties (ρ, P, T, γ, R) are absent in this velocity formulation as well. It is important to note that in order to use equation (3), several requirements must be satisfied. The first requirement is that the thermodynamic speed of sound through the medium be approximately equal along stream-wise and transverse direction. The second requirement is that the flow velocity in the *y*-direction be negligible when compared to the *x*-direction. If any of these requirements are not satisfied, the velocity measurement will produce invalid results. In practical applications, such as jet measurements, the flow properties are not

typically uniform along the propagation medium. A numerical approach, as outlined in the following section, may be used when handling these types of configurations.

2.2. Non-Uniform Velocity Solution

Figure 3.3 depicts the configuration for case 2 (the non-uniform medium described in the introduction to Section 2).

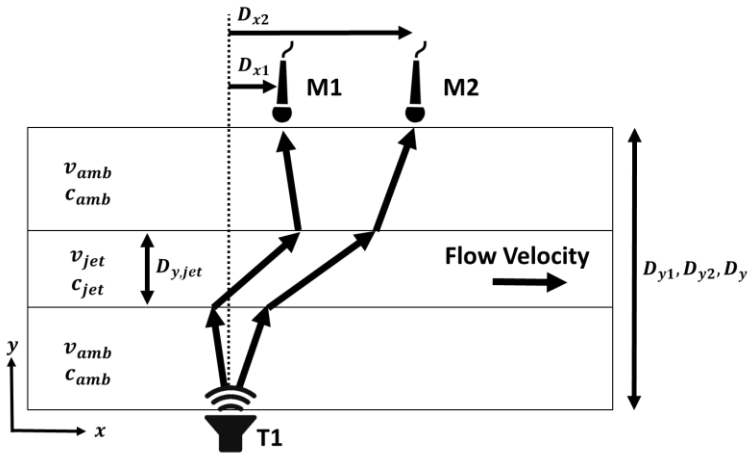

Figure 3.6. *Application of MSA in a non-uniform flow medium with known ambient conditions.*

In order to resolve v_{jet} and c_{jet} in the non-uniform flow configuration, a numerical approach is necessary. Using a Snell's law for convected mediums approach, the flow properties were iteratively obtained. According to this principle, the wavelength (or wavenumber) component parallel to a fluid boundary remains constant on both sides of the interface (Ostashev et al. 2001). To better explain this phenomena, consider a plane wave front "exiting" a jet into an ambient domain as shown in Figure 3.4 below:

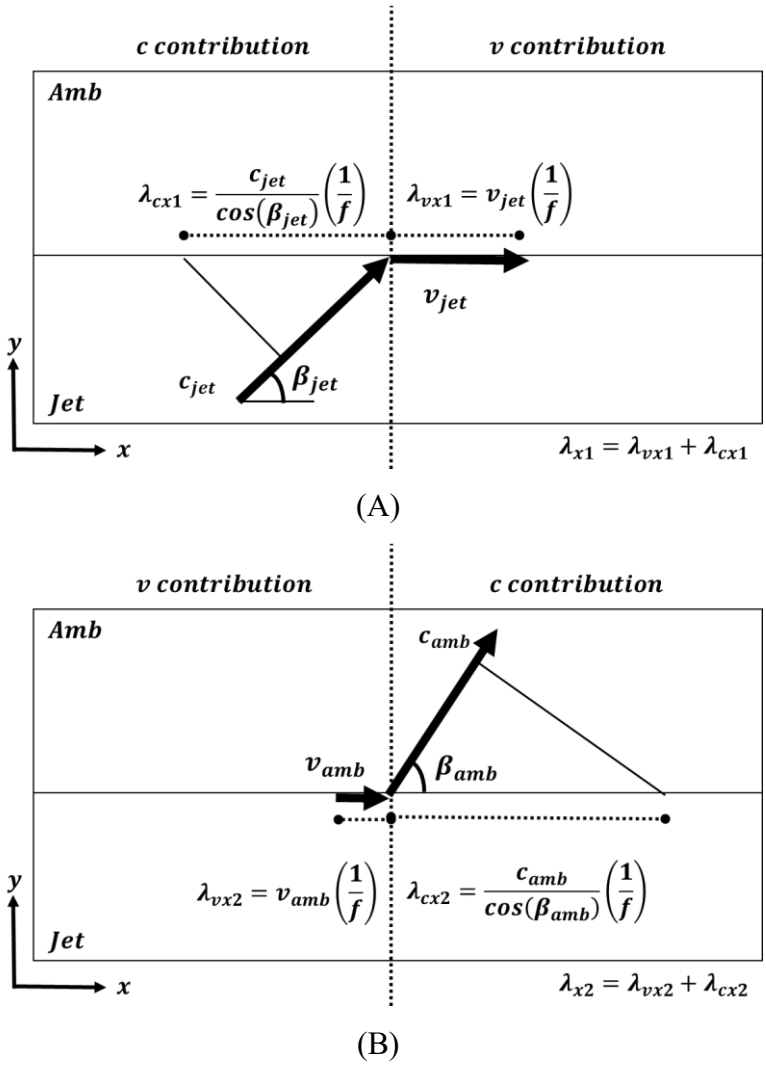

Figure 3.7. *Schematic of stratified flow where plane acoustic wave travels from a jet section to an ambient section. (A) Incident wave. (B) Transmitted wave.*

In Figure 3.4, the incident and transmitted wavelengths along the fluid boundary are represented by contributions from v and c (λ_{vx} and λ_{cx}). Setting λ_{x1} equal to λ_{x2}, a Snell's Law for convected medium equation can be determined:

$$\lambda_x = \frac{2\pi}{k_x} = \frac{1}{f}\left(\frac{c_{jet}}{cos(\beta_{jet})} + v_{jet}\right) = \frac{1}{f}\left(\frac{c_{amb}}{cos(\beta_{amb})} + v_{amb}\right) \quad (4)$$

Since λ_x (or k_x) and f are constant, equation (4) can be further reduced to obtain

$$\frac{\omega}{k_x} = \frac{c_{amb}}{cos(\beta_{amb})} + v_{amb} = \frac{c_{jet}}{cos(\beta_{jet})} + v_{jet} = constant \quad (5)$$

Using equations (1) and (5), the acoustic path and TOF between a transmitter and microphone can be obtained for an assumed jet thermodynamic speed of sound and flow velocity. The assumed jet parameters can be iterated until the numerical TOF values converge upon the measured values. A high level overview of the iterative method used in this experiment is shown in Figure 3.5:

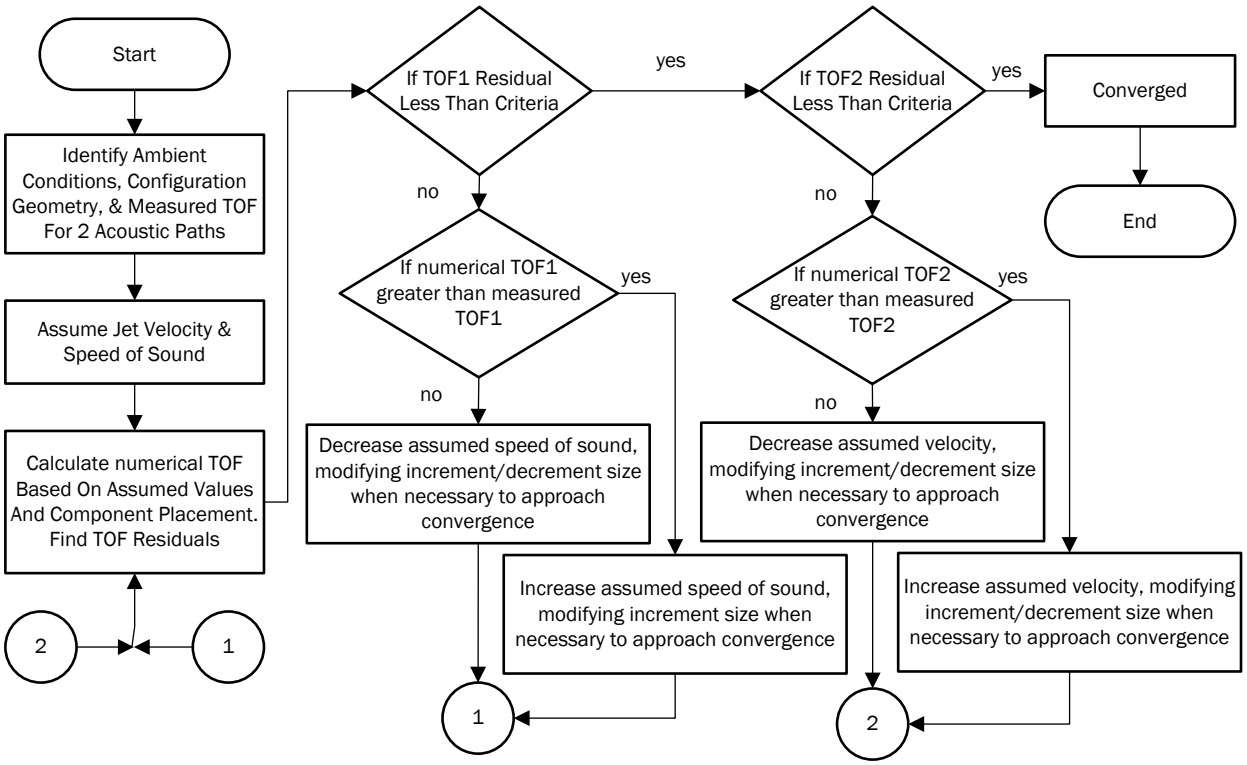

Figure 3.8. *High-level flow diagram highlighting steps necessary to iteratively solve for jet properties.*

Iterating the assumed jet velocity and thermodynamic speed of sound, and properly defining the increment/decrement parameters, this approach can be used to converge on the flow velocity. For the experimental results presented, this method was used.

3. Experimental Setup & Procedures

In order to validate the theory presented in Section 2, experiments were conducted at a Virginia Tech jet facility, capable of attaining plenum pressures up to 2 MPa, and mass flow rates up to 0.25 kg/s (Brooks et al, 2014). Throughout the experiment, a 50.8 mm diameter converging nozzle was used to produce high subsonic Mach number flow. The measurement conditions spanned between Mach 0 and 0.83, and diameter Reynolds numbers up to 900,000. The expected potential core length was approximately 5 jet diameters downstream of the exit plane (Lau et al, 1979).

To operate the facility, a feedback-controlled pneumatic valve was used to control the plenum pressure upstream of the nozzle exit. Using the known ambient pressure at the exit of the nozzle, the nozzle pressure ratio was determined and used to control the operating isentropic Mach number.

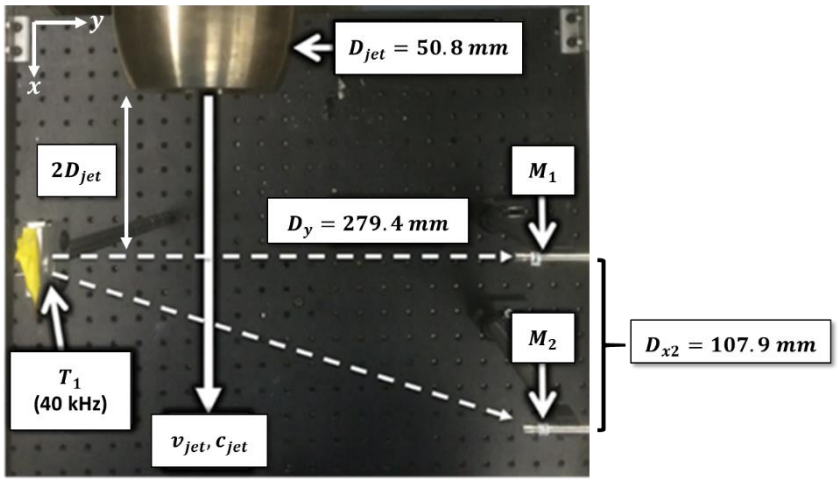

Figure 3.9. *Diagram of experimental setup for iterative MSA measurements.*

To generate the acoustic tone for measurements, an ultrasonic American Piezo 40 kHz transmitter, which is capable of achieving sound pressure levels up to 117 dB (measured 30 cm from transmitter) with a driving voltage of 10 Vrms, was used. Two 6.35 mm PCB microphones were used to measure the acoustic waveforms across the jet. An NI USB 6356 data acquisition system was used to simultaneously sample the transmitter and microphone outputs at 1.25 MS/s each.

3.1. Transmitter Characteristics & Signal Processing

Since acoustic signals in real environments are attenuated by stratified media and polluted by acoustic noise (Ostashev 2001), the accuracy of each TOF measurement will vary according to SNR (Mylvaganam 1989). In high subsonic Mach number flows, determination of the true TOF will require a robust sound source and proven signal processing technique.

Although various sound source options exist, an amplitude modulated burst approach was selected for the current work due to a desire for low noise acoustic measurements. Since flow noise generally decreases with increasing frequency, a high frequency acoustic tone was used to maximize SNR. A sample signal, collected using the experimental test equipment, is shown in Figure 3.7 below:

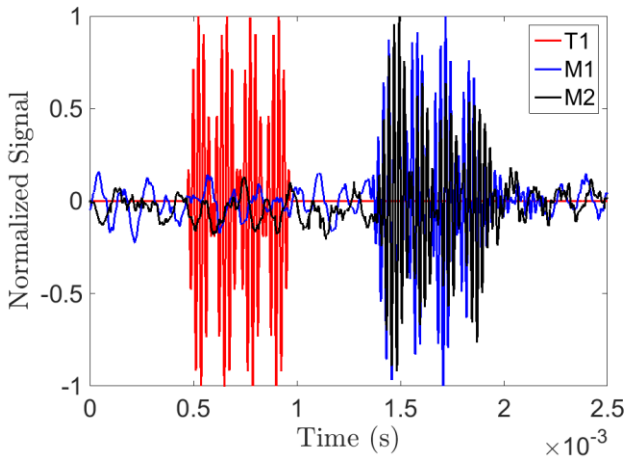

Figure 3.10. *Sample of amplitude modulated burst signals (one measurement set) collected at 3 different locations.*

The acoustic signal is comprised of a 40 kHz carrier frequency (f_c) that is cycled by a 4 kHz modulation frequency (f_m). A signal burst duration of 0.5 milliseconds was used.

$$F(t) = \begin{cases} \sin(2\pi f_m t)\sin(2\pi f_c t), & |t| \le 2/f_m \\ 0, & |t| > 2/f_m \end{cases} \tag{6}$$

The selected waveform characteristics exhibit a few benefits in the current application. Primarily, the short burst of amplitude modulated signal produces a more distinct acoustic signature that can be emitted multiple times during the measurement duration. Using multiple measurement sets (Figure 3.7 represents a measurement set), the standard error of TOF estimation can be greatly reduced (Bendat & Piersol 2011).

Throughout the experiment, 30 measurement sets were sampled continuously for one second at 9 different Mach numbers up to Mach 0.83. The acquired data was primarily used to identify TOF along each acoustic path. An illustration of the signal processing approach is shown in Figure 3.8 below and described further to follow:

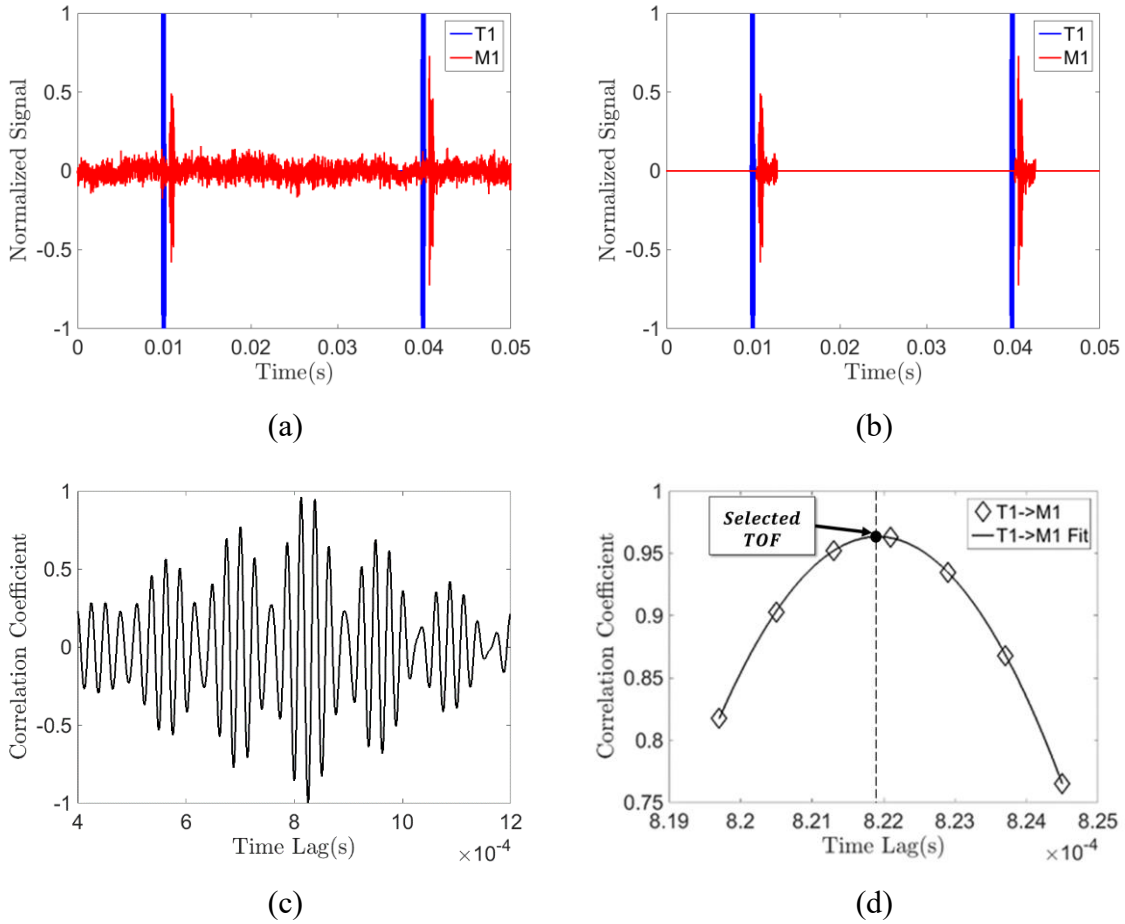

Figure 3.11. *Overview of TOF estimation procedure. (a) Raw T1 and M1 acoustic signal (b) Pre-conditioned T1 and M1 acoustic signals (c) Cross Correlation of T1-M1 signal. (d) 3rd order polynomial peak fit used to enhance precision of time-lag detection.*

A cross-correlation approach, similar to the one outlined by Omologo et al. (1994), was used to estimate TOF between the transmitter and microphones. Before correlating the measured signals, each measurement was pre-conditioned to improve the accuracy of the estimator (Knapp & Carter 1976). This pre-conditioning was performed by setting to zero any signal regions known not to have originated from the sound source. A range of conceivable time delays were determined using the maximum and minimum expected flow velocities and temperatures. This step served to minimize the effect of flow noise on the cross-correlation results. After conditioning the measurement data to reduce the effects of flow noise, cross correlation of the entire one second signal (30 measurement sets) was performed. In Figure 3.8c, the results of a sample cross-correlation are shown. In this correlation there appears to be two maxima. This behavior was attributed to the sound source frequency characteristics and should not be considered a technique limitation. Sound pulses with more distinct time-series signatures may be used to minimize this ambiguity. For the current research, this issue was resolved using Fermat's principle of least propagation time. In the figure, the correlation minima appears between these two peaks. Fermat's principle of least time indicates that the true correlation maxima should occur before the correlation minima. Combining the known relative distances and measured TOF values, the jet velocity was iteratively resolved using the procedure outlined in Section 2.

4. Measurement Uncertainty

The correlation results shown in Figure 3.8c highlight the importance of using distinct, high SNR, acoustic signals when performing an MSA measurement. Even with the amplitude modulated approach, the correlation maxima can be mistaken if the measurement contains sufficient noise. In addition to signal strength, the cross-correlation method used to estimate TOF must be carefully considered to minimize the effects of SNR. From the previous section, it is important to note that the full signal, comprised of 30 measurement sets, was correlated in this experiment rather than binning each measurement set in the one second signal. While correlating each set individually would provide a greater number of TOF samples, Monte Carlo simulation results (see Appendix B) indicate that single-set (binned) correlations with low SNRs are associated with increased variation.

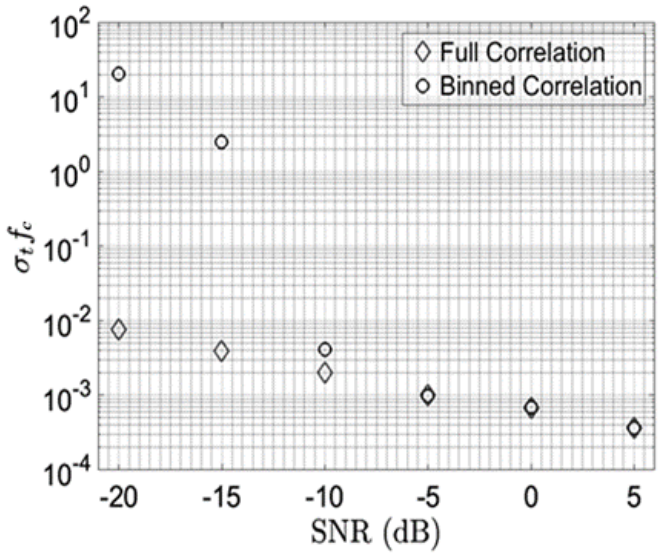

Figure 3.12. *Cross correlation estimator non-dimensional TOF standard deviation. "Full Correlation" refers to the correlation of the entire 1-second signal, while "Binned Correlation" correlates individual measurement sets and compiles them to find an ensemble average.*

In Figure 3.9, the relationship between signal SNR and standard deviation of two post-processing techniques is shown. When SNR is greater than -5 dB, binned and full correlations give similar standard deviation results. However, as the SNR decreases, the full correlation gives a smaller standard deviation, indicating improved post-processing performance. In the following Section, the impact of TOF standard deviation on velocity estimation uncertainty will be explored in detail.

4.1. Velocity Estimation Uncertainty

Prior to conducting an MSA measurement, it is important to understand the driving factors of velocity uncertainty. Fundamentally, the MSA measurement is a function of two acoustic path measurements of TOF and displacement measurements. For a uniform flow configuration, equation (3) may be used to quantify velocity uncertainty in a relatively straight forward manner. For a non-uniform flow configuration, velocity uncertainty must be quantified numerically.

Combining equation (1) for two acoustic paths, it is evident that velocity can be expressed as a function of $c, \delta\tau, ds_{\Gamma_1}$, and ds_{Γ_2}:

$$\tau_2 - \tau_1 = \delta\tau = \int_{\Gamma_2} \frac{ds}{(c\hat{\boldsymbol{n}} + \boldsymbol{v}) \cdot \mathbf{t}_{\boldsymbol{\Gamma_2}}} - \int_{\Gamma_1} \frac{ds}{(c\hat{\boldsymbol{n}} + \boldsymbol{v}) \cdot \mathbf{t}_{\boldsymbol{\Gamma_1}}} \tag{7}$$

Using Fermat's principle of least time, a derivative expression that minimizes each propagation path may be derived from equation (1). Since the y-direction displacement is known for each section of propagation, the derivative expression can be written as:

$$0 = \frac{\partial(\tau_2)}{\partial(\theta_{M2})} \tag{8}$$

$$0 = \frac{\partial(\tau_1)}{\partial(\theta_{M1})} \tag{9}$$

Combining equations (7-9), the equation for velocity uncertainty can be generalized as:

$$u_{v_x} = \sqrt{\left[\left(\frac{\partial v_x}{\partial(\delta\tau)}\right)^2\right] u_{\delta\tau}^2 + \left[\left(\frac{\partial v_x}{\partial(\theta_{M2})}\right)^2 + \left(\frac{\partial v_x}{\partial(\theta_{M1})}\right)^2\right] u_\theta^2} \tag{10}$$

Assuming the effect of u_θ on u_{v_x} is dependent on time uncertainty (equipment distances can be calibrated using ambient measurements), the effect of stream-wise microphone placement on velocity uncertainty can be iteratively resolved using the results of the TOF Monte Carlo simulation presented in the previous section.

In order to quantify the velocity uncertainty for this experiment, another Monte Carlo analysis was performed. First, a simulated flow field was created. Next, two acoustic propagation paths (same arrangement as experimental setup) were iteratively resolved using Snell's Law for convected flows and the known ambient medium conditions. The simulated acoustic propagation model was used to determine the expected TOF for each acoustic path. Assuming a worst case SNR of -20 dB in TOF measurements, Figure 3.9 was used to specify a worst case TOF standard deviation of approximately $2.5 * 10^{-7}$ seconds. Adding random noise (of the specified standard deviation) to the expected TOF values of 1000 samples, the effect of TOF noise on velocity estimation error at various microphone 2 angles (microphone 1 angle was set to 0) was quantified

for several Mach number (unheated jet) conditions. It is important to note that the TOF standard deviation did not change for each Mach number throughout this study. Under realistic conditions, the SNR of acoustic measurements are expected to decrease with increasing Mach number due to jet noise scaling with flow velocity (Lighthill 1963). The results of the velocity standard deviation Monte Carlo study are shown in Figure 3.10 below.

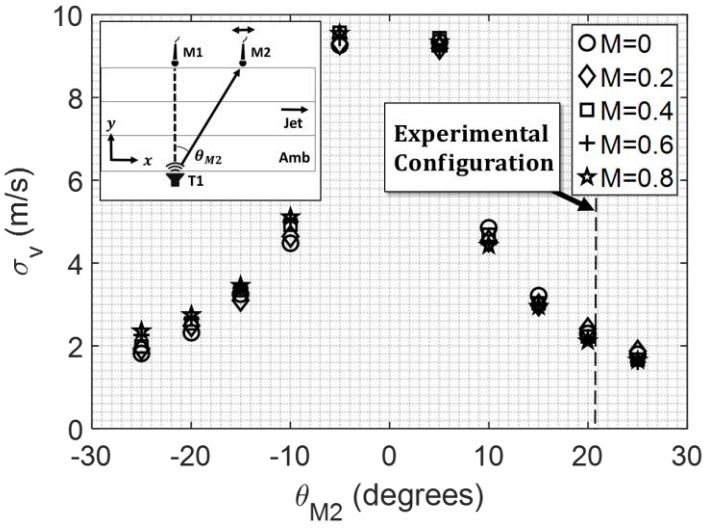

Figure 3.13. *Effect of microphone 2 placement on the MSA technique's ability to determine flow velocity in a non-uniform flow configuration with a 50.8 mm jet.*

From the data points shown in Figure 3.10, it is evident that velocity standard deviation diverges as the second microphone approaches the stream-wise position of the first microphone. Another important observation is the fact that the σ_v does not significantly change with Mach number. The relatively small sensitivity to Mach number can be observed when TOF difference is plotted against microphone 2 angle:

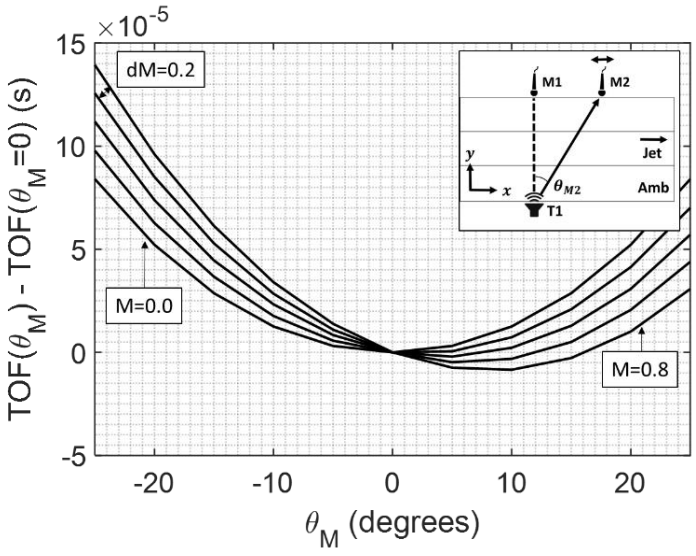

Figure 3.14. *Effect of microphone 2 angle on difference in TOF between the two acoustic paths.*

Notably, the spacing between each Mach line at a given angle is approximately the same, or:

$$\left(\frac{\partial(\delta\tau)}{\partial(M)}\right)_{\theta} \cong Constant$$

From the Mach uncertainty equation, which is analogous to the velocity uncertainty equation,

$$u_M = \sqrt{\left(\frac{\partial(M)}{\partial(\delta\tau)} u_{\delta\tau}\right)^2}$$

it is evident that the uncertainty in Mach (and consequently velocity) should be constant for a constant $u_{\delta\tau}$ (2.5e-7 s).

For the current experiment, the microphone 2 position corresponds with an angle of 20°. Since it has been shown that the measurement error does not strongly depend on Mach number, the velocity measurement standard deviation is expected to be approximately 2.21 m/s. Using a 95% confidence interval, the measurement results are expected to be within $\pm$4.42 m/s of the true value.

5. Results & Discussion

Using the experimental setup and procedures outlined in Section 3, MSA measurements were collected for 9 Mach number cases. The first step was to identify the TOF for each acoustic path:

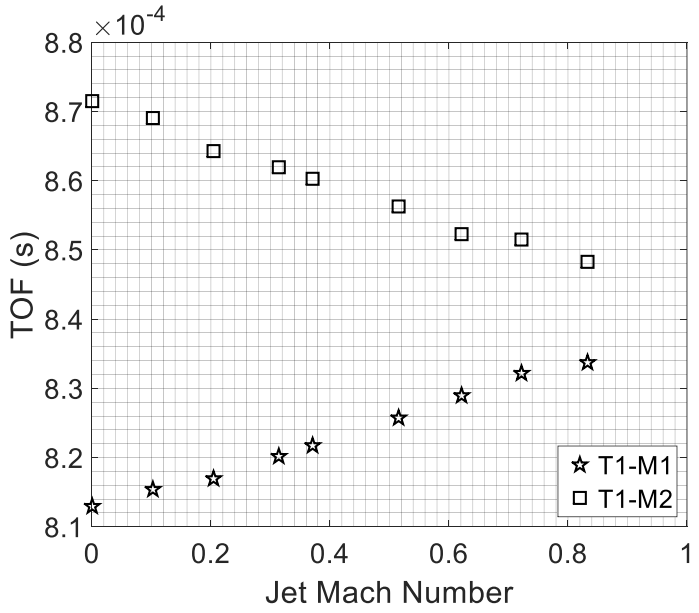

Figure 3.15. *Mach number effect on TOF for the non-uniform flow configuration. The star markers indicate the TOF measurements between the transmitter and microphone 1, and the square markers indicate the TOF measurements between the transmitter and microphone 2 (see Figure 3.6).*

Cross-correlation of the acoustic measurements resulted in the TOF values presented in Figure 3.12. As expected, the TOF between the transmitter and microphone 1 increased as jet Mach number goes up because the convective medium reduces the denominator of equation (1) ($\boldsymbol{v} \cdot \hat{\boldsymbol{n}} < 0$). Conversely, the TOF between the transmitter and microphone 2 decreases with increasing Mach number because the flow "pushes" the acoustic (ray) towards microphone 2 and the equation (1) denominator increases ($\boldsymbol{v} \cdot \hat{\boldsymbol{n}} > 0$).

The key validation results of the current study are provided in Figure 3.13 below. The standard for comparison was a measurement of plenum conditions, which were used to obtain

expected velocity values assuming isentropic expansion to atmospheric pressure. Additionally, the velocity uncertainty, obtained in Section 4 (4.42 m/s), is reported as an error bar for each Mach number case.

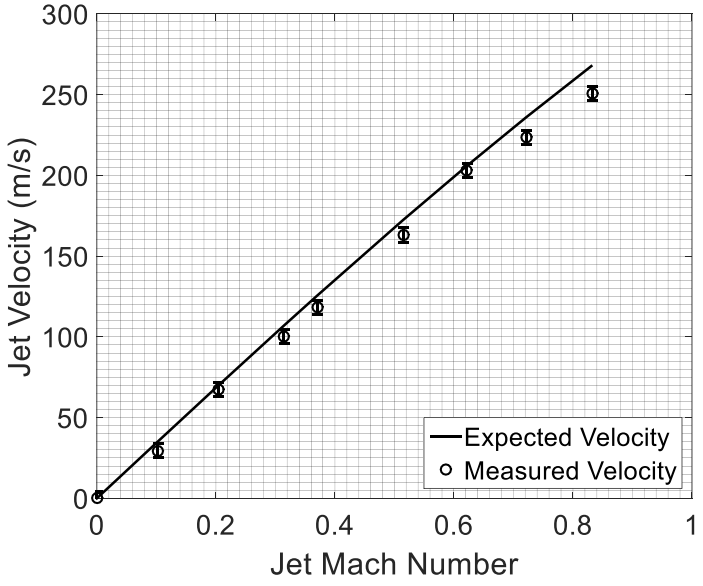

Figure 3.16. *MSA jet velocity measurements compared with the expected values at various Mach numbers. The MSA measured velocity shows a negative bias when compared with the expected (intrusive measurement) results.*

For most Mach numbers measured, the expected velocities fell close to the predicted error range. Notably, higher deviation from the nominal values can be seen at higher Mach numbers. The generally negative bias in the MSA measurements and pronounced difference at high subsonic Mach numbers is believed to be associated with a systematic error in the component placement measurements. An RMS error of 8.79 m/s was found across the measurement span.

6. Conclusions

A modified sonic anemometry technique was introduced and test results for jet flow conditions up to Mach 0.83 were presented. The experimental results support the use of acoustics for high subsonic flow characterization provided SNR is adequately strong. To the authors' knowledge, this is the first time SA has been used to characterize flow velocity beyond Mach 0.3.

Using the classical acoustic ray propagation equation, the proposed MSA technique provides additional design flexibility which can be used to mitigate the effects of critical angle reflection. Two fundamental configurations (uniform and non-uniform flow) were briefly described and the solution approach for each case was outlined. The focus of this paper has been primarily on the measurement of flow velocity in a non-uniform medium (jet) configuration with known ambient conditions (Case 2 in Section 2).

For the non-uniform jet configuration, the flow velocity had to be determined numerically. Using the procedure outlined in Section 2, measured velocities showed an RMS error of 8.79 m/s when compared with intrusive measurements. To better assess the sensitivity of the proposed MSA technique, Monte Carlo simulations were used to first determine the effect of SNR on TOF estimation. Using the results of this numerical study, the effect of microphone placement on velocity measurement error was also explored. For the configuration used in this experiment, the analysis showed that random error was expected to be within $\pm$4.42 m/s using a 95% confidence interval. Later comparison of intrusive and non-intrusive measurements indicated a negative bias in the MSA measured velocities. This type of error was attributed to component placement uncertainties. In the future, this type of error will be minimized through more accurate component placement measurements.

Acknowledgments.

The authors are grateful for the support from Rolls Royce and the Commonwealth of Virginia, and would like to give a special thanks to Dr. Srinath Ekkad, Dr. Lin Ma, and MS student Chuyoung Kim, for their contributions to this work.

References

[1] Lighthill, M. J. (1963). Jet noise. AIAA Journal, 1(7), 1507-1517.

[2] Schlinker, R. H., & Amiet, R. K. (1980). Refraction and scattering of sound by a shear layer (Vol. 3371). National Aeronautics and Space Administration, Scientific and Technical Information Branch.

[3] Ostashev, V. E., & Wilson, D. K. (2015). Acoustics in moving inhomogeneous media. CRC Press.

[4] Voulgaris, G., & Trowbridge, J. H. (1998). Evaluation of the Acoustic Doppler Velocimeter (ADV) for Turbulence Measurements. Journal of Atmospheric and Oceanic Technology, 15(1), 272-289.

[5] Kiminki, S. (2005). Sound propagation theory for linear ray acoustic modelling (Doctoral dissertation, Master's thesis, Helsinki University of Technology).

[6] Jovanovic, I., Sbaiz, L., & Vetterli, M. (2006, May). Acoustic tomography method for measuring temperature and wind velocity. In *2006 IEEE International Conference on Acoustics Speech and Signal Processing Proceedings* (Vol. 4, pp. IV-IV). IEEE.

[7] Fox, M. D., & Gardiner, W. M. (1988). Three-dimensional Doppler velocimetry of flow jets. Biomedical Engineering, IEEE Transactions on, 35(10), 834-841.

[8] Cuerva, A., & Sanz-Andrés, A. (2000). On sonic anemometer measurement theory. Journal of Wind Engineering and Industrial Aerodynamics, 88(1), 25-55.

[9] Wyngaard, J. C. (1981). Cup, propeller, vane, and sonic anemometers in turbulence research. Annual Review of Fluid Mechanics, 13(1), 399-423.

[10] Rehmel, M. (2007). Application of acoustic Doppler velocimeters for streamflow measurements. Journal of Hydraulic Engineering, 133(12), 1433-1438.

[11] Kraus, N. C., Lohrmann, A., & Cabrera, R. (1994). New acoustic meter for measuring 3D laboratory flows. Journal of Hydraulic Engineering, 120(3), 406-412.

[12] Cuerva, A., & Sanz-Andrés, A. (2003). Sonic anemometry of planetary atmospheres. Journal of Geophysical Research: Planets (1991–2012),108(E4).

[13] Banfield, D., & Dissly, R. (2005, March). A Martian sonic anemometer. In Aerospace Conference, 2005 IEEE (pp. 641-647). IEEE.

[14] Wang, S., Yernaux, M., & Deltour, J. (1999). A networked two-dimensional sonic anemometer system for the measurement of air velocity in greenhouses. Journal of Agricultural Engineering Research, 73(2), 189-197.

[15] Sozzi, R., & Favaron, M. (1996). Sonic anemometry and thermometry: theoretical basis and data-processing software. Environmental Software, 11(4), 259-270.

[16] McKeon, B., Comte-Bellot, G., Foss, J., Westerweel, J., Scarano, F., Tropea, C., ... & Cuerva, A. (2007). Velocity, vorticity, and Mach number. In Springer Handbook of Experimental Fluid Mechanics (pp. 215-471). Springer Berlin Heidelberg.

[17] Kato, N., Ohkuma, T., Kim, J. R., Marukawa, H., & Niihori, Y. (1992). Full scale measurements of wind velocity in two urban areas using an ultrasonic anemometer. Journal of Wind Engineering and Industrial Aerodynamics, 41(1), 67-78.

[18] Mylvaganam, K. S. (1989). High-rangeability ultrasonic gas flowmeter for monitoring flare gas. Ultrasonics, Ferroelectrics, and Frequency Control, IEEE Transactions on, 36(2), 144-149.

[19] Tack, D. H., & Lambert, R. F. (1965). Influence of shear flow on sound attenuation in a lined duct. The Journal of the Acoustical Society of America, 38(4), 655-666.

[20] Ingard, U., & Singhal, V. K. (1973). Upstream and downstream sound radiation into a moving fluid. The Journal of the Acoustical Society of America, 54(5), 1343-1346.

[21] Ostashev, V. E., Hohenwarter, D., Attenborough, K., Blanc-Benon, P., Juvé, D., & Goedecke, G. H. (2001). On the refraction law for a sound ray in a moving medium. Acta Acustica united with Acustica, 87(3), 303-306.

[22] Brooks, D. R., Ecker, T., Lowe, K. T., & Ng, W. F. (2014). Experimental Reynolds stress spectra in hot supersonic round jets. In AIAA SciTech (52nd Aerospace sciences meeting).

[23] Lau, J. C., Morris, P. J., & Fisher, M. J. (1979). Measurements in subsonic and supersonic free jets using a laser velocimeter. Journal of Fluid Mechanics, 93(01), 1-27.

[24]Bendat, J. S., & Piersol, A. G. (2011). Random data: analysis and measurement procedures (Vol. 729). John Wiley & Sons.

[25] Omologo, M., & Svaizer, P. (1994, April). Acoustic event localization using a crosspower-spectrum phase based technique. In Acoustics, Speech, and Signal Processing, 1994. ICASSP-94., 1994 IEEE International Conference on (Vol. 2, pp. II-273). IEEE.

[26] Knapp, C. H., & Carter, G. C. (1976). The generalized correlation method for estimation of time delay. IEEE Transactions on Acoustics, Speech and Signal Processing, 24(4), 320-327.

Appendix A: Modified Sonic Anemometry Technique Derivation

Using trigonometry, flow velocity can be determined using two acoustic path measurements. Like the existing technique, the measurement of velocity is a function of time delays and distances, but the SNR of the measurement can be significantly improved through microphone placement flexibility.

Consider the configuration shown in Figure A.1 below.

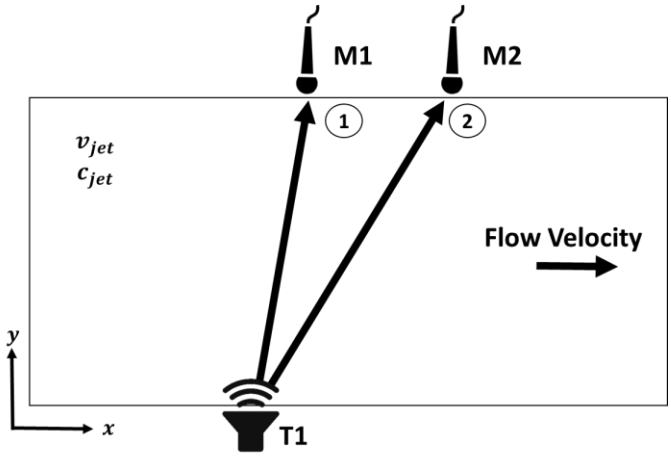

Figure A.1. *Example modified sonic anemometry technique measurement configuration*

In order to conduct the sonic anemometry measurement, three devices are used. A transmitter, which is placed on one side of the flow, and two microphones, which are placed on the other side of the flow. The two microphones are located at the same y position and displaced in the *x*-direction (streamwise direction). An acoustic signal is emitted from the transmitter and picked up at the two microphone locations. Using the measured acoustic propagation time delay for each acoustic path, along with the measured distances between the equipment, it is possible to determine the average flow velocity as shown below.

Consider the first acoustic path:

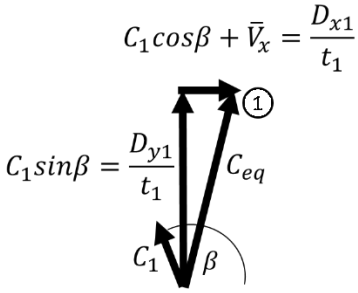

Figure A.2. *Vector diagram of first acoustic path measurement*

Using a well-known trigonometric identity, the x and y components can be combined to create an equation for speed of sound C_1:

$$C_1 * \cos(\beta) + \bar{V}_x = \frac{D_{x1}}{t_1} \quad \text{(A1)}$$

$$C_1 * \sin(\beta) = \frac{D_{y1}}{t_1} \quad \text{(A2)}$$

$$1 = \cos^2 \beta + \sin^2 \beta \quad \text{(A3)}$$

$$\cos(\beta) = \frac{\left(\frac{D_{x1}}{t_1} - \bar{V}_x\right)}{C_1} \quad \text{(A4)}$$

$$\sin(\beta) = \frac{\left(\frac{D_{y1}}{t_1}\right)}{C_1} \quad \text{(A5)}$$

$$1 = \left(\frac{\left(\frac{D_{x1}}{t_1} - \bar{V}_x\right)}{C_1}\right)^2 + \left(\frac{\left(\frac{D_{y1}}{t_1}\right)}{C_1}\right)^2 \quad \text{(A6)}$$

$$C_1^2 = \left(\frac{D_{x1}}{t_1} - \bar{V}_x\right)^2 + \left(\frac{D_{y1}}{t_1}\right)^2 \quad \text{(A7)}$$

Next, consider the second acoustic path

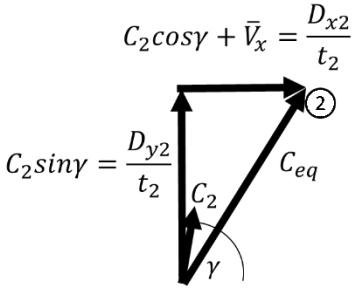

Figure A.3. *Vector diagram of the second acoustic path measurement.*

Using the same manipulation described for path one:

$$C_2 * \cos(\gamma) + \bar{V}_x = \frac{D_{x2}}{t_2} \tag{A8}$$

$$C_2 * \sin(\gamma) = \frac{D_{y2}}{t_2} \tag{A9}$$

$$1 = \cos^2\gamma + \sin^2\gamma \tag{A10}$$

$$\cos(\gamma) = \frac{\left(\frac{D_{x2}}{t_2} - \bar{V}_x\right)}{C_2} \tag{A11}$$

$$\sin(\gamma) = \frac{\left(\frac{D_{y2}}{t_2}\right)}{C_2} \tag{A12}$$

$$1 = \left(\frac{\left(\frac{D_{x2}}{t_2} - \bar{V}_x\right)}{C_2}\right)^2 + \left(\frac{\left(\frac{D_{y2}}{t_2}\right)}{C_2}\right)^2 \tag{A13}$$

$$C_2^2 = \left(\frac{D_{x2}}{t_2} - \bar{V}_x\right)^2 + \left(\frac{D_{y2}}{t_2}\right)^2 \tag{A14}$$

Finally, the equations are combined by assuming that $C_1 \cong C_2$, and $\bar{V}_x$ can be determined:

$$\left(\frac{D_{x1}}{t_1} - \bar{V}_x\right)^2 + \left(\frac{D_{y1}}{t_1}\right)^2 = \left(\frac{D_{x2}}{t_2} - \bar{V}_x\right)^2 + \left(\frac{D_{y2}}{t_2}\right)^2 \tag{A15}$$

$$\left(\frac{D_{x1}}{t_1}\right)^2 - \frac{2\bar{V}_x D_{x1}}{t_1} + \bar{V}_x^2 + \left(\frac{D_{y1}}{t_1}\right)^2 = \left(\frac{D_{x2}}{t_2}\right)^2 - \frac{2\bar{V}_x D_{x2}}{t_2} + \bar{V}_x^2 + \left(\frac{D_{y2}}{t_2}\right)^2 \quad \text{(A16)}$$

$$\bar{V}_x = \frac{\left(\left(\frac{D_{x2}}{t_2}\right)^2 + \left(\frac{D_{y2}}{t_2}\right)^2 - \left(\frac{D_{x1}}{t_1}\right)^2 - \left(\frac{D_{y1}}{t_1}\right)^2\right)}{\left(\frac{2D_{x2}}{t_2} - \frac{2D_{x1}}{t_1}\right)} \quad \text{(A17)}$$

Appendix B: Acoustic Time-of-Flight Estimation Monte Carlo Simulation

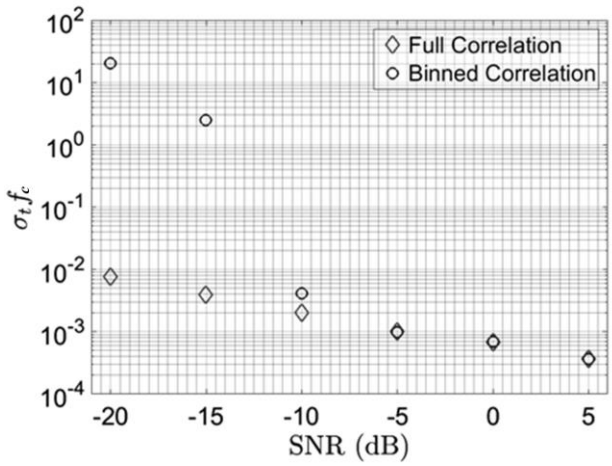

Figure B.1. *Cross correlation estimator TOF variance. "Full Correlation" refers to the correlation of the entire 1-second signal, while "Binned Correlation" correlates individual measurement sets and compiles them to find an ensemble average.*

In order to perform the Monte Carlo simulation, 100 one second signals where simulated for a transmitter and microphone pair. Each one second signal contained 30 bursts of a 40 kHz waveform modulated for two modulation cycles at 4 kHz that lasted 0.5 milliseconds. Gaussian white noise was added to the signal to obtain desired values of signal-to-noise ratio. All steps of the signal conditioning and processing, as depicted in Figure 3.6, were applied to the synthetic signals to obtain time delay estimates.

In the first approach, referred to as "Full Correlation" in Figure B.1, the full one second transmitter signal was cross-correlated with the entire one second microphone signal. After the time delay estimate was obtained, the process was repeated for the remaining 99 signal pairs. Using 100 time delay samples, the standard deviation of the samples was determined and specified for the set SNR value.

In the second approach, referred to as "Binned Correlation" in Figure B.1, the one second signal pairs were first divided into 30 different time bins, each containing an acoustic burst measurement. Each sound transmitter bin was then cross correlated with its corresponding

microphone bin to find 30 time delay estimates for the one second signals. The 30 time delays from binned signals were averaged, and one time delay estimate was found for a one second signal pair. The process was repeated for the remaining 99 signal pairs, and the standard deviation was determined for the set SNR value.

While binning and full signal cross correlation provided similar results above an SNR of -5 dB, high noise (SNR < -5dB) causes errors in some of the binned time delay estimates, resulting in a higher variation in the overall time delay estimation. From Figure B.1, it is evident that the full signal cross-correlation approach is more practical in a high noise environment due to its lower standard deviation, and linear logarithmic error behavior in low SNR conditions.

Part IV. Heated Laboratory Jet Experiment

Preface

The text presented in Part IV was recently recommended for publication in the Measurement Science and Technology journal by referees pending minor revisions. Note that the appendices referred to in the text are included at the end of the manuscript, not the end of this dissertation.

The major takeaways of this manuscript are:

- SAT technique can be used to measure single-stream temperatures in compressible flows
- Compressible flow acoustic tomography is required for improved measurement accuracy

Non-Intrusive Acoustic Measurement of Flow Velocity and Temperature in a High Subsonic Mach Number Jet

R Otero Jr[1], K T Lowe[2] and W F Ng[3]

[1]Graduate Research Assistant, Department of Mechanical Engineering,
Virginia Tech, Blacksburg, VA, USA,

[2]Associate Professor, Department of Aerospace and Ocean Engineering,
Virginia Tech, Blacksburg, VA, USA.

[3]Chris C. Kraft Endowed Professor, Department of Mechanical Engineering,
Virginia Tech, Blacksburg, VA, USA.

E-mail: raul1991@vt.edu

Abstract. In previous studies, sonic anemometry and thermometry have generally been used to measure low subsonic Mach flow conditions. Recently, a novel configuration was proposed and used to measure unheated jet velocities up to Mach 0.83 non-intrusively. The objective of this investigation is to test the novel configuration in higher temperature conditions and explore the effects of fluid temperature on mean velocity and temperature measurement accuracy. The current work presents non-intrusive acoustic measurements of single-stream jet conditions up to Mach 0.7 and total temperatures from 299 K to 700 K. Comparison of acoustically measured velocity and static temperature with probe data indicate root mean square (RMS) velocity errors of 2.6 m/s (1.1% of the maximum jet centerline velocity), 4.0 m/s (1.2%), and 8.5 m/s (2.4%), respectively, for 299, 589, and 700 K total temperature flows up to Mach 0.7. RMS static temperature errors of 7.5 K (2.5% of total temperature), 8.1 K (1.3%), and 23.3 K (3.3%) were observed for the same respective total temperature conditions. To the authors' knowledge, this is the first time a non-intrusive acoustic technique has been used to simultaneously measure mean fluid velocity and static temperatures in high subsonic Mach numbers up to 0.7. Overall, the findings of this work support the use of acoustics for non-intrusive flow monitoring. The ability to measure mean flow conditions at high subsonic Mach numbers and temperatures makes this technique a viable candidate for gas turbine applications, in particular.

Keywords: Sonic Anemometry (SA), Sonic Thermometry (ST), Compressible Flows, Acoustic Temperature Measurement, Acoustic Velocity Measurement, Non-Intrusive Flow Measurement, Time of Flight Techniques

Nomenclature

c	Thermodynamic speed of sound
c_{amb}	Thermodynamic speed of sound in an ambient medium
c_{jet}	Thermodynamic speed of sound in a jet medium
D_{jet}	Jet diameter
D_x	Stream-wise displacement between microphones
D_y	Distance between transmitter and microphones in direction perpendicular to flow
FFT	Fast Fourier Transform
K	Mach number uncertainty constant (function of relative equipment displacements)
L	Distance between sound transmitter and microphone
M	Mach number
M_{ref}	Reference microphone
M_1	Microphone 1
M_2	Microphone 2
MSA	Modified sonic anemometry
MW	Molecular Weight
$\hat{\boldsymbol{n}}$	Unit vector normal to the acoustic wave front
P_s	Static pressure
$\bar{R}$	Universal ideal gas constant
RMS	Root mean square
SA	Sonic anemometry
SAT	Sonic anemometry and thermometry
ST	Sonic thermometry
$T1$	Transmitter 1
$T2$	Transmitter 2
TOF	Acoustic propagation time of flight

T_o	Total temperature
T_s	Static temperature
$T_{s,jet}$	Jet static temperature
$\boldsymbol{t_n}$	Unit vector tangent to nth ray path
u_c	Uncertainty in thermodynamic speed of sound measurements
u_{T_s}	Uncertainty in static temperature measurements
u_τ	Uncertainty in time of flight measurements
$\boldsymbol{v}$	Flow velocity
v_{amb}	Flow velocity in an ambient medium
v_{jet}	Flow velocity in a jet medium
v_{max}	Maximum jet velocity at a specific total temperature setting
γ	Specific heat ratio
ϵ_v	Root mean square error in velocity
ϵ_{T_s}	Root mean square error in static temperature
τ_n	Acoustic propagation time of flight of nth path
τ_d	Acoustic propagation time of flight in downstream direction
τ_u	Acoustic propagation time of flight in upstream direction
$\sum\tau$	Sum of acoustic propagation time of flight in upstream and downstream direction

1. Introduction

In recent years, the use of acoustic measurements for non-intrusive gas turbine engine flow monitoring has been proposed and several studies have been conducted to assess its feasibility in practical applications [1–5]. An acoustic approach is of particular interest because it offers several unique advantages over optical methods (such as particle image velocimetry) in gas turbine engine environments. Among these advantages are the ability to simultaneously measure flow velocity and temperature, operate without seeding the flow, avoid equipment fouling due to engine soot, and operate effectively in a high vibration environment.

In 2013, Siemens presented a comparison between intrusive (probe) and non-intrusive (acoustic) flow temperature measurements at the exhaust of a ground-based gas turbine engine [2]. Using tomographic reconstruction, researchers were able to use multiple microphones and sound

sources, spread azimuthally around the exhaust of the engine, to measure temperature non-uniformities. Reported results showed that acoustically measured gas turbine exhaust temperatures were within 10 $°C$ of thermocouple data. Siemens conducted a similar study in 2015, this time using improved sound source design for better time-of-flight estimation, and reported 0.36% bulk mean temperature error in temperatures up to 600 °C [3]. In both experiments, the impact of flow velocity on the measurements was not addressed in detail. The first article mentions that the assumption of sound traveling in a straight line is a "good starting point for reconstruction of temperature maps" [2], while the second article specifies that velocity was measured "by other means" and used to correct the temperature values [3]. While the negligible velocity effects may be justified at low Mach numbers, the inability to properly account for acoustic refraction, convection, and increased fluid compressibility at higher Mach numbers would result in significant errors if flow velocity is not considered.

To overcome this challenge, a similar technique known as sonic anemometry (SA) could be coupled with sonic thermometry (ST) to non-intrusively measure mean jet flow velocity and temperature simultaneously [6–9]. The issue with classical combined sonic anemometry and thermometry (SAT) is that it has only been proven in low Mach number (M<0.3) applications due to insufficient SNR, curvilinear acoustic ray propagation, and a limited range of practical applications. To overcome these difficulties, the current work uses a novel approach outlined by Otero et al. [9] to measure temporally averaged compressible jet flow velocities and temperatures. The primary objective of this study is to verify that Otero et al.'s [9] acoustic technique can be used in high temperature flows while investigating the effects of fluid temperature on temporally averaged velocity and static temperature measurement accuracy. Overall, this work serves as an incremental step towards the development of a health monitoring system for gas turbine engines.

2. Principles of Combined Sonic Anemometry and Thermometry (SAT)

Before describing the high subsonic Mach number SAT approach, it is useful to first consider the classical SAT method. Figure 4.1 presents a sample configuration of acoustic sound sources and microphones that could be used to simultaneously measure mean fluid velocity and temperature. The acoustic equipment is characteristically arranged to measure upstream and downstream acoustic propagation times.

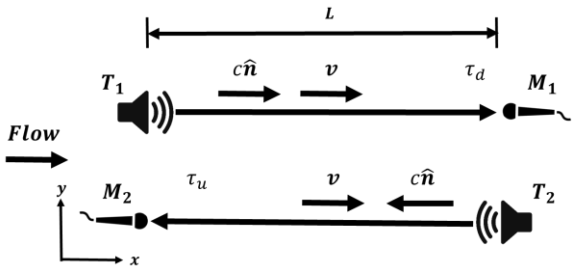

Figure 4.1. *Modified from [9]. Example configuration used for classical sonic Anemometry and thermometry.*

The acoustic wave is expected to travel faster in the downstream direction than the upstream direction due to medium convection. The propagation time along each trajectory exhibits a sensitivity to the flow direction and group velocity ($c\hat{\boldsymbol{n}} + \boldsymbol{v}$) as expressed in equations (1) and (2) [10,11].

$$\tau_d = \int_0^L \frac{ds}{(c\hat{\boldsymbol{n}} + \boldsymbol{v}) \cdot \mathbf{t_1}} = \frac{L}{c + v} \tag{1}$$

$$\tau_u = \int_0^L \frac{ds}{(c\hat{\boldsymbol{n}} + \boldsymbol{v}) \cdot \mathbf{t_2}} = \frac{L}{c - v} \tag{2}$$

Assuming that the fluid velocity and thermodynamic speed of sound ($c = \sqrt{\gamma \bar{R} T_s / MW}$) remain constant along both acoustic paths, and the mean flow direction is known, equations (1) and (2) can be rearranged to obtain equations (3) and (4) below [6,8,9]:

$$v = \frac{L}{2}\left(\frac{1}{\tau_d} - \frac{1}{\tau_u}\right) \tag{3}$$

$$c = \frac{L}{\tau_u} + v = \frac{L}{\tau_d} - v \tag{4}$$

Supposing that the fluid is air that behaves as an ideal gas, its molecular weight and the empirical relationship between air temperature and specific heat can be used to determine static temperature as shown in equation (5).

$$T_s = \frac{c^2}{\gamma(T_s)\bar{R}/MW} \tag{5}$$

Similar procedures to the one outlined above have been previously used to measure low Mach number (Mach<0.3) fluid properties under atmospheric [12] and wind tunnel [13,14] conditions. Although the setup in Figure 4.1 is oriented for acoustic propagation that is parallel with the fluid velocity vector, modifications can be made to equations (3) and (4) to account for other flow directions. These modified equations also require previous knowledge of the mean flow direction. Generally, the measurement results presented in the literature indicate good agreement between intrusive and non-intrusive measurements at low Mach numbers. In the following section, advancements in high subsonic Mach number acoustic anemometry and thermometry are discussed.

2.1. SAT Measurements in High Subsonic Mach Number Flows

As mentioned in Section 1, various factors such as insufficient SNR and complex curvilinear propagation in the presence of fluid gradients have generally limited SAT applications to low Mach number conditions. Using a novel configuration of acoustic sound source and microphone equipment, a less restrictive method was developed by Otero et al. [9] to simultaneously measure temporally averaged jet flow velocity and static temperature in a high subsonic Mach number jet. To facilitate further discussion of this approach, consider the arrangement of acoustic equipment shown in Figure 4.2.

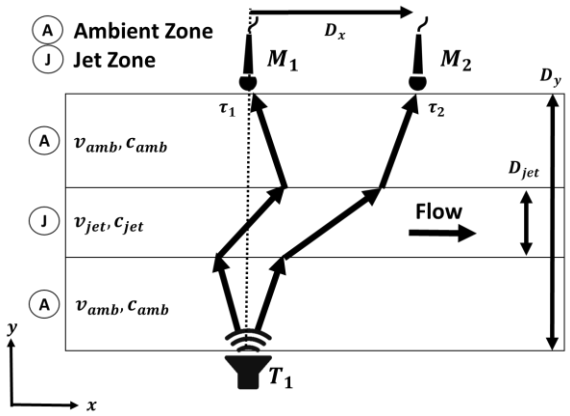

Figure 4.2. *Modified from Otero et al. [9]. Application of MSA in a non-uniform flow medium with known ambient conditions.*

As the acoustic waves travel to each microphone position, medium convection will cause differences in the acoustic time-of-flight (TOF). The difference in TOF along each path is proportional to the Mach number of the moving medium and the direction of the fluid velocity vector. This concept is similar to the classical SAT approach presented at the beginning of Section 2, but sound source and microphone positions are no longer confined to an upstream and downstream position. Like the classical approach, the high subsonic Mach number technique also requires previous knowledge of the mean flow velocity vector direction. While limiting, this approximation is justified in jet applications because the velocity in the stream-wise direction is much greater than the transverse direction. While the canonical approach maximizes TOF difference due to medium convection (and consequently minimizes TOF related uncertainty) by using an upstream and downstream propagation path, the added flexibility in the proposed technique facilitates system design for reduced attenuation, improved SNR, and critical angle reflection avoidance in inhomogeneous flow applications. Figure 5 of Otero et al. [9] highlights the major steps involved in solving for mean flow jet conditions (see Figure C.1 in Appendix C). Once flow velocity and thermodynamic speed of sound are identified, the static temperature is determined using equation (5).

Using the procedure outlined above, Otero et al. performed acoustic measurements in an unheated jet operating at conditions up to Mach 0.83 [9]. Root mean square (RMS) velocity errors of ± 9 m/s in flows up to ~270 m/s were observed, but temperature values were not discussed due to the unheated nature of the jet. In the unheated jet experiment, it is important to note that the

results were a spatial (across the jet diameter) and temporal average of the jet conditions. Since only two stream-wise displaced propagation paths were used, additional information about the medium could not be obtained. Although the two-zone model required for the Figure 4.A1 approach is used in the current work as well, the authors hypothesize that an acoustic tomography method can be developed to avoid this sort of spatial averaging in the future. Such an approach could ultimately be used to monitor temporally averaged flow velocity and temperature gradients, as well as mass flow rates and thrust in a variety of applications (this work serves as an incremental step towards the development of such a system).

Building on the unheated jet work, a proof of concept measurement was conducted on a Pratt and Whitney JT15D bypass turbofan engine to assess the feasibility of applying this technique in a gas turbine engine environment [5]. Due to the non-uniform nature of the two-stream (bypass) gas turbine engine exhaust, an integrated path parameter was used to compare intrusive probe data with the non-intrusive acoustic measurements. Engine conditions were varied between idle and maximum exhaust Mach numbers of 0.48. RMS errors in integrated path velocity (3.8 m/s) and temperature (2.3 K) were reported. Otero et al. [5] also indicated that advancements in acoustic tomography would be necessary to reduce measurement errors and capture shear layer effects.

In the current work, a single stream jet is once again considered to fundamentally investigate sensitivity to fluid temperature. Using the same jet facility described by Otero et al. [9], intrusive and non-intrusive flow velocity and static temperature measurements were collected for a range of Mach numbers and temperatures, and later compared. The following section outlines the experimental setup and procedures used to perform these measurements.

3. Experimental Setup & Procedures

In the current experiment, a similar arrangement to the one described by Otero et al. [9] (with some modifications to improve signal strength) is used to measure temporally and spatially (across jet diameter) averaged jet velocity and temperature. The relative placement of acoustic equipment is described in Figure 4.3.

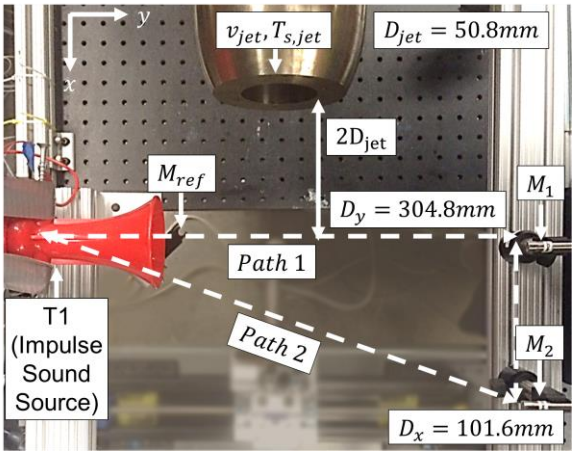

Figure 4.3. *Diagram of experimental setup for MSA measurements.*

Upstream of the jet exhaust plane, a total temperature and total pressure probe was used to monitor facility operating conditions while the acoustic measurements were collected. Previous experiments conducted in this jet facility have shown the upstream measurements to be a good indicator of potential core characteristics. Although a shear layer is present at the $2D_{jet}$ streamwise position, its relatively small size (see Appendix D) justifies the use of a two-zone model as described in Section 2.1. Using the upstream measurements, as well as the known static pressure of the room and compressible flow isentropic equations, the jet static temperature and velocity at the $2D_{jet}$ stream-wise position were approximated.

To carry out this experiment, an electric spark, enclosed in a horn housing, was used to produce impulse sound signals at a rate of 30 Hz ($\pm$3 Hz). The impulse sound signal generated by each spark lasted approximately 0.002 seconds and was measured at three distinct positions (M_{ref}, M_1, M_2) using a 1.25 MS/s data sampling rate. A sample spark signal, as measured by M_{ref}, M_1, and M_2, is shown in Figure 4.4.

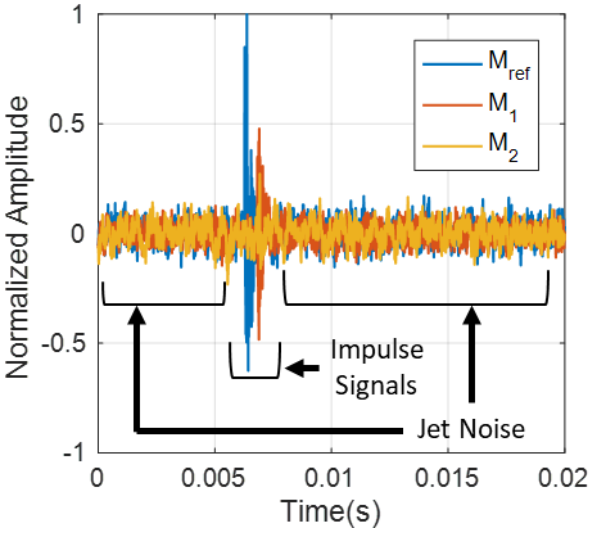

Figure 4.4. *Sample of impulse acoustic signals measured at 3 different locations, normalized by the maximum* M_{ref} *amplitude. Test conditions were* $Mach \cong 0.7,\ T_o = 700\ K,\ P_s = 94.39\ kPa.$

Throughout the experiment, 25 one-second data sets (see Figure 4.5 in Section 3.1 for sample one-second data set) were collected at each facility operating condition described in Table 4.1.

Table 4.1. *Facility operating conditions*

T_o	299 K	589 K	700K
Mach #	0→0.7	0.4→0.7	0.4→0.7
Mach Increment	0.1	0.1	0.1

3.1. Signal Processing

Once the microphone measurements were collected, the acoustic signals were processed to obtain TOF for each acoustic path. First, each one-second data set was mean subtracted to avoid correlation errors. Figure 4.5 shows a sample one-second data set normalized by the maximum amplitude of the reference microphone measurement.

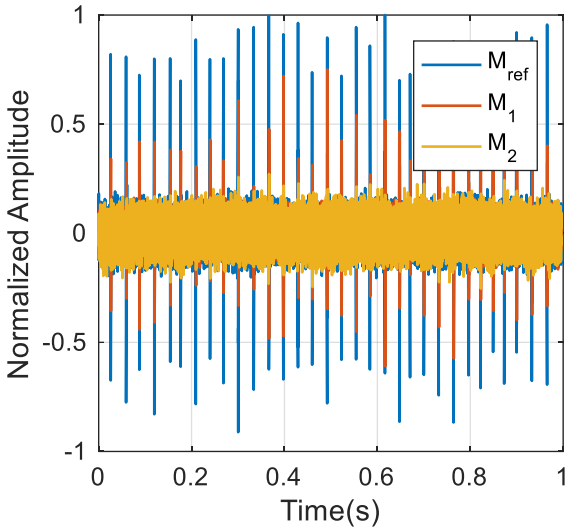

***Figure 4.5**. Sample of mean-subtracted one-second acoustic signal data set at 3 different locations, normalized by the maximum M_{ref} amplitude. Test conditions were $Mach \cong 0.7,\ T_o = 700\ K,\ P_s = 94.39\ kPa$.*

Next, the acoustic signals were filtered using a bandpass FFT filter (1 kHz – 100 kHz) to remove low and high frequency noise. The high-pass frequency of 1kHz was selected to minimize the effects of dominant jet noise on impulse signal cross correlation, while the low-pass frequency was chosen to prevent microphone harmonics from influencing impulse cross correlation accuracy. Once the signals were bandpass filtered, maximum and minimum expected TOF values (obtained using equipment displacements and worst case jet velocities/static temperatures) were used to trim acoustic signals known not to have originated from the impulse sound source. This step was performed to further reduce the impact of jet noise on signal cross correlation when identifying acoustic TOF. An example of the bandpass filtered and trimmed signal is shown in Figure 4.6.

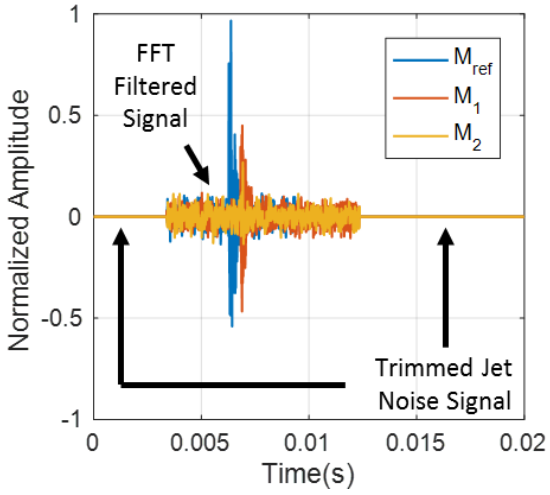

Figure 4.6. *Sample of filtered acoustic data set at 3 different locations, normalized by the maximum* M_{ref} *amplitude. Test conditions were* $Mach \cong 0.7,\ T_o = 700\ K,\ P_s = 94.39\ kPa.$

After filtering, a time correction was applied to the measured acoustic signals to account for the time delay between the emission of the acoustic signal and the arrival at the reference microphone. Finally, each one-second data set was cross correlated and the 25 correlation coefficient sets obtained at a specific test condition were averaged. Figure 4.7 shows the averaged correlation coefficients (normalized by the maximum correlation amplitude of each path) and corresponding time lag. The TOF value for each path (see Figure 4.3 for path definition) corresponds with the time lag that has a maximum correlation coefficient.

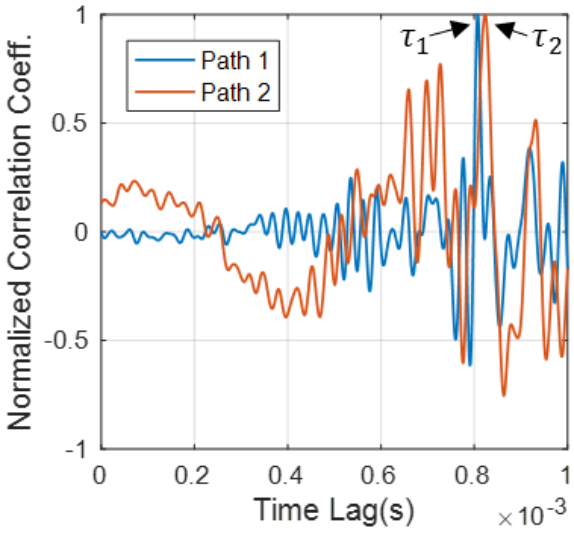

Figure 4.7. *Sample of averaged correlation coefficients for each acoustic path, normalized by the maximum correlation coefficient of the given path. Test conditions were* $Mach \cong 0.7,\ T_o = 700\ K,\ P_s = 94.39\ kPa.$

4. Experimental Results & Discussion

Using the procedure outlined in Section 3.1, TOF values were identified for each jet operating condition and acoustic path. The TOF results are shown in Figure 4.8.

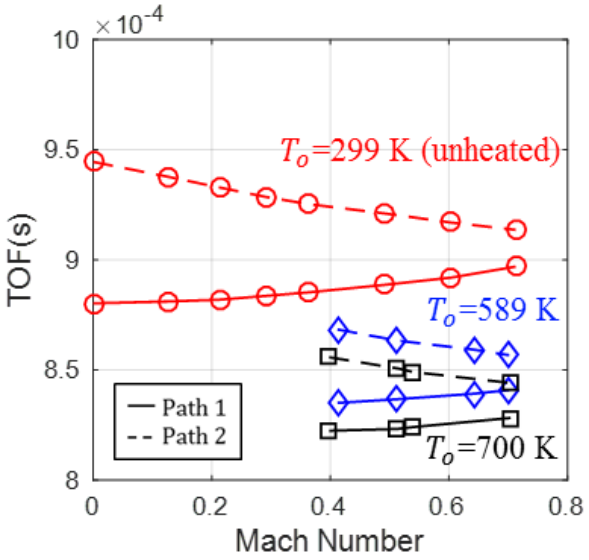

Figure 4.8. *Acoustic TOF measurements in 299 K (unheated), 589 K, and 700 K total temperature flows for various Mach numbers.*

As shown in Figure 4.8, flow speed and temperature have a significant impact on TOF for each acoustic path. Although both parameters influence the sound speed, flow temperature has a more dominant effect on TOF magnitude than velocity, while the velocity largely influences the difference in TOF between the two acoustic paths. It is evident that, as the temperature increases, the magnitude of the TOF drops. The relative difference in TOF between paths 1 and 2, however, does not change significantly for different temperatures at the same Mach number. Conversely, as the Mach number rises, the relative difference in TOF decreases for a set temperature. Although the rate of increase or decrease of TOF difference is also dependent on microphone placement, flow velocity can be determined when microphone and sound source displacements are known. Using this information, temporally averaged fluid velocity and static temperature values were determined using the algorithm in Figure 4.A1.

4.1. Velocity and Temperature Results

Using the measured TOF values, jet width (jet exit diameter), and known distances between the sound source and the microphones, the procedure outlined in Section 2.1 was used to determine the velocity and thermodynamic speed of sound of the jet. Using equation (5), the jet static temperature was then determined. A comparison of the acoustically measured fluid properties with

upstream probe measured values is presented in Figure 4.9. The RMS errors in jet velocity and static temperature are shown in Table 4.2 (for the derivation of temperature and speed of sound uncertainty equations, see Appendix E).

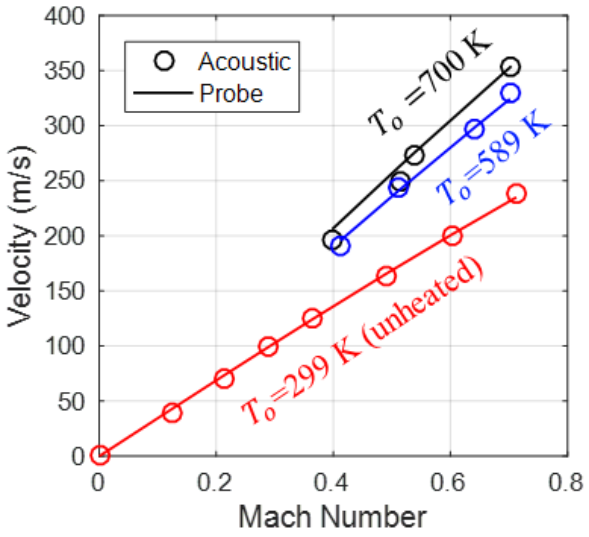

(a)

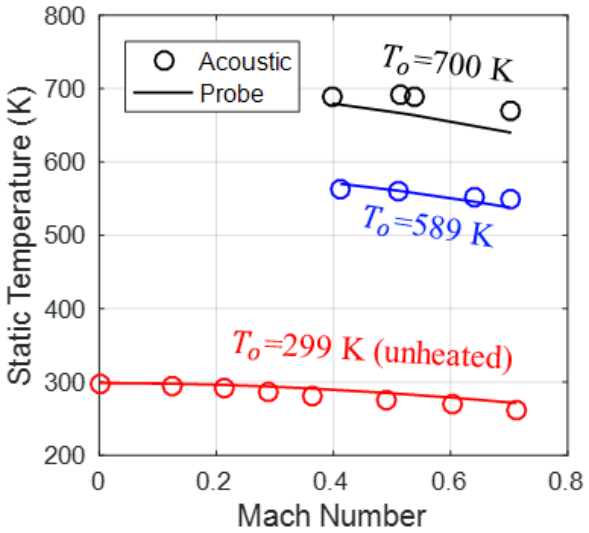

(b)

Figure 4.9. *Comparison of acoustic and probe measured jet (a) velocity and (b) static temperature in 299 K (unheated), 589 K, and 700 K total temperature flows for various Mach numbers.*

Table 4.2. *Acoustic measurement RMS error in jet velocity and static temperature at 299 K (unheated), 589 K, and 700 K total temperature flows.*

T_o	ϵ_v	$\frac{\epsilon_v}{v_{max}}$	ϵ_{T_s}	$\frac{\epsilon_{T_s}}{T_o}$
299 K	2.6 m/s	1.1%	7.5 K	2.5%
589 K	4.0 m/s	1.2%	8.1 K	1.3%
700 K	8.5 m/s	2.4%	23.3 K	3.3%

The acoustic results shown in Figure 4.9 appear to follow similar trends when compared to the upstream probe measured parameters. Notably, Table 4.2 shows a growth in both velocity and static temperature RMS error with increasing jet total temperature. Although a trend in velocity errors is not immediately evident in Figure 4.9a, an interesting behavior can be observed in Figures 5.9b. In the unheated case, the acoustic technique appears to underestimate the temperature values while the higher temperature cases appear to overestimate them. These errors are believed to be an outcome of the two-zone assumption required to solve the non-uniform flow problem (see Figure 4.2 for ambient and jet zone definitions).

In Otero et al.'s algorithm (see Figure 4.A1), the solver assumes that there is an "ambient" and a "jet" zone. Due to fluid entrainment and heat dissipation, the two-zone approximation is expected to cause some measurement error. Since ambient convection velocity and temperature serve as inputs to the algorithm, it is plausible that the ambient temperature inputs to the model slightly differed from the true ambient zone average values. For the unheated case, the jet may have cooled the air surrounding the jet, causing an overestimation of the ambient temperature. By over-estimating the ambient temperature, the algorithm would compensate by outputting a lower jet temperature. In the 589 and 700 K cases, an underestimated ambient temperature may have caused higher acoustic temperature outputs. In future experiments, tomography will be used to non-intrusively and simultaneously measure the ambient and jet conditions in order to significantly reduce the errors associated with the two-zone model.

5. Conclusion

The work presented extends the concepts for the modified sonic anemometry technique reported by Otero et al. [5,9] into simultaneous mean velocity and temperature measurements.

Using a similar sound source and microphone configuration, the MSA technique [9] was used to measure single stream jet velocities and static temperatures. Jet conditions were varied between room temperature and 700 K, and Mach numbers were tested up to Mach 0.7. Upstream total pressure and total temperature measurements in the plenum were used to assess the acoustic measurement accuracy. Observed velocity RMS and percentage (percent of maximum jet centerline velocity) errors for the 299, 589, and 700 K total temperature measurements were 2.6 m/s (1.1%), 4.0 m/s (1.2%), and 8.5 m/s (2.4%), respectively. Static temperature RMS and percentage (percent of total temperature) errors were 7.5 K (2.5%), 8.1 K (1.3%), and 23.3 K (3.3%), respectively. In addition to the observed measurement errors, an interesting behavior was denoted in Figure 4.8. Generally, it was observed that the difference in TOF between the two stream-wise displaced acoustic paths is more sensitive to jet Mach number than fluid temperature.

Overall, the findings of the current work support the use of acoustics for non-intrusive mean flow velocity and temperature measurements in high subsonic Mach number flows. Although jet conditions were only varied up to Mach 0.7 and 700 K, the authors believe that higher Mach numbers and temperatures could also be resolved due to the systematic nature of the observed static temperature errors with increasing Mach number and Otero et al.'s [9] previous implementation in Mach 0.83 unheated flows. In order to resolve these higher test conditions, additional research is necessary to resolve the shear layer behavior and improve measurement accuracy. Generally, the errors observed in this experiment were largely attributed to the two-zone assumption required by the Figure 4.A1 algorithm. Since much of the error is thought to have been caused by fluid entrainment and heat dissipation, future error reduction will likely require resolution of fluid non-uniformities via acoustic tomography.

Acknowledgments

The authors are grateful for the support of Rolls Royce and would like to give a special thanks to Dr. Srinath Ekkad, Dr. Lin Ma, and Mr. Chuyoung Kim, for their support of this work.

References

[1] Kleppe J, Sanchez J and Fralick G 1998 The Application of Acoustic Pyrometry to Gas

Turbines and Jet Engines *34th AIAA/ASME/SAE/ASEE Joint Propulsion Conference and Exhibit* (Cleveland: AIAA) pp 1–10

[2] DeSilva U, Bunce R H and Claussen H 2013 Novel Gas Turbine Exhaust Temperature Measurement System *Proceedings of ASME Turbo Expo 2013* (San Antonio: ASME) pp 1–8

[3] DeSilva U, Bunce R H, Schmitt J M and Claussen H 2015 Gas Turbine Exhaust Temperature Measurement Approach Using Time-Frequency Controlled Sources *Proceedings of ASME Turbo Expo 2015* (Montreal: ASME) pp 1–7

[4] Wassmer D, Schuermans B, Paschereit C O and Moeck J P 2016 An Acoustic Time-of-Flight Approach for Unsteady Temperature Measurements: Characterization of Entropy Waves in a Model Gas Turbine Combustor *Proceedings of ASME Turbo Expo 2016: Turbine Technical Conference and Exposition* vol 139(Seoul: ASME)pp 1–11

[5] Otero R, Lowe K T, Ng W F, Ma L and Kim C-Y 2016 Non-Intrusive Gas Turbine Engine Exhaust Characterization using Acoustic Measurements *32nd AIAA Aerodynamic Measurement Technology and Ground Testing Conference* (Washington D.C.: AIAA) pp 2016–4160

[6] Sozzi R and Favaron M 1996 Sonic anemometry and thermometry: Theoretical basis and data-processing software *Environ. Softw.* **11** 259–70

[7] Kaimal J C and Gaynor J E 1991 Another look at sonic thermometry *Boundary-Layer Meteorol.* **56** 401–10

[8] McKeon B 2007 Velocity, Vorticity, and Mach Number *Springer Handbook of Experimental Fluid Mechanics* (Springer Science+Business Media) pp 215–471

[9] Otero Jr. R, Lowe K T and Ng W F 2017 Extension of sonic anemometry to high subsonic mach number flows *Meas. Sci. Technol* **28** 1–12

[10] Kiminki S 2005 *Sound Propagation Theory for Linear Ray Acoustic Modelling* (Helsinki University of Technology)

[11] Ostashev V E and Wilson D K 2015 *Acoustics in moving inhomogeneous media* (CRC Press)

[12] Liu H, Peters G and Foken T 2001 New equations for sonic temperature variance and buoyancy heat flux with an omnidirectional sonic anemometer *Boundary-Layer Meteorol.* **100** 459–68

[13] Barth M and Raabe A 2011 Acoustic tomographic imaging of temperature and flow fields in air *Meas. Sci. Technol. Meas. Sci. Technol* **22** 35102–13

[14] Lanzinger E and Langmack H 2005 Measuring Air Temperature by using an Ultrasonic Anemometer *WMO Tech. Conf. Meteorol. Environ. Instruments Methods Obs.* 1–8

Appendix C: Numerical Procedure Outlined By Otero et al. [9]

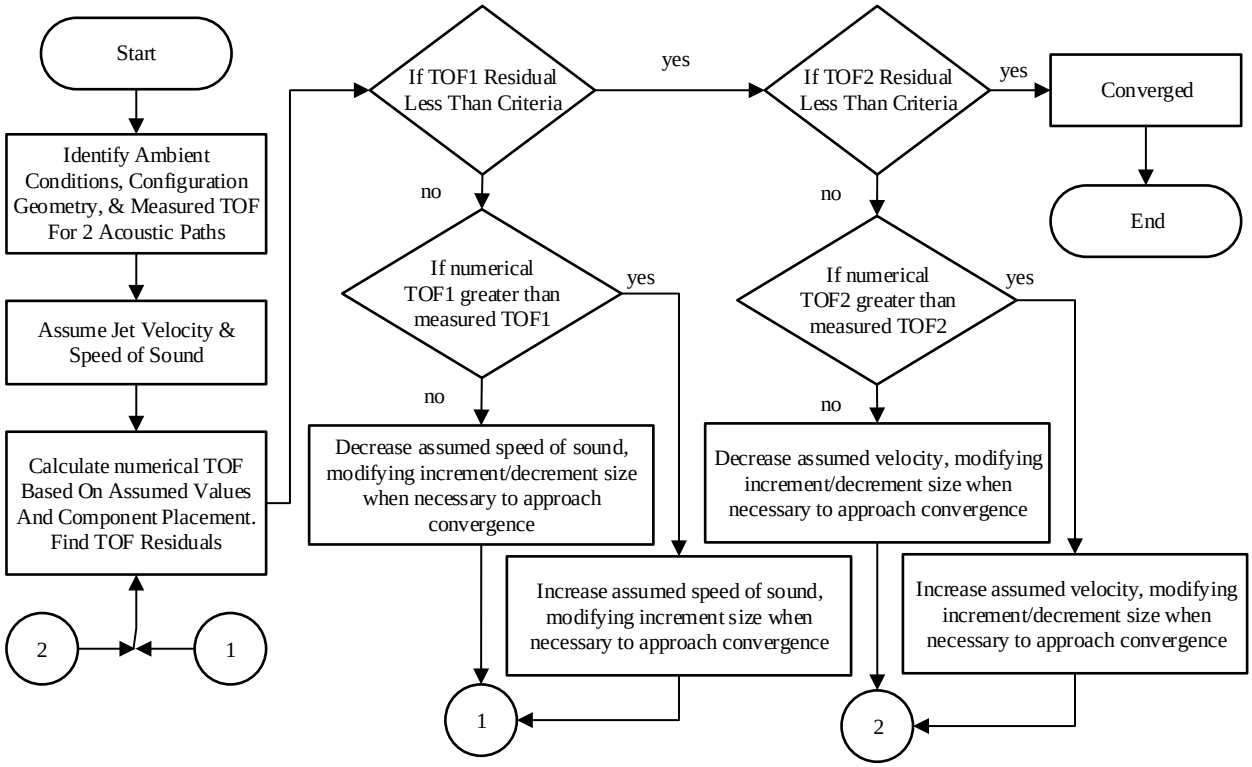

Figure C.1. *High-level flow diagram highlighting steps necessary to iteratively solve for jet properties.*

Appendix D: Normalized Jet Velocity and Static Temperature Profile at $2D_{jet}$ Stream-wise Position

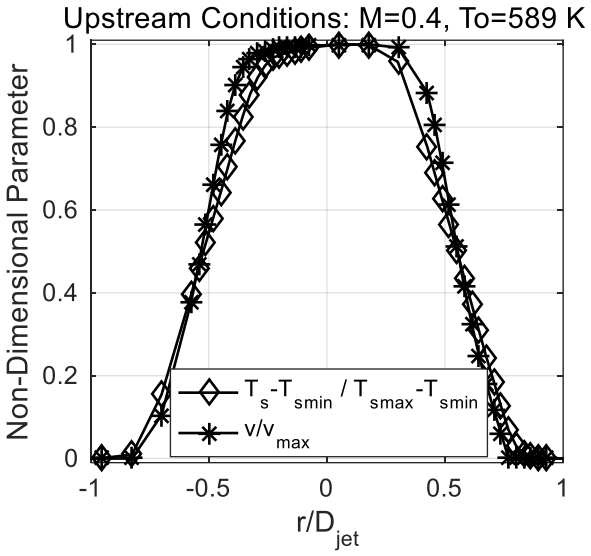

Figure D.1. *Normalized downstream static temperature and velocity profiles at $2D_{jet}$ stream-wise position for exit conditions of M=0.4 and T_o=589 K.*

Appendix E: Speed of Sound and Temperature Measurement Uncertainty

In the unheated jet study [9], the authors described velocity estimation uncertainty in detail, but speed of sound and temperature accuracy were not explored due to the unheated nature of the jet. To simplify the derivation of a temperature uncertainty expression, consider the classical SAT configuration presented in Figure 4.1. From equations (1) and (2), it is evident that flow velocity and temperature are a function of acoustic path trajectories and TOF values. From Otero et al. [9], Mach number uncertainty can be approximately described by equation (E1)

$$u_M \cong \sqrt{(Ku_\tau)^2} \tag{E1}$$

where K is a constant that is a function of relative microphone placement and u_τ is the uncertainty in time-of-flight estimation. Writing equation (4) in terms of speed of sound and Mach number (rather than velocity) and noting that both paths are critical for determining fluid velocity, the average expression for thermodynamic speed of sound shown in equation (E2) is obtained:

$$c \cong \frac{c_d + c_u}{2} = \frac{L}{\sum\tau}\left(\frac{1}{(1 - M^2)}\right) \tag{E2}$$

Incorporating the known gas composition and specific heat ratio of the fluid, equation (E3) can be used to specify static temperature as well.

$$T_s = \left(\frac{L}{(1 - M^2)\sum\tau}\right)^2 / \gamma R \tag{E3}$$

Assuming the distance uncertainty is small due to ambient calibration measurements, equations (E2) and (E3) can be used to approximate speed of sound and temperature uncertainties as shown in equations (E4) and (E5).

$$u_c \cong u_\tau \sqrt{\left(\frac{\partial c}{\partial \sum \tau}\right)^2 + \left(K \frac{\partial c}{\partial M}\right)^2} \tag{E4}$$

$$u_{T_s} \cong u_\tau \sqrt{\left(\frac{\partial T_s}{\partial \sum \tau}\right)^2 + \left(K \frac{\partial T_s}{\partial M}\right)^2} \tag{E5}$$

While the above expressions were derived using the classical SAT configuration, both equations are a good approximation measurement uncertainty in Otero et al.'s [9] configuration since both arrangements rely on displacement and TOF measurements to measure fluid characteristics.

Part V. Gas Turbine Engine Experiment

Preface

The text presented in Part V was originally published in the 32nd AIAA Aerodynamic Measurement Technology and Ground Testing Conference in 2016. *Otero, R., Lowe, K. T., & Ng, W. F., Ma, L., Kim, C. Y. (2016). Non-Intrusive Gas Turbine Engine Exhaust Characterization using Acoustic Measurements, 32nd AIAA Aerodynamic Measurement Technology and Ground Testing Conference, AIAA 2016-4160, DOI: 10.2514/6.2016-4160.* The text has since been amended to include a mass flow rate and thrust estimation procedure and its corresponding results. The current text was recently recommended for publication in the AIAA Journal of Propulsion and Power by referees pending minor revisions. Note that the appendices referred to in the text are included at the end of the manuscript, not the end of this dissertation.

The major takeaways of this manuscript are:

- SAT technique was implemented in a Turbofan engine's exhaust for the first time
- Acoustic measurements can be used to sense velocity and temperature changes in non-uniform flow fields
- A normalized shape-function approach can be used to estimate engine mass flow rate and thrust non-intrusively

Non-Intrusive Gas Turbine Engine Exhaust Characterization using Acoustic Measurements

Raul Otero Jr[1], K. Todd Lowe[2], Wing F. Ng[3], Lin Ma[4], Chu-young Kim[1]
Virginia Polytechnic Institute and State University, Blacksburg, VA, 24060

This paper reports exhaust measurements performed using a non-intrusive acoustic technique on a JT15D-1A turbofan research engine. Using multiple stream-wise displaced microphones, integrated exhaust velocity and static temperature were measured simultaneously in engine flows with bypass Mach numbers up to 0.48. A combination pressure and thermocouple probe was used to assess the accuracy of the acoustic measurements. Integrated velocity and static temperature root mean square errors of 3.8 m/s and 2.3 K were identified. Using probe-based measurements at a low engine power setting, two calibration constants were identified for conversion from integrated flow parameters to mass flow and thrust. Applying the calibration constants to the acoustic measurements, 1.1 kg/s and 200 N root mean square errors in mass flow and thrust were observed. These promising results indicate that the acoustic technique may be used to characterize and monitor gas turbine engine performance. To the authors' knowledge, this is the first time a non-intrusive acoustic technique has been used to characterize engine flows with Mach numbers greater than 0.3.

[1] Graduate Research Assistant, Department of Mechanical Engineering, Student Member AIAA.

[2] Assistant Professor, Department of Aerospace and Ocean Engineering, Associate Fellow AIAA.
[3] Chris C. Kraft Endowed Professor, Department of Mechanical Engineering, Associate Fellow AIAA.
[4] Professor, Department of Aerospace and Ocean Engineering, Associate Fellow AIAA.

Nomenclature

c = speed of sound (m/s)

$\bar{c}_{jet}$ = temporally integrated jet speed of sound (m/s)

D_x = distance between acoustic equipment in transverse direction (m)

D_y = distance between acoustic equipment in stream-wise direction (m)

F_{jet} = Jet exhaust thrust (N)

$\bar{F}_{A,jet}$ = Arbitrary momentum flux defined using integrated parameters (N/m^2)

K_1 = Mass flow calibration constant defined at 35% corrected fan speed probe measurements

K_2 = Thrust calibration constant defined at 35% corrected fan speed probe measurements

$\bar{\dot{m}}_{A,jet}$ = Arbitrary mass flow flux term defined using integrated parameters (kg/m^2s)

$\dot{m}_{jet}$ = Jet exhaust mass flow rate (kg/s)

$\hat{n}$ = Unit vector normal to the acoustic wave front

M = local Mach number

P_s = local static pressure (Pa)

P_t = local total pressure (Pa)

Q = acoustic directivity index

r = distance between acoustic source and receiver (m)

R = ideal gas constant (J/kgK)

s = acoustic propagation distance (m)

T_s = local static temperature (K)

$\bar{T}_{s,jet}$ = temporally integrated jet static temperature (K)

t_i = time-of-flight along the ith acoustic path (s)

v = local velocity (m/s)

$\bar{V}_{jet}$ = temporally integrated jet velocity (m/s)

γ = specific heat ratio

Γ = unit vector that is everywhere tangent to acoustic ray path

τ = acoustic propagation time (s)

1. Introduction

GAS turbine engine manufactures have long sought an efficient and robust method to characterize the engine flow conditions of in-flight vehicles. In the past, instrumentation available for the direct measurement of desirable flow properties have primarily been intrusive, and consequently inefficient and infeasible for in-flight application. More recently, minimally-intrusive and non-intrusive methods such as Particle Image Velocimetry (PIV), Global Doppler Velocimetry (GDV), and Tunable Diode Laser Absorption Spectroscopy (TDLAS) have been proposed and used to measure flow characteristics in ground-based, high-speed applications [1-6]. While effective and widely used, these techniques rely on laser equipment that is often prone to misalignment, optical fouling, and is generally expensive to implement.

Throughout this document, a non-intrusive acoustic method, as outlined by Otero et al.[7], is proposed for future in-flight measurement of engine exhaust properties. The proposed acoustic technique relies on the fundamentals of sonic anemometry and thermometry, which have been around for many years [8-14], but uses a new configuration to estimate higher subsonic Mach number flow characteristics simultaneously. While the first implementation of this acoustic technique was in a 50.8 mm, unheated uniform jet [7], the current work indicates that flow velocity and static temperature in non-uniform flows could be resolved if the signal-to-noise ratio (SNR) is adequately strong and sufficient acoustic path measurements are collected. Throughout this investigation, Otero et al's acoustic technique has been applied in a much larger coaxial jet with flow Mach numbers up to 0.48. Integrated path results of intrusive (probe) and non-intrusive (acoustic) engine measurements were compared and the error associated with the acoustic technique have been quantified. While the spatial distribution of exhaust velocity and temperature could not be resolved due to equipment limitations, the authors believe that tomographic reconstruction methods could be used to resolve these non-uniform flow features in the future. Before going into the specifics of the proposed acoustic technique and the experimental methodology, it is necessary to briefly discuss the theory behind existing acoustic techniques and elaborate on the state of the art.

2. State of the Art

Sonic anemometry is a non-intrusive acoustic technique that uses multiple acoustic time-of-flight and position displacement measurements to determine flow velocity, independent of medium temperature [8]. Conventionally, acoustic source and receiver pairs are arranged in a manner that allows for downstream and upstream acoustic time-of-flight measurements [8, 9, 11-13]. The convective impact of the flow's velocity on the acoustic wave creates a difference in the acoustic time-of-flight, depending on direction of propagation, which can be used to determine the integrated path velocity. This conventional method, which has been implemented for many years in applications such as meteorological, pipe flow, and wind tunnel measurements, is often limited by SNR, and the adverse convective effects of upstream and downstream acoustic propagations [15-17]. Until recently, these adverse effects have limited the measurement technique to low subsonic Mach numbers (Mach < 0.3) [7]. In Otero et al.'s high subsonic Mach number investigation, a new configuration for sonic anemometry measurements was explored and results indicated root mean square errors of approximately 9 m/s for unheated jet flows up to Mach 0.83. The successful application of sonic anemometry at high subsonic Mach numbers makes the new configuration a viable approach for aero-gas turbine engine measurements, provided the SNR is sufficiently large.

Sonic thermometry, on the other hand, is a non-intrusive acoustic technique that measures integrated path temperature using acoustic time-of-flight and position displacement measurements. At low Mach numbers, the effects of velocity are assumed to be negligible, and a single line-of-sight acoustic measurement can be used to determine the temperature of a medium in the following fashion [18].

$$c = \sqrt{\gamma R T_s} = \frac{s}{\tau} \tag{1}$$

$$T_s = \frac{s^2}{\gamma R \tau^2} \tag{2}$$

This approach has been used for a wide range of applications including furnace, boiler, and gas turbine combustor measurements [13, 19, 20] because of the relatively low cost and robustness of the acoustic equipment. More recently, a Siemens experiment implemented sonic thermometry on a ground based gas turbine exhaust [18]. Throughout the experiment, a plurality of sonic thermometry measurements were sequentially collected and used to reconstruct the temperature

map of the engine's exhaust. The results of Siemens investigation indicated a temperature error of less than 10K [18]. In 2015, Siemens presented a follow up investigation of a micro-turbine's exhaust which showed bulk mean errors of $\pm 0.36\%$ in temperature [21]. It is important to note that all of these sonic thermometry measurements were carried out in flow Mach numbers less than 0.3. In order to measure higher Mach number temperatures, such as an aero- gas turbine engine's exhaust, the flow velocity cannot be neglected. Hybrid techniques that couple sonic anemometry and sonic thermometry, have been used in the past to enhance temperature measurement accuracy [13, 14]. However, the previously discussed limitations of conventional sonic anemometry techniques have limited flow measurements to below Mach 0.3.

3. Principles of Proposed Acoustic Technique

Building on the principles discussed in the previous section, the proposed acoustic technique allows for the approximation of integrated path velocity and static temperature in flows with Mach numbers greater than 0.3 using two stream-wise displaced acoustic path measurements as illustrated in Figure 5.1 below.

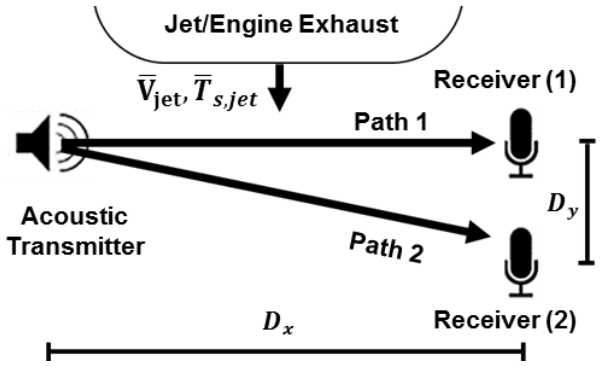

Figure 5.1. *Non-intrusive acoustic technique configuration.*

To determine these flow variables, the concepts described in Otero et al.'s unheated jet experiment [7] were used to estimate the integrated path velocity and speed of sound as shown in equations (3) and (4). The procedure for estimating the right hand side of equations (3) and (4) is outlined in Appendix F:

$$\bar{V}_{jet} = \frac{1}{\tau}\int V dt \cong \frac{\frac{D_x^2 + D_y^2}{t_2^2} - \left(\frac{D_x}{t_1}\right)^2}{\frac{2D_y}{t_2}} \tag{3}$$

$$\bar{c}_{jet} = \frac{1}{\tau}\int c dt \cong \sqrt{\left(-\bar{V}_{jet}\right)^2 + \left(\frac{D_x}{t_1}\right)^2} = \sqrt{\left(\frac{D_y}{t_2} - \bar{V}_{jet}\right)^2 + \left(\frac{D_x}{t_2}\right)^2} \tag{4}$$

The equations above result in a first order approximation of the integrated path parameters because they do not incorporate the effects of fluid refraction through the non-uniform convected medium (method requires a straight-line propagation assumption). Using the gas composition molecular weight, determined using the fuel flow rate or assumed based on operating conditions, the static temperature of the flow can be estimated using equation (5).

$$\bar{T}_{s,jet} = \frac{\bar{c}_{jet}{}^2}{\gamma R} \tag{5}$$

Throughout our investigation, it was noted that the ideal gas constant of exhaust products differs from air by less than 1%. Therefore, the ideal gas properties of air were used in this analysis.

Generally, the acoustic technique described in this section is prone to two main sources of uncertainty, time-of-flight (TOF) estimation and relative equipment displacement measurements. The TOF uncertainty is strongly correlated with measurement SNR since jet noise directly affects the clarity of the measured acoustic signals. From Otero et al.'s unheated jet investigation [7], a minimum SNR of -5 dB is recommended when estimating acoustic TOF. If the sound source frequency remains below the sampling Nyquist frequency and the SNR is sufficiently strong, the effect of jet noise can be mitigated by collecting a large amount of data and minimizing the standard error of the TOF estimation. This approach, however, requires that engine conditions remain constant throughout the acoustic measurement which may introduce other potential sources of error.

The second fundamental source of error, relative equipment displacement measurements, cannot be reduced by simply collecting more data throughout the experiment. Instead, this type of error must be handled with proper acoustic equipment calibration and high accuracy distance

measurement devices. Using a set of ambient measurements, along with the known ambient temperature of the air, D_x and D_y can be calibrated using the classical speed of sound equation (speed=Distance/time). Since only two time differences can be obtained from the ambient measurements, however, there may still be some distance uncertainty associated with this calibration (receiver 1 may not be aligned with source, etc…). One final source of uncertainty that is expected in this set of measurements is associated with the straight line propagation assumption that is used to approximate the integrated path velocity and speed of sound in equations (3) and (4). In the engine application, the acoustic paths will undoubtedly deviate from a straight line path to the receivers. The variation in path trajectory will ultimately result in an over or underestimation of fluid properties, depending on engine conditions. Since the current work serves as a proof of concept experiment to verify technique sensitivity to engine conditions, and a method for resolving non-uniformities is still being developed, the authors have chosen not to explore this type of error.

4. Experimental Setup and Procedures

To assess the performance of the proposed acoustic method in engine exhaust flows, intrusive (probe) and non-intrusive (acoustic) measurements were collected at the Virginia Tech JT15D-1A engine test facility, 0.58 m (2.275 core diameters) downstream of the core exhaust plane. Figure 5.2 below illustrates the configurations used for the probe and acoustic measurements at the exhaust of the turbofan engine.

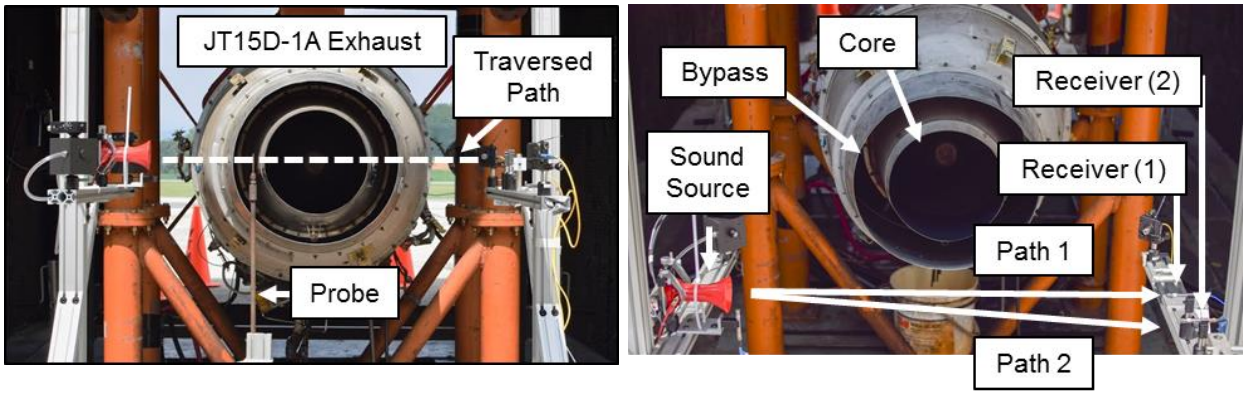

(a) (b)

Figure 5.2. *Experimental configurations: a) Intrusive (probe) setup b) Non-intrusive (acoustic) setup.*

Throughout the experiment, data was first collected using the traversing probe configuration and later using the acoustic configuration. Probe measurements would ultimately serve as the benchmark for acoustic error quantification. As illustrated in Figure 5.2a, the linear traverse was oriented to collect data at various radial positions using a 1/8 inch combination Kiel pressure and K-type thermocouple probe. In the acoustic measurement configuration, a spark sound source was used to generate an acoustic impulse signal and three microphones were used to collect acoustic data as shown in Figure 5.3 below:

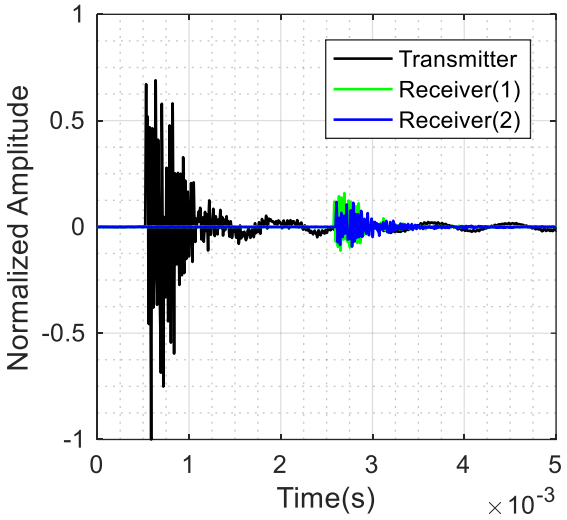

Figure 5.3. *Sample acoustic signals generated by spark transmitter.*

All three microphones used in the experiment were 6.35 mm PCB microphones. The transmitter and receivers were displaced 81.3 cm in the radial direction, and the two receivers, on the other side of the exhaust plume, were 10.2 cm apart. For each engine operating condition, 1500 sets of measurements (Figure 5.3 represents one measurement set) were collected and used to determine the acoustic time-of-flight along each propagation path using a proprietary cross correlation algorithm. It is important to note that the probe and acoustic measurements were collected at different times throughout the day. While ambient temperature and pressure did not vary significantly, there is a slight discrepancy to be expected between the acoustic and probe measurements.

5. Experimental Results & Discussion

Results, to be outlined in this section, were obtained for three different engine power settings, as well as the engine-off condition, in the plume of the research engine at Virginia Tech. First, the probe measurements are discussed to facilitate understanding of the engine's exhaust characteristics. Next, the procedure used to temporally integrate the intrusive probe data is discussed. Finally, the acoustic time-of-flight measurements will be presented, and the integrated flow parameters are compared.

5.1. Probe Measured Flow Parameters

Using the probe measurement configuration outlined in Section 4, radially displaced total pressure and total temperature probe data was collected. Assuming the measurements were locally isentropic, a known gas composition, and ideal gas behavior, the relevant flow variables were determined using Equations (6-8):

$$M = \sqrt{\frac{2}{\gamma - 1}\left(\left(\frac{P_t}{P_s}\right)^{\frac{\gamma-1}{\gamma}} - 1\right)} \tag{6}$$

$$T_s = \frac{T_t}{\left(\frac{P_t}{P_s}\right)^{\frac{\gamma-1}{\gamma}}} \tag{7}$$

$$v = M\sqrt{\gamma R T_s} \tag{8}$$

The local flow variables, determined using the intrusive probe measurements, are shown in Figure 5.4 below.

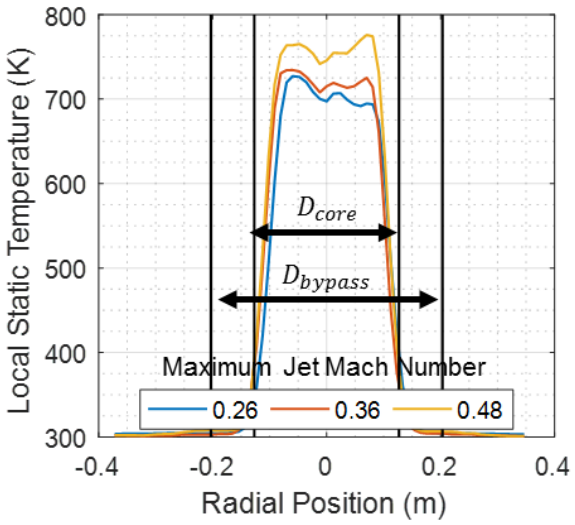

(a)

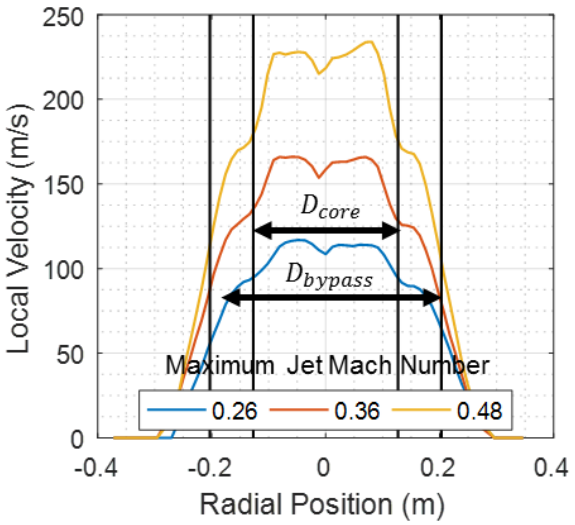

(b)

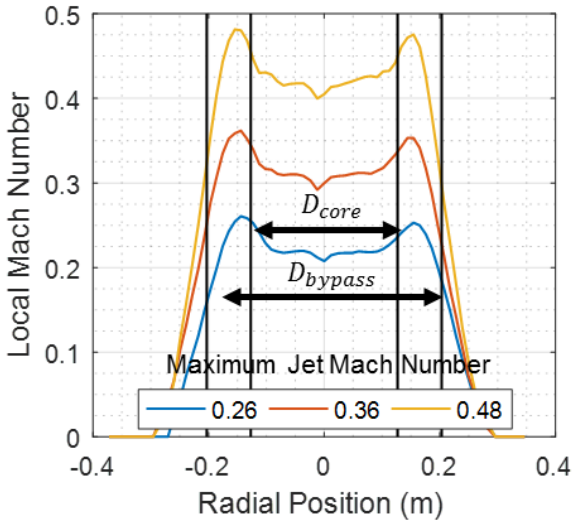

(c)

Figure 5.4. *Flow properties 2.275 core diameters downstream of engine exhaust plane: a) Static Temperature b) Velocity c) Mach Number.*

Figure 5.4 depicts the operating flow conditions at the JT15D-1A engine's exhaust. Each line represents a different engine power setting, corresponding with 35%, 50%, and 65% corrected fan speed. Maximum jet Mach numbers are used to specify the curve of interest.

Referring to the static temperature plot, it can be seen that the bypass region has a relatively low static temperature when compared to the core region of the engine. However, the velocity profile shows that the bypass velocity is only slightly lower than the core velocity. The relatively large difference in static temperature and relatively small difference in velocity when comparing core and bypass regions ultimately result in higher Mach numbers for the bypass region as shown in Figure 5.4c. Furthermore, the plots above give insight into the symmetry of the engine's exhaust. While the Mach number and velocity plots appear to be symmetric, some asymmetry can be observed in the static temperature plot, where one side is slightly hotter than the other at 0.26 and 0.36 maximum jet Mach number flows. The asymmetry in the speed of sound and temperature values was confirmed by alternating traversing directions between engine operating conditions.

5.2. Temporal Integration of Probe Measurements

To compare the integrated path parameters, the spatial probe measurements must be temporally integrated using the following relationships:

$$\bar{V}_{jet} = \frac{1}{\tau}\int_0^{\tau} v * dt = \frac{1}{\tau}\int_0^{s} \frac{v}{(c\hat{n} + \vec{v}) \cdot \Gamma} * ds \tag{9}$$

$$\bar{T}_{s,jet} = \frac{1}{\tau}\int_0^{\tau} T * dt = \frac{1}{\tau}\int_0^{s} \frac{T}{(c\hat{n} + \vec{v}) \cdot \Gamma} * ds \tag{10}$$

From Equation (9-10) above, the temporally integrated velocity and temperature terms are a function of the speed of sound in the medium, fluid velocity, acoustic propagation vector, and time-of-flight. In order to resolve these components, a numerical approach was used to model propagation between acoustic equipment.

As a first order approximation, the radial flow parameters are assumed to not change significantly in the stream-wise direction. An algorithm was developed to model the propagation trajectory of each acoustic path based on Snell's Law for moving mediums [22,23] and Fermat's principle of least time [23,24]. For more information regarding this approach, refer to Section 2.2 of Otero et al.'s unheated jet investigation [7].

Before implementing this numerical tool, the algorithm results were verified using simple propagation scenarios that have been previously explored in the literature. First, a stagnant, variable temperature grid was used to compare the results of the algorithm with a Snell's Law for non-moving mediums expression [25]. Next, a variable velocity, constant temperature grid was used to compare the results of the numerical tool with Amiet's model for acoustic propagation through a shear layer[26-29]. After successfully testing both scenarios, the numerical tool was deemed valid and implemented using the probe measured results. The numerically resolved acoustic propagation paths (based on the probe measurements) for 0.26, 0.36, and 0.48 maximum jet Mach number flows are shown in Figure 5.5. The left hand column presents the propagation paths overlaid on the engine's velocity profile while the right hand column shows the same paths on the static temperature profile.

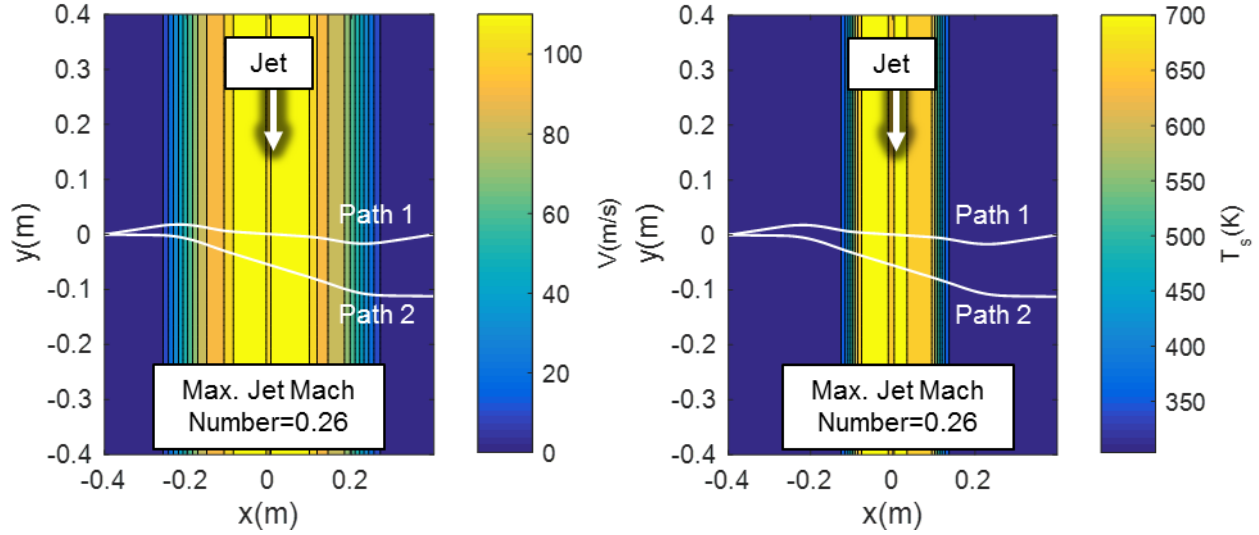
Jet
Path 1
Path 2
Max. Jet Mach Number=0.26
y(m)
x(m)
V(m/s)
T_s(K)

(a) (b)

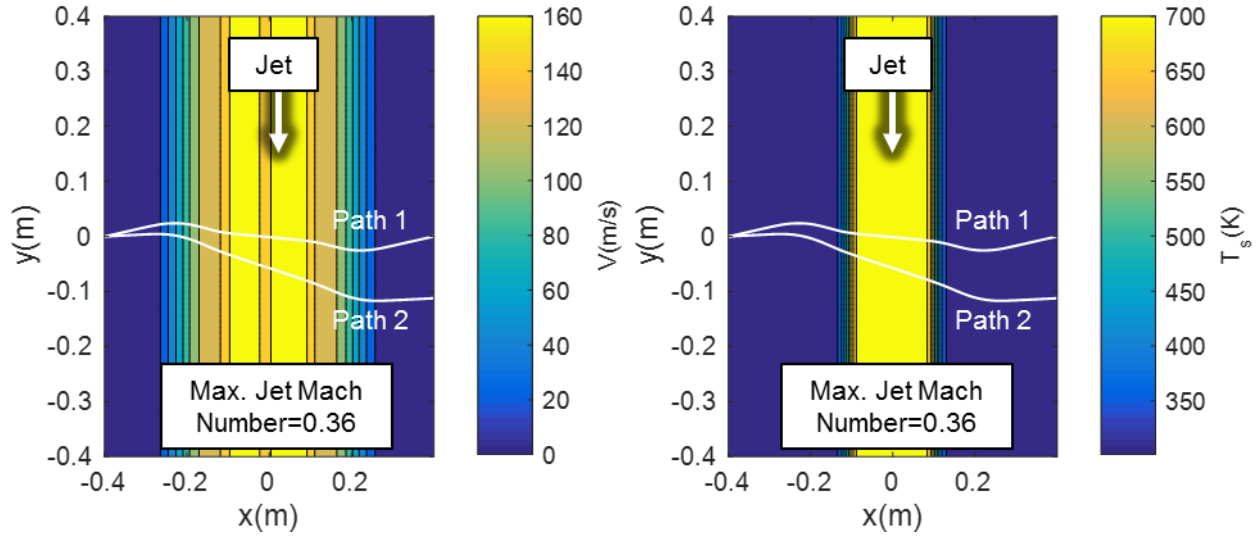
Jet
Path 1
Path 2
Max. Jet Mach Number=0.36
y(m)
x(m)
V(m/s)
T_s(K)

(c) (d)

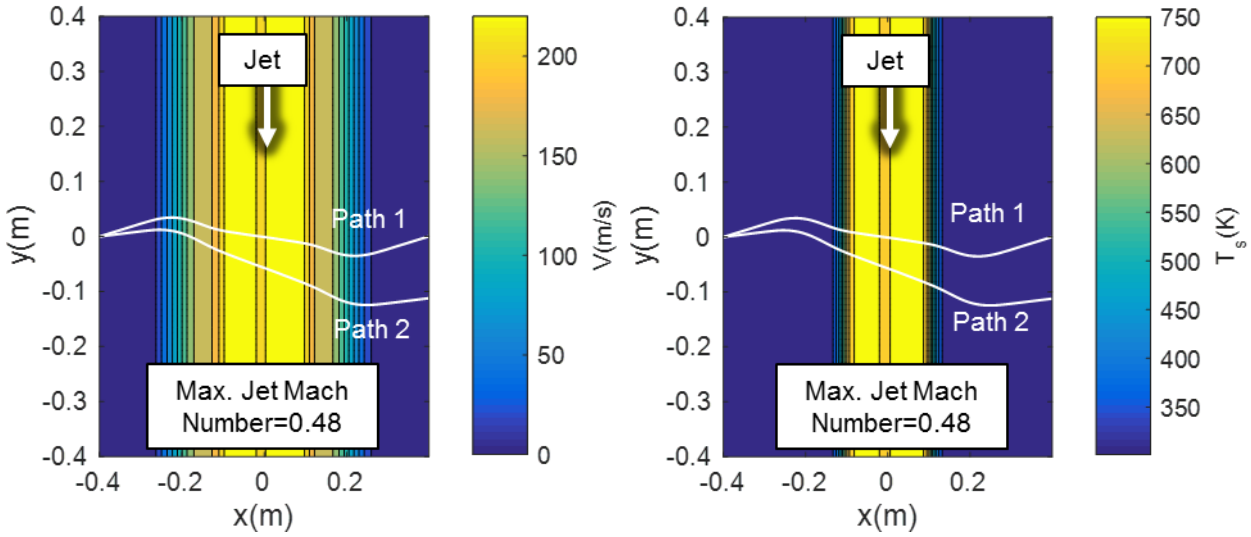

Figure 5.5. *Numerically resolved acoustic propagation paths determined using intrusive probe measurements. Left column illustrates acoustic propagation through velocity contour. Right column illustrates the same acoustic propagation through the static temperature contour.*

In Figure 5.5, the refractive effects of varying flow parameters can be seen more clearly. For the low Mach number case, the propagation path is approximately linear whereas the high Mach number case exhibits significantly more deviation from a linear path. Once the acoustic propagation paths were identified, temporal integration of the flow parameters was carried out along each acoustic path using Equation (9). The results of the temporal integration of probe measurements will be presented in Section 5 (D).

5.3. Non-Intrusive Time Delay Measurements

Using the non-intrusive configuration (see Figure 5.2b), raw voltage signals were collected using three microphones. Using the cross correlation procedure, outlined by Otero et al.[7], time-of-flight values were determined for each acoustic path at each corrected fan speed. The results of the signal cross correlations are shown in Figure 5.6 below.

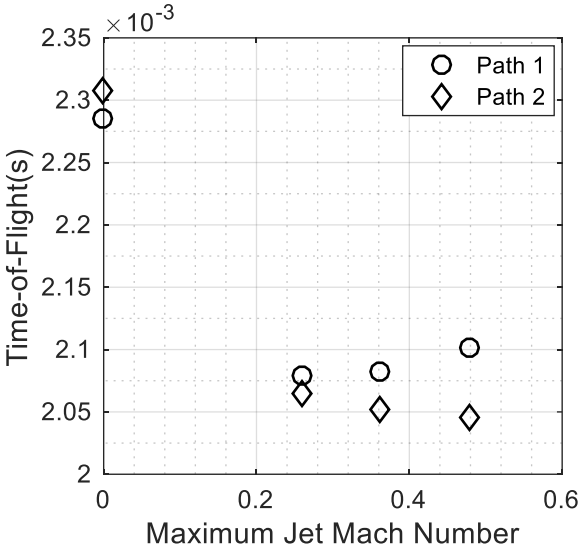

Figure 5.6. *Time-of-Flight measurements performed using acoustic equipment at various engine conditions.*

Analyzing the results in Figure 5.6, a few trends in the time-of-flight behavior can be seen with increasing jet Mach number. First of all, it can be seen that the ambient case correctly depicts the relative distance between acoustic components. Path 1, which has the shortest ambient path length, has the shortest time-of-flight. As the engine's maximum Mach number increases, the relative difference in times-of-flight also increases. Above Mach 0.26, Figure 5.6 shows that path 2 has a shorter time-of-flight than path 1 because the convective medium favorably "pushes" the acoustic ray towards receiver (2). Another trend shown in Figure 5.6 is the curvature of the time-of-flight curves. In the 0.26, 0.36, and 0.48 maximum jet Mach number cases, a parabolic trend for paths 1 and 2 is visible, shifted downwards and to the right with increasing path number.

5.4. Comparison of Probe and Acoustic Measurement Results

Using the time-of-flight parameters presented in Figure 5.6, integrated flow velocity and temperature were determined using the procedure outlined in Section 3. The results in Figure 5.7 show a direct comparison of the temporally integrated probe and acoustic measurements.

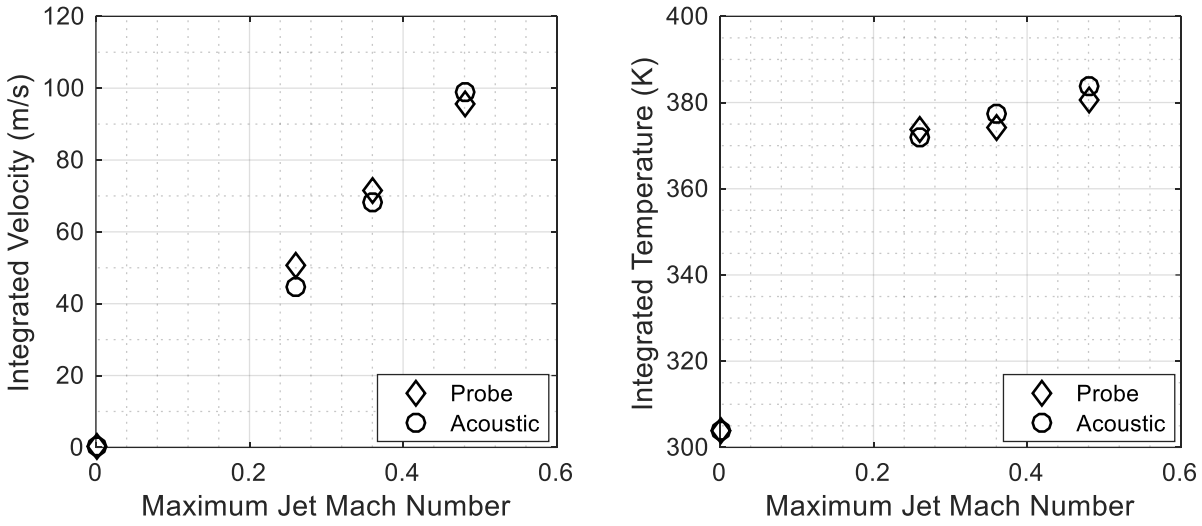

(a) (b)

Figure 5.7. *Comparison of acoustic and probe measurements: a) Integrated velocity b) Integrated static temperature.*

From the data presented in Figure 5.7, it is evident that the probe and acoustic measurement results match up fairly well. Assuming the operating conditions did not vary significantly between the time each measurement was collected, the deviation is hypothesized to be a consequence of assumed linear propagation between acoustic components and differences in data acquisition time periods. As mentioned in Section 3, the linear propagation assumption was made to enable the use of Equations (3) and (4) in the current work. In future experiments, the linear propagation assumption may be avoided if fluid non-uniformities can be resolved in a non-intrusively manner. Ultimately, the approach used in the current work served as a good first order approximation of the engine's operating conditions. Integrated path velocity and static temperature root mean square errors where shown to be 3.8 m/s and 2.3 K respectively.

5.5. Resolving Engine Mass Flow Rate and Thrust from Integrated Parameters

As evidenced by the results in Section 5 (D), the integrated probe and acoustic results were very promising. Using the integrated temperature and velocity acoustic measurements, it is also possible to estimate the engine mass flow rate and thrust performance using a calibration constant identified at low engine power levels. First, an arbitrary mass and momentum flux term are defined which are functions of the integrated terms:

$$\bar{m}_{A,jet} \cong \frac{P_s}{R\bar{T}_{jet}} \bar{v}_{jet} \tag{11}$$

$$\bar{\mathrm{F}}_{A,jet} \cong \frac{P_s}{R\bar{T}_{jet}} \left(\bar{v}_{jet}\right)^2 \tag{12}$$

The flux terms above are expected to relate to engine mass flow and thrust by some multiple for two main reasons. First, the area of the jet at the stream-wise position of the acoustic equipment is not expected to vary significantly with Mach number. Second, the normalized distribution of flow Mach number (shown in Figure 5.8 below) indicate that the non-uniform "shape function" is approximately constant for different Mach numbers.

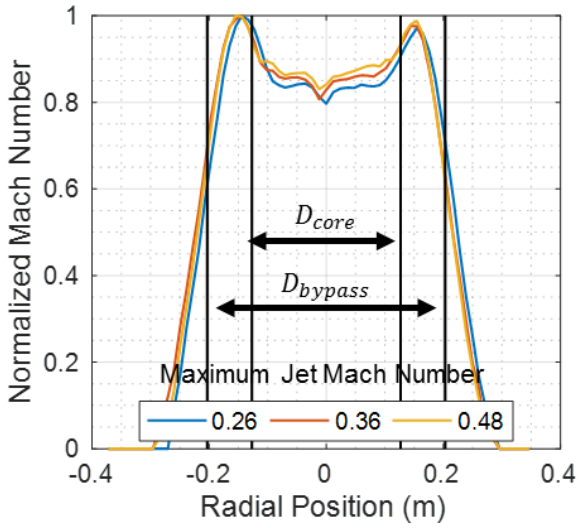

Figure 5.8. *Normalized Mach number distributions at measured engine power levels.*

Using the assumptions indicated above, the relationships between the arbitrary flux terms and the true mass flow and thrust terms were defined as:

$$\dot{m}_{jet} = K_1 \bar{m}_{A,jet} \tag{13}$$

$$F_{jet} = K_2 \bar{\mathrm{F}}_{A,jet} \tag{14}$$

Using the temporally integrated probe measurements at 35% corrected fan speed, along with the true mass flow and thrust parameters found using data in Figure 5.4, the constants K_1 and K_2 were found to be 0.298 and 0.453. Multiplying these constants by the acoustically determined flux terms, the exhaust mass flow and thrust of the JT15D-1A engine could be approximated at higher engine power levels:

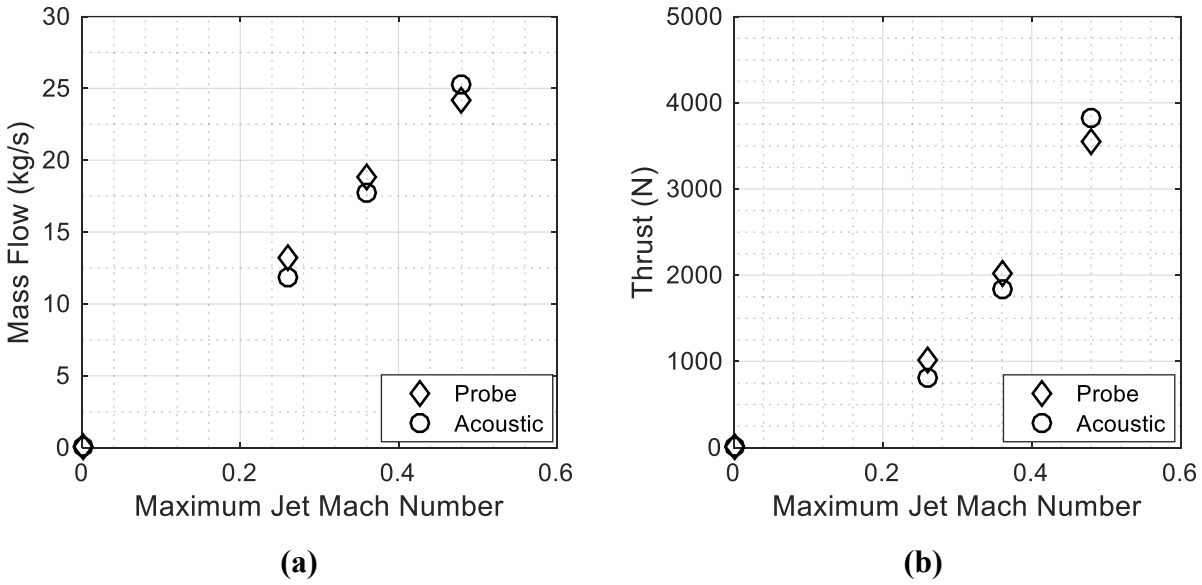

Figure 5.9. *Comparison of acoustic and probe measurements: a) Mass Flow Rate b) Thrust.*

The results presented in Figure 5.9 indicate this may be a viable way to estimate engine mass flow rates and thrust. Mass flow and thrust root mean square errors were shown to be 1.1 kg/s and 200 N respectively. Once again, the differences exemplified in Figure 5.9 are believed to be a function of the linear propagation assumption associated with equations (3-4) in Section 3, and differences in engine operating conditions associated with probe and acoustic data acquisition time periods. Future experiments should also be performed on a thrust stand facility so that acoustically determined values can be compared in real-time with intrusive measurements.

6. Conclusion and Future Work

This study tested the performance of a non-intrusive acoustic flow characterization system, thought to be feasible for in-flight gas-turbine engine exhaust measurements. A proof of concept, ground-based experiment was performed on a modified JT15D-1A turbofan research engine operating up to a maximum non-uniform jet Mach number of 0.48. Intrusive (probe) and non-intrusive (acoustic) measurements were collected at three different engine operating conditions for comparison.

Using a numerical ray tracing approach, implementing Snell's Law for convected flows [22,23] and Fermat's principle of least time modeling [23,24], the probe measurements were temporally integrated for comparison with the acoustic measurements. Assuming linear propagation between acoustic equipment, the equations outlined by [7] were used to approximate the integrated path velocity and static temperature of the turbofan engine's exhaust. The integrated path velocity and static temperature root mean square errors where shown to be 3.8 m/s and 2.3 K respectively. In order to estimate the mass flow rate and thrust of the engine, a calibration constant was identified using the intrusive probe measurements at 35% corrected fan speed. Applying this calibration constant to the acoustic measurements, engine mass flow rate and thrust root mean square errors were found to be 1.1 kg/s and 200 N respectively.

Overall, these results indicate that the acoustic technique may be used to characterize and monitor gas turbine engine performance. This sort of instrument could be used to reduce engine down-time due to catastrophic failure or performance checks and improve cost efficiency. Future work will seek to reduce uncertainty and assess measurement accuracy at higher Mach numbers. To the authors' knowledge, this is the first time a non-intrusive acoustic technique has been used to characterize engine flows with Mach numbers greater than 0.3.

Acknowledgments

The authors gratefully acknowledge the Rolls-Royce Corp. for funding this research, as well as Prof. Walter O'Brien and the Virginia Tech Turbomachinery and Propulsion Lab for enabling the use of the JT15D-1A engine research facility.

References

[1] Nelson, M., Lowe, K. T., O'Brien, W. F., Hoopes, K. M., "Stereoscopic PIV Measurements of Swirl Distortion on a Full-Scale Turbofan Engine Inlet," *52nd Aerospace Sciences Meeting*, AIAA 2014-0533, Jan. 2014, pp. 1-13.
doi: 10.2514/6.2014-0533

[2] Meyers, J. F., and Komine, H., "Doppler Global Velocimetry: A New Way to Look at Velocity," Laser Anemometry, Vol. 1, Jan. 1991, pp. 289-296.

[3] Cadel, D. R., Ecker, T., Lowe, K. T., "Time-Domain Cross-Correlation Scan DGV (CCS-DGV) for Mean-Velocity Boundary Layer Measurements," *52nd Aerospace Sciences Meeting*, AIAA 2014-1104, Jan. 2014, pp. 1-12.
doi: 10.2514/6.2014-1104

[4] Ecker, T., Ng W. F., Lowe, K. T., Henderson, B. S., Leib, S. J., "Velocity Statistics and Spectra in Three-Stream Jets," *52nd Aerospace Sciences Meeting*, AIAA 2016-1633, Jan. 2016, pp. 1-14.
doi: 10.2514/6.2016-1633

[5] Li, F., Yu, X., Gu, H., Li, Z., Zhao, Y., Ma, L., Chen, L., and Chang, X., "Simultaneous Measurements of Multiple Flow Parameters for Scramjet Characterization using Tunable Diode-Laser Sensors," *Applied Optics*, 20 Dec. 2011, Vol. 40, No. 36, 2011, pp. 6697-6707
doi: 10.1364/AO.50.006697

[6] Chang, L. S., Strand, C. L., Jeffries, J. B., Hanson, R. K., Kiskin, G. S., Gaffney, R. L., and Capriotti, D. P., "Supersonic Mass-Flux Measurements via Tunable Diode Laser Absorption and Nonuniform Flow Modeling," *AIAA Journal*, Vol. 49, No. 12, 2011, pp. 2783-2791.
doi: 10.2514/1.J051118

[7] Otero Jr., R., Lowe, K. T., and Ng, W. F., "Extension of Sonic Anemometry to High Subsonic Mach Number Flows," *Measurement Science and Technology*, published online 20 Dec. 2016.

[8] Cuerva, A., and Sanz-Andrés, A., "On Sonic Anemometer Measurement Theory," *Journal of Wind Engineering and Industrial Aerodynamics*, Vol. 88, No. 1, 2000, pp. 25-55.
doi: 10.1016/S0167-6105(00)00023-4

[9] Cuerva, A., Sanz-Andrés, A., and Lorenz, R. D., "Sonic Anemometry of Planetary Atmospheres," *Journal of Geophysical Research*, Vol. 108, No. E4, 2003, pp. 295-302.
doi: 10.1029/2002JE001944

[10] Banfield, D., and Dissly, R., "A Martian Sonic Anemometer," *Institute of Electrical and Electronics Engineers Aerospace Conference*, 2005, pp. 641-647.
doi: 10.1109/AERO.2005.1559354

[11] Wyngaard, J. C., "Cup, Propeller, Vane, and Sonic Anemometers in Turbulence Research," *Annual Review of Fluid Mechanics*, Vol. 13., Jan. 1981, pp. 399-423.
doi: 10.1146/annurev.fl.13.010181.002151

[12] Sozzi, R., and Favaron, M., "Sonic Anemometry and Thermometry: Theoretical Basis and Data-Processing Software," *Environmental Software*, Vol. 11, No. 4, 1996, pp. 259-270.
doi: 10.1016/S0266-9838(96)00046-9

[13] McKeon, B., Comte-Bellot, G., Foss, J., Westerweel, J., Scarano, F., Tropea, C., Meyers, J., Lee, J., Cavone, A., Schodl, R. and Koochesfahani, M., "Velocity, Vorticity, and Mach number," *Springer Handbook of Experimental Fluid Mechanics*, 1st ed., Springer Science & Business Media., New York, 2007, pp. 215-471.
doi: 10.1007/978-3-540-30299-5_5

[14] Kaimal, J. C., and Gaynor, J. E., "Another Look at Sonic Thermometry," *Boundary-Layer Meteorology*, Vol. 56, No. 4, 1991, pp. 401-410.
doi: 10.1007/BF00119215

[15] Tack, D. H., and Lambert, R. F., "Influence of Shear Flow on Sound Attenuation in a Lined Duct," *The Journal of the Acoustical Society of America*, Vol. 38, March 1965, pp. 655-666.
doi: 10.1121/1.1909770

[16] Ingard, U., and Singhal, V. K., "Sound Attenuation in Turbulent Pipe Flow," *The Journal of the Acoustical Society of America*, Vol. 55, No. 3, 1974, pp. 535–538.
doi: 10.1121/1.1914532

[17] Ingard, U., and Singhal, V. K., "Upstream and Downstream Sound Radiation into a Moving Fluid," *The Journal of the Acoustical Society of America*, Vol. 54, No. 5, 1973, pp. 1343–1346.
doi: 10.1121/1.1914431

[18] DeSilva, U., Bunce, R. H., and Claussen, H., "Novel Gas Turbine Exhaust Temperature Measurement System," *American Society of Mechanical Engineers Turbo Expo*, GT2013-95152, Jun. 2013, pp. 1-8.
doi: 10.1115/GT2013-95152

[19] Bramanti, M., Salerno, E. A., Tonazzini, A., Pasini, S., and Gray, A., "An Acoustic Pyrometer System for Tomographic Thermal Imaging in Power Plant Boilers," *Institute of Electrical and Electronics Engineers Transactions on Instrumentation and Measurement*, Vol. 45, No. 1, pp. 159-167.
http://dx.doi.org/10.1109/19.481329

[20] Zhang, S. P., An, L. S., Shen, G. Q., and Niu, Y. G., "Acoustic Pyrometry System for Environmental Protection in Power Plant Boilers," *Journal of Environmental Informatics*, Vol. 23, No. 2, 2014, pp. 24–35.
doi: 10.3808/jei.201400265

[21] DeSilva, U., Bunce, R. H., Schmitt, J. M., and Claussen, H., "Gas Turbine Exhaust Temperature Measurement Approach Using Time-Frequency Controlled Sources," *American Society of Mechanical Engineers Turbo Expo*, GT2015-42139, Jun. 2015, pp. 1-7.
doi: 10.1115/GT2015-42139

[22] Ostashev, V. E., Hohenwarter, D., Attenborough, K., Blanc-Benon, P., Juvé, D., and Goedecke, G. H., "On the Refraction Law for a Sound Ray in a Moving Medium," *Acta Acustica*, Vol. 87, No. 3, 2001, pp. 303–306.

[23] Ostashev, V. E., and Wilson, D. K., *Acoustics in moving inhomogeneous media*, 2nd ed., Vol. 1, CRC Press, New York, 2015.

[24] Ugincius, P., "Ray Acoustics and Fermat's Principle in a Moving Inhomogeneous Medium," *Journal of Acoustical Society of America*, Vol. 51, No. 5 (part 2), 1972, pp. 1759–1763.
doi: 10.1121/1.1913024

[25] Keller, J. B., "Rays, Waves and Asymptotics," *Bulletin of the American Mathematical Society*, Vol. 84, No. 5, 1978, pp.727-750.
doi: 10.1090/S0002-9904-1978-14505-4

[26] Amiet, R. K. K., "Refraction of Sound by a Shear Layer," *Journal of Sound and Vibration*, Vol. 58, No. 4, 1978, pp. 467–482.
doi: 10.1016/0022-460X(78)90353-X

[27] Schlinker, R. H., and Amiet, R. K., "Refraction and Scattering of Sound by a Shear Layer," *Journal of the Acoustical Society of America*, Vol. 70, No. 6, 1981, pp. 1797-1799.
http://dx.doi.org/10.1121/1.2033269

[28] Amiet, R. K., "Correction of Open Jet Wind Tunnel Measurements for Shear Layer Refraction," *2nd AIAA Aeroacoustics Conference*, AIAA 75-532, Mar. 1975, pp. 1-10. http://dx.doi.org/10.2514/6.1975-532

[29] Candel, S. M., Guedel, A., and Julienne, A., "Radiation, Refraction and Scattering of Acoustic acoustic waves in a free shear flow," *3rd AIAA Aero-Acoustics Conference*, AIAA 76-544, Jul. 1976, pp. 1-17. http://dx.doi.org/10.2514/6.1976-544

Appendix F. Integrated Path Variable Derivation

Using a kinematic manipulation, integrated path velocity and speed of sound can be determined using two downstream measurements. Similar to existing sonic anemometry and thermometry techniques, the measurement of velocity and speed of sound/temperature becomes a function solely of time delays and distances. Consider the configuration shown in Figure F.1 below.

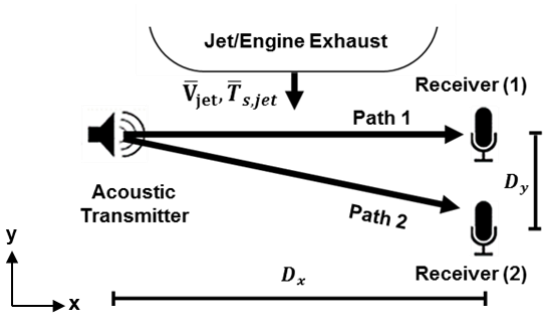

Figure F.1. *Acoustic equipment configuration for integrated path variable estimation.*

The first acoustic path can be represented using the diagram below:

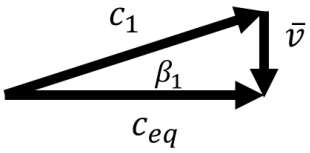

Figure F.2. *Variables associated with the first acoustic path propagation measurement.*

The path vector can be described as a combination of the medium's average velocity, $\bar{v}$, and the average speed of sound along the acoustic path c_1. This relationship can be described in terms of vector components as shown below.

$$c_1 \sin(\beta) + \bar{v} = \frac{D_{y1}}{t_1} \tag{F1}$$

$$c_1 \cos(\beta_1) = \frac{D_{x1}}{t_1} \tag{F2}$$

Using equations (F1) and (F2), the velocity measurement's dependency on angle of propagation can be discarded through the use of a trigonometric relationship described below.

$$1 = \cos^2 \beta_1 + \sin^2 \beta_1 \tag{F3}$$

$$\cos(\beta_1) = \frac{\left(\frac{D_{y1}}{t_1} - \bar{v}\right)}{c_1} \tag{F4}$$

$$\sin(\beta_1) = \frac{\left(\frac{D_{x1}}{t_1}\right)}{c_1} \tag{F5}$$

$$c_1^2 = \left(\frac{D_{y1}}{t_1} - \bar{v}\right)^2 + \left(\frac{D_{x1}}{t_1}\right)^2 \tag{F6}$$

Next, consider the second acoustic path

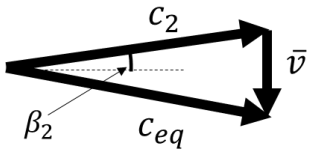

Figure F.3. *Variables associated with the second acoustic path propagation measurement.*

The acoustic path vector can once again be described as a combination of the medium's average velocity, $\bar{v}$, and the average speed of sound along the acoustic path c_2. Using the same manipulation described for path one, equation (F7) can be obtained.

$$c_2^2 = \left(\frac{D_{y2}}{t_2} - \bar{v}\right)^2 + \left(\frac{D_{x2}}{t_2}\right)^2 \tag{F7}$$

If, $c_1 \cong c_2$ is assumed, equations (F6) and (F7) can be combined to determine the integrated path velocity as shown below.

$$\bar{v} = \frac{\left(\left(\frac{D_{y2}}{t_2}\right)^2 + \left(\frac{D_{x2}}{t_2}\right)^2 - \left(\frac{D_{y1}}{t_1}\right)^2 - \left(\frac{D_{x1}}{t_1}\right)^2\right)}{\left(\frac{2D_{y2}}{t_2} - \frac{2D_{y1}}{t_1}\right)} \tag{F8}$$

The velocity expression in equation (F8) may be substituted into equation (F6) or equation (F7) to obtain the integrated path speed of sound as shown below:

$$c_1^2 = c_2^2 = \left(\frac{D_{y1}}{t_1} - \bar{V}_x\right)^2 + \left(\frac{D_{x1}}{t_1}\right)^2 \tag{F9}$$

Finally, flow temperature is determined using the known specific heat ratio and ideal gas constant of the fluid.

$$T_s = \frac{c_1^2}{\gamma R} \tag{F17}$$

Part VI. Compressible Flow Tomography Experiment

Preface

The text presented in chapter 6 is currently pending journal submission. The reader may reference appendix G for additional information regarding the algorithm used to solve the coupled acoustic tomography problem.

The major takeaways of this manuscript are:

- The difference in TOF between both ray paths in an SAT configuration is more sensitive to velocity than the thermodynamic speed of sound. Conversely, the summation of TOF is more sensitive to the thermodynamic speed of sound than the velocity of the convected fluid.
- A compressible flow acoustic tomography technique was developed using the sensitivity observations described above.
- Experimental results showed an ability to measure disturbance shape and location well
- A numerical sensitivity study revealed the impact of orientation count on measurement accuracy. More measurement orientations will be required in future experiments to improve performance.
- If a flow field is axisymmetric, the author recommends that measurements along a single orientation be projected onto other azimuthal orientations to solve the tomographic problem. This approach was used on the experimental data and there was a noticeable improvement in accuracy
- Additional errors are attributed to the relatively small size of the jet and tomography numerical errors. Error reduction will require additional research since tomography is dependent on gradient magnitudes, non-uniformity distributions, number of acoustic paths, convergence criteria, and several other variables.

Coupled Velocity and Temperature Acoustic Tomography in High Subsonic Mach Number Flows

R Otero Jr[1], K T Lowe[2], W F Ng[3], and K A Silas[1]

[1]Graduate Research Assistant, Department of Mechanical Engineering,
Virginia Tech, Blacksburg, VA, USA,

[2]Associate Professor, Department of Aerospace and Ocean Engineering,
Virginia Tech, Blacksburg, VA, USA.

[3]Chris C. Kraft Endowed Professor, Department of Mechanical Engineering,
Virginia Tech, Blacksburg, VA, USA.

E-mail: raul1991@vt.edu

Abstract. The application of acoustic tomography for simultaneous velocity and static temperature estimation has generally been restricted to low subsonic Mach number applications due to the increased complexities associated with acoustic refraction, high computational resource requirements, and a limited range of practical applications. The current work describes a novel acoustic tomography method for application in such conditions and presents the results of a proof of concept laboratory jet experiment. Using a traversed set of acoustic sound source and microphones, acoustic propagation time measurements were collected at Mach 0.48 and 0.72 jet conditions (with total temperatures of 675 K) along three azimuthal orientations and used to perform acoustic tomography. A comparison of intrusive and non-intrusive measurements showed that the three orientation reconstruction was effective in determining the general shape and location of the jet plume characteristics. Several sensitivity studies were subsequently conducted to further assess the behavior and limitations of the proposed acoustic tomography method. In particular, the effect of orientation count, reconstruction resolution, and displacement errors were investigated. The findings of these sensitivity studies were ultimately used to make recommendations for future experiments. Overall, the findings of this work are very promising. This application is the first time an acoustic method is used to non-intrusively and simultaneously measure jet velocity and static temperature distributions in high subsonic Mach number flows.

Keywords: Coupled Acoustic Tomography, Sonic Anemometry (SA), Sonic Thermometry (ST), Compressible Flows, Acoustic Temperature Measurement, Acoustic Velocity Measurement, Non-Intrusive Flow Measurement, Time of Flight Techniques, Tomography, Tomographic Reconstruction

Nomenclature

AT	Acoustic tomography
$b(x - x_j, y - y_j)$	User defined interpolation basis function
c	Thermodynamic speed of sound
$c_{j_{max}}$	Maximum thermodynamic speed of sound of all voxels
c_j^{q+1}	jth voxel thermodynamic speed of sound for next cycle
CVTT	Coupled velocity and temperature acoustic tomography
D_{jet}	Jet diameter
D_z	Distance between microphone planes
$d\ell$	Projection variable
$d\theta$	Angle of rotation between tomography orientations
$f(x, y)$	Field function that is a function of x and y position
i	Path index
j	Voxel or object function index
k	Wave number
$\boldsymbol{k}$	Wave vector
L	Canonical sonic anemometry and thermometry path length
L_i	ith Path length
ℓ_{ij}	Distance travelled through jth voxel by ith path
M	Mach number
M_j^q	Mach number of jth voxel in q cycle
M_j^{q+1}	jth voxel Mach number for next cycle
MART	Multiplicative algebraic reconstruction technique

MW_{air}	Molecular weight of air
$\boldsymbol{n}$	Unit vector normal to the acoustic wave front
N	Number of orientations used for tomographic reconstruction
O_j	Object function - field function definition at discrete positions j
P	Number of paths
P_t	Total pressure
P_s	Static Pressure
r_{jet}	Jet radius
$\bar{R}$	Universal ideal gas constant
R_{ji}^q	MART coefficient of jth voxel, ith path, and q cycle
R_i	Ray displacement along i coordinate
$\left(R_{ji}^q\right)_c$	Thermodynamic speed of sound MART Coefficient of ith path, jth voxel and q cycle
$\left(R_{ji}^q\right)_M$	Mach number MART Coefficient of ith path, jth voxel and q cycle
$RMSE_{T_s}$	Static temperature root mean square error
$RMSE_v$	Velocity root mean square error
$\boldsymbol{s}$	Wave slowness vector
$SR_{\Delta\tau}$	Sensitivity ratio of $\Delta\tau$
$SR_{\sum\tau}$	Sensitivity ratio of $\sum\tau$
$\boldsymbol{t}$	Ray path unit vector
T_s	Static Temperature
$T_{s_{max}}$	Maximum jet static temperature
T_t	Total Temperature
T_{amb}	Ambient temperature
TOF	Time-of-flight
q	Cycle index
u_{D_z}	Uncertainty in plane displacement measurement
v	Flow velocity
$\boldsymbol{v}$	Flow velocity vector

v_{max}	Maximum jet velocity
v_j^{q+1}	jth voxel velocity for next cycle
$v_{j_{max}}$	Maximum velocity of all voxels
X	Number of voxels in x direction
x_j	Voxel center x coordinate
Y	Number of voxels in y direction
y_j	Voxel center y coordinate
β_i	Initial angle of propagation of ray vector projected onto XZ plane
γ	Specific heat ratio
Γ	Correlation Coefficient
Δ	Image error
δx_j	jth voxel width
δy_j	jth voxel height
ζ	Arbitrary measurement variable
θ_i	Initial angle of propagation of ray vector projected onto XY plane
θ_{M2}	Microphone two angle relative to microphone one
λ	MART relaxation parameter
λ_c	Thermodynamic speed of sound relaxation parameter
λ_M	Mach number relaxation parameter
τ_i	Time-of-flight along ith path
$\Delta\tau$	Difference in acoustic time-of-flight between two paths
$\Delta\tau_i$	Measured TOF difference of ith path and i+P/2 path
$\Delta\tau_i^q$	Reconstructed TOF difference of ith path and q cycle
$\sum\tau$	Summation of acoustic time-of-flight of two paths
$\sum\tau_i^q$	Reconstructed TOF sum of ith path and q cycle
$\sum\tau_i$	Measured TOF sum of ith path and i+P/2 path
ψ_i	Integrated path measurement
ψ_i^q	Integrated path measurement of ith path and q cycle
ω	Wave angular frequency

1. Introduction

In the past, acoustic tomography (AT) methods have been used to characterize fluid velocity and static temperature gradients in a non-intrusive manner [1–7]. Although AT has been around for several decades, high subsonic Mach number applications ($0.3 < \text{Mach} < 1$) have not been explored in detail because of increased complexities associated with acoustic refraction, high computational resource requirements, and a limited range of practical applications. Due to recent proof of concept acoustic measurements performed by Otero et al. [8–10] in compressible jet flows, the use of AT for high subsonic Mach number flow sensing is worth exploring. Since modern AT methods require that fluid velocity be much smaller than the speed of sound, additional development of modern tomography methods is necessary for implementation in compressible flow regimes.

Throughout this paper, a novel AT approach for simultaneous velocity and static temperature estimation in compressible flows is described. Using classical sonic anemometry and thermometry concepts, the enabling characteristics of the technique are first presented and later used to formulate an effective multiplicative algebraic reconstruction technique (MART) expression that can be used to iteratively identify fluid velocity and temperature. Next, the results of a Mach 0.48 and 0.72 heated laboratory jet experiment are used to assess technique performance in realistic operating conditions. This experiment largely consisted of both intrusive (probe) and non-intrusive (acoustic) measurements, which were used to quantify fluid velocity and static temperature estimation error. Finally, a series of numerical simulations were used to perform sensitivity studies to better understand technique limitations. While additional research is necessary to better understand the limits of the proposed technique, the overall findings of the current work strongly support the use of acoustics for high subsonic Mach number flow sensing. Though the focus of this work is primarily velocity and temperature estimation, the technique could also be used to deduce mass flow rates and momentum flux in high speed applications. This capability is of significant interest to the gas turbine engine community.

1.1 Limited Data Acoustic Tomography

Before discussing the novel acoustic tomography approach, it is instrumental to first describe the concept of limited data AT. In practice, a wide variety of tomography algorithms have

been developed for solving the inverse problem (unknown integrand in integral expression) [11–13]. Generally, the objective of these algorithms is to use multiple integrated path measurements ψ_i to estimate a field function $f(x,y)$. The relationship between these two variables is generally described by equation (1).

$$\psi_i = \int_{L_i} f(x,y)d\ell\,, \qquad i = 1,2,\dots,P \tag{1}$$

Since the exact relationship is indeterminate due to the absence of complete information, a series expansion of equation (1) can be used to approximate $f(x,y)$ using an object function O_j and an arbitrary basis function $b(x-x_j, y-y_j)$[12]. The object function is simply a field function definition at discrete positions j in the measurement domain, and the basis function is a user defined interpolation expression that is used to approximate the field function behavior between discrete positions. Substituting the object and basis functions into equation (1), equation (2) can be obtained[12].

$$\psi_i \cong \sum_{j=1}^{XY} O_j \int_{L_i} b\big(x-x_j, y-y_j\big)d\ell\,, \qquad i = 1,2,\dots,P \tag{2}$$

Given that the projection variable $d\ell$ is confined by the field function and initial trajectory in acoustics (see Fermat's principle of least time [14]), the primary goal of an acoustic tomography algorithm is to approximate the correct object function O_j.

While many tomography algorithms exist for iteratively updating the object function, the MART approach is of particular interest because it has been shown to converge quickly and produce better accuracy when compared to several other limited data tomography algorithms[11–13]. The MART approach can be described using equation (3) as shown below[12].

$$\begin{gathered} O_j^{q+1} = R_{ji}^q O_j^q, \qquad \psi_i^q \neq 0, \qquad j = 1,2,\dots,XY \\ R_{ji}^q = 1 - \lambda \frac{\ell_{ij}}{L_i}\left(1 - \frac{\psi_i}{\psi_i^q}\right) \end{gathered} \tag{3}$$

To begin a tomographic reconstruction, a guess object function is specified at each coordinate (x_j, y_j), and the start and end position for each path are defined. Using the basis function of choice, a smooth mesh is defined for propagation modelling. Starting with the first projection, the propagation path is identified (using ray acoustics and Fermat's principle of least time) to determine the weighting that will be used to scale the object function. The weighting is defined as the ratio of distance traveled in a voxel to the overall path length, multiplied by a relaxation parameter λ (Note that a voxel refers to the area confined by $x_j - \frac{\delta x_j}{2}, x_j + \frac{\delta x_j}{2}, y_j - \frac{\delta y_j}{2}, y_j + \frac{\delta y_j}{2}$). Solving equation (2) for the first projection between start and end coordinates, an integrated variable ψ_i^q is identified and compared with the experimentally measured (true) value ψ_i. Using the weights and ratio of the integrated parameters, equation (3) is used to update the object function. This process is repeated for each projection to complete one cycle. At the end of each cycle, a criteria for convergence is checked. This process is repeated until the object function converges, or an exit criteria is met. Using the concepts described in this section (with several key modifications), the novel tomographic reconstruction method was developed to simultaneously resolve temperature and velocity gradients in high subsonic Mach number flows. The details of this procedure are outlined in the following section.

2. Principles of Proposed Coupled Velocity and Temperature Acoustic Tomography

In order to simultaneously resolve flow velocity and temperature gradients using integrated acoustic measurements, a method for decoupling the effects of temperature and velocity on acoustic propagation is necessary. To accomplish this decoupling, the authors will first assume that the mean flow direction is known a-priori (although limiting, this is generally a good assumption for high subsonic Mach number jets), which enables the use of Otero et al.'s coupled sonic anemometry and thermometry configuration [8,10]. To facilitate further discussion, consider the example CVTT configuration shown in Figure 6.1 which is comprised of multiple orientations of Otero et al.'s configuration.

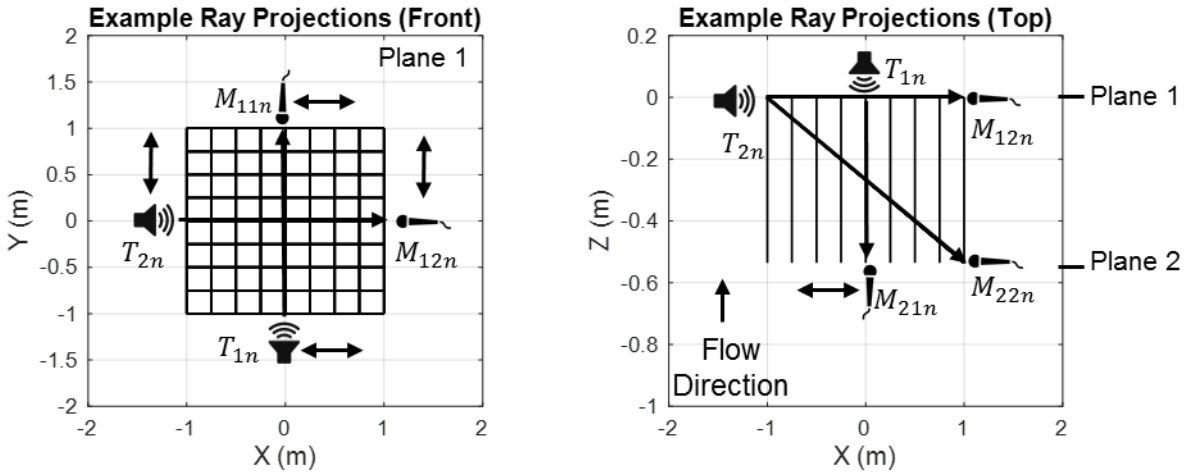

(a) (b)

Figure 6.1. *Example coupled velocity and temperature tomography configuration. (a) Front view of example CVTT tomography set up. (b) Top view of example CVTT tomography setup.*

The principle feature that distinguishes this technique from other tomography applications is the use of two stream-wise displaced microphones for each sound source positions. In Otero et al.'s heated laboratory jet experiment [10], it was observed that the difference in acoustic time-of-flight ($\Delta\tau = \tau_2 - \tau_1$) between two stream-wise displaced paths was more sensitive to flow velocity than the temperature of the jet. To quantitatively describe this behavior, consider the classical sonic anemometry and thermometry configuration shown in Figure 6.2.

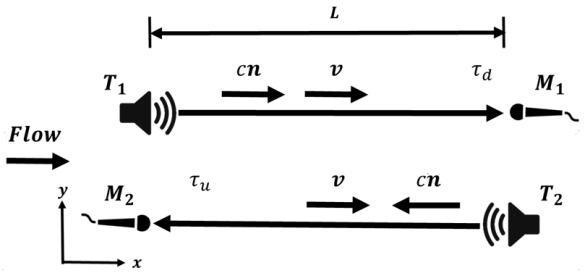

Figure 6.2. *Classical sonic anemometry and thermometry configuration.*

Using the time-of-flight (TOF) equations for each path, an expression for the $\Delta\tau$ can be written as shown in equation (4).

$$\Delta\tau = \frac{L}{c - v} - \frac{L}{c + v} = \frac{2Lv}{c^2 - v^2} \tag{4}$$

To show that $\Delta\tau$ is more sensitive to fluid velocity (v) than the thermodynamic speed of sound (c), which is analogous to temperature, consider the non-dimensional ratio (sensitivity ratio) of partial derivatives with respect to each variable shown in equation (5), and the corresponding plot shown in Figure 6.3.

$$SR_{\Delta\tau} = \left|\frac{\partial\Delta\tau/\partial v}{\partial\Delta\tau/\partial c}\right| = \frac{1 + M^2}{2M} \tag{5}$$

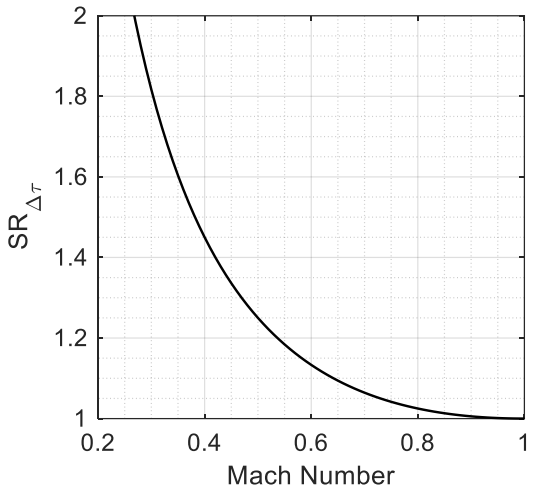

Figure 6.3. *Sensitivity ratio of $\Delta\tau$ at subsonic Mach numbers for the canonical sonic anemometry configuration shown in Figure 6.2.*

From equation (5) and Figure 6.3, it is evident that the $\Delta\tau$ relationship (equation (4)) remains more sensitive to v than c for subsonic Mach number flows. Noting that the c has a stronger influence on TOF magnitude at low Mach numbers ($c \gg v$), a similar analysis can also be used to show that the summation of TOF is more sensitive to c than v. Using the TOF equations for each path, an expression for the TOF summation ($\sum\tau$) can be written as shown in equation (6).

$$\sum\tau = \frac{L}{c-v} + \frac{L}{c+v} = \frac{2Lc}{c^2 - v^2} \tag{6}$$

Solving for the $\sum\tau$ sensitivity ratio,

$$SR_{\sum\tau} = \left|\frac{\partial\sum\tau/\partial v}{\partial\sum\tau/\partial c}\right| = \frac{2M}{1+M^2} \tag{7}$$

it is evident that the $\sum\tau$ is more sensitive to c than v. Additionally, the $\sum\tau$ sensitivity ratio is the inverse of the $\Delta\tau$ sensitivity ratio! These two sets of observations are used as the framework for updating the object function in the CVTT technique.

As a final note on the classical configuration observations, it is clear that $\Delta\tau$ and $\sum\tau$ become equally sensitive to v and c as the Mach number approaches one. This behavior is largely due to the inherent inability for acoustic waves to propagate upstream in the classical configuration. One of the major benefits of using Otero et al.'s configuration is that two downstream paths can be used to measure velocity and temperature. This capability could allow for an optimization of the sensitivity ratio for improved tomography performance. The optimization of equipment placement will not be explored in the current work.

Now that the enabling characteristics of the sonic anemometry and thermometry setups have been explored, the CVTT process can be described. Generally, the CVTT technique is divided into two main task, identifying the acoustic propagation path between start and end coordinates (eigenray) and iteratively updating the mesh velocity and thermodynamic speed of sound object functions. These two tasks are described in sections 2.1 and 2.2 respectively.

2.1. Eigenray Detection

To obtain the eigenray between a start and end coordinate for a fully defined mesh, an iterative ray shooting method was implemented. First, the unit vector normal to the wave front ($\boldsymbol{n}$) is defined using initial angles of propagation. The two initial angles used (θ_i and β_i) are defined in Figure 6.4.

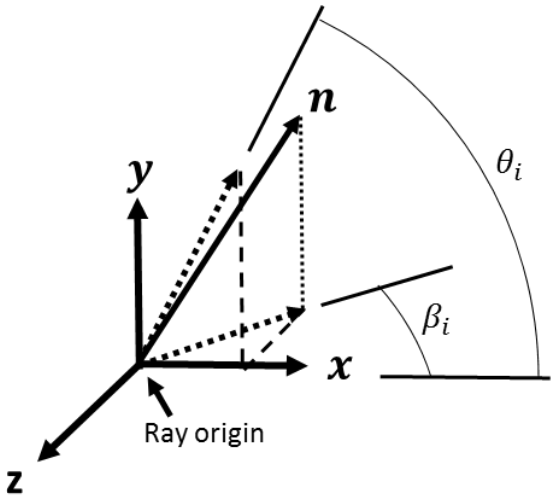

Figure 6.4. *Initial angles of propagation associated with the unit vector normal to the wave front:* $\boldsymbol{n}$

It is important to note that the unit vector $\boldsymbol{n}$ and the ray path do not coincide in inhomogeneous moving flows. The relationship between $\boldsymbol{n}$ and the ray path unit vector $\boldsymbol{t}$ is defined by equation (8).

$$\boldsymbol{t} = \frac{c\boldsymbol{n} + \boldsymbol{v}}{|c\boldsymbol{n} + \boldsymbol{v}|} \tag{8}$$

Using the initial $\boldsymbol{n}$ definition, and assuming geometric acoustics is valid, the Hamilton – Jacobi equations described by Ostashev [15](see equations (9-11)) are used to solve for the acoustic ray paths using a predefined set of initial θ_i and β_i angles.

$$\frac{dR_i}{dt} = \frac{c^2 s_i}{(1 - \boldsymbol{s}\cdot\boldsymbol{v})} + v_i \tag{9}$$

$$\frac{ds_i}{dt} = -\frac{(1 - \boldsymbol{s}\cdot\boldsymbol{v})}{c}\frac{\partial c}{\partial x_i} - \sum_{j=1}^{3} s_j \frac{\partial v_j}{\partial x_i} \tag{10}$$

$$\boldsymbol{s} = \frac{\boldsymbol{k}}{\omega} = \frac{k^2}{\omega^2}(c + \boldsymbol{n}\cdot\boldsymbol{v})\boldsymbol{n} \tag{11}$$

After projecting the ray using the user specified initial angles, the minimum distance between the ray path and the final location is determined. Using information about the minimum relative distances between the ray and the final location, the initial angles are adjusted, and the procedure is repeated until an exit criteria is met. The eigenray trajectory is then stored and later used to update the object function. Depending on the fluid properties and mesh characteristics, this procedure can become computationally intensive. The following subsection describes the expressions that are used to update the object function.

2.2. CVTT MART Procedure

In Otero et al.'s unheated laboratory jet experiment [8], the effect of varying plane two displacement relative to plane one on $\Delta\tau$ were plotted for various Mach numbers as shown in Figure 6.5.

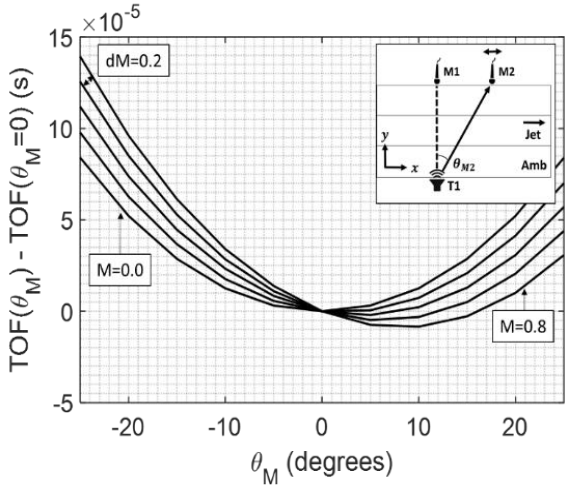

Figure 6.5. *From Otero et al [8]. Effect of microphone 2 angle on difference in TOF between two stream-wise displaced acoustic paths.*

One of the key findings of this data, was that $\partial\Delta\tau/\partial M$ remains approximately constant for fixed microphone positions and a constant thermodynamic speed of sound. This observation complements the sensitivity discussion presented at the beginning of Section 2 for the classical configuration.

In addition to the sensitivity observations described above, Figure 6.5 also shows that for negative θ_{M2} angles, $\Delta\tau$ increases as the Mach number increases. Since the MART equation is simply a framework for updating the object function, and the sensitivity ratios derived at the beginning of Section 2 are inverses of each other, we will assume that equation (12) and (13) can be used to approximate the Mach number and thermodynamic speed of sound of the flow since $\Delta\tau$ and Mach number are positively correlated, and $\sum\tau$ is negatively correlated with the thermodynamic speed of sound.

$$M_j^{q+1} = \left(R_{ji}^q\right)_M M_j^q, \qquad \Delta\tau_i^q \neq 0, \qquad j = 1,2,\dots,XY$$
$$\left(R_{ji}^q\right)_M = \left(1 - \left(\lambda_M \frac{\ell_{ij}}{L_i}\right)_1 \left(1 - \frac{\Delta\tau_i}{\Delta\tau_i^q}\right)\right) \tag{12}$$

$$c_j^{q+1} = c_j^q / \left(R_{ji}^q\right)_c, \qquad \sum\tau_i^q \neq 0, \qquad j = 1,2,\dots,XY$$
$$\left(R_{ji}^q\right)_c = \left(1 - \left(\lambda_c \frac{\ell_{ij}}{L_i}\right)_1 \left(1 - \frac{\sum\tau_i}{\sum\tau_i^q}\right)\right) \tag{13}$$

To solve equations (12) and (13), a coupled set of ray paths (path from source to plane one and two at same XY position) are first identified using the procedure outlined in Section 2.1. Using the TOF magnitudes obtained for both paths, $\Delta\tau$ and $\sum\tau$ can be identified. Assuming that the x-y projection of both acoustic paths do not vary significantly in the x-y plane, the weighting function ($\lambda\ell_{ij}/L_i$), is defined using the plane one propagation path.

After the new Mach number and speed of sound values have been identified for each voxel, velocity can be determined using equation (14) below.

$$v_j^{q+1} = M_j^{q+1} c_j^{q+1}, \qquad j = 1,2,\dots,XY \tag{14}$$

Once the new velocity and speed of sound object functions have been defined, a cubic b-spline basis function, defined by Hou and Andrews [16], was used to interpolate between the voxel

coordinates. The interpolated thermodynamic speed of sound was later used to determine the temperature of the flow using the specific heat ratio and ideal gas constant of air.

3. Experimental Setup & Procedures

Throughout the experiment, acoustic and probe data were collected in the 50.8 mm (2 inch) diameter jet facility used by Otero et al. [8,10]. The acoustic and probe equipment used to carry out the experiment are shown in Figure 6.6.

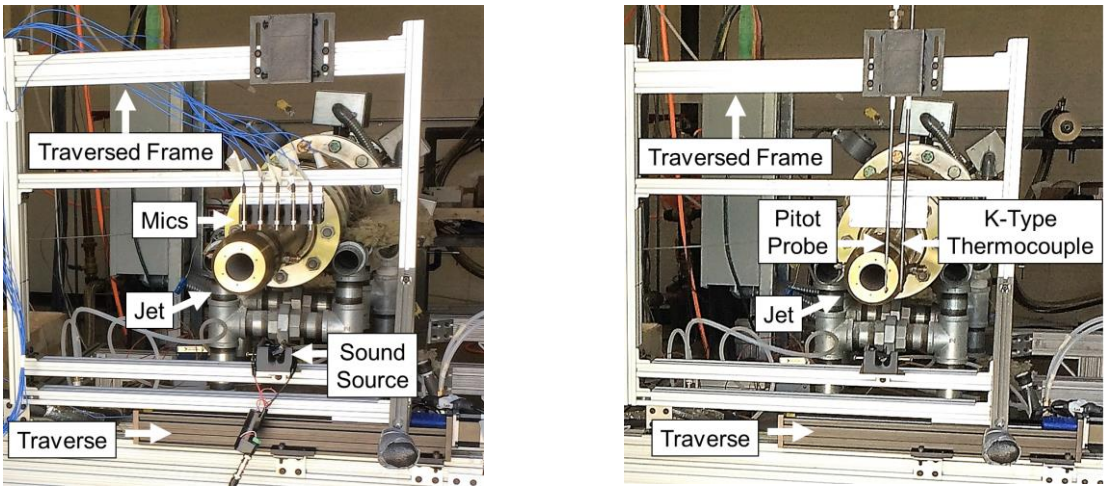

(a) (b)

Figure 6.6. *Acoustic and probe equipment oriented for horizontal (0°) traversing. (a) Acoustic configuration. (b) Probe configuration.*

Since few microphones and probes were available for data acquisition, a traversing mechanism was used to collect data at different spatial coordinates. Although fluid characteristics will undoubtedly vary in time, the current configuration serves as a proof of concept test of the CVTT technique.

For the acoustic measurements, a spark impulse sound source was used to emit acoustic signals and 11 PCB microphones were used to collect data. One of the 11 microphones was used as a reference to monitor spark discharging time, and the remaining 10 microphones were split across multiple plane one and two locations as shown in Figure 6.7.

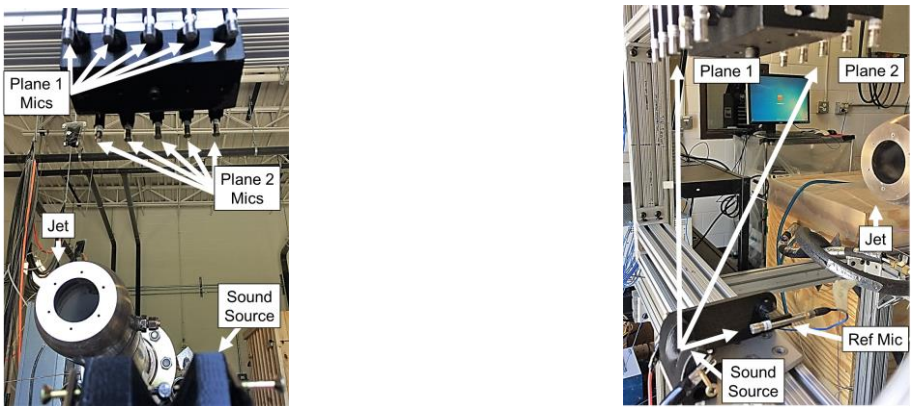

(a) (b)

Figure 6.7. *Close up of Acoustic sound source and microphones. (a) Front view. (b) Side view.*

The stream-wise position of plane one was 5 D_{jet} away from the jet exit plane, and plane two was positioned 2.125 D_{jet} upstream of plane one. A total of three orientations (horizontal - 0°, vertical - 90°, and diagonal - 45°) of the linear traverse were used to collect acoustic data for CVTT. Although additional orientations would result in better reconstruction accuracy, re-orientation and calibration time, as well as difficulties associated with upside down mounting discouraged the pursuit of additional orientations.

The acoustic equipment moved a span of $4D_{jet}$ in steps of $1/8^{th}$ D_{jet}, and signals were collected for 3 seconds at each traversed location. Figure 6.8 illustrates the acoustic paths at all traversed locations and orientations relative to the jet position.

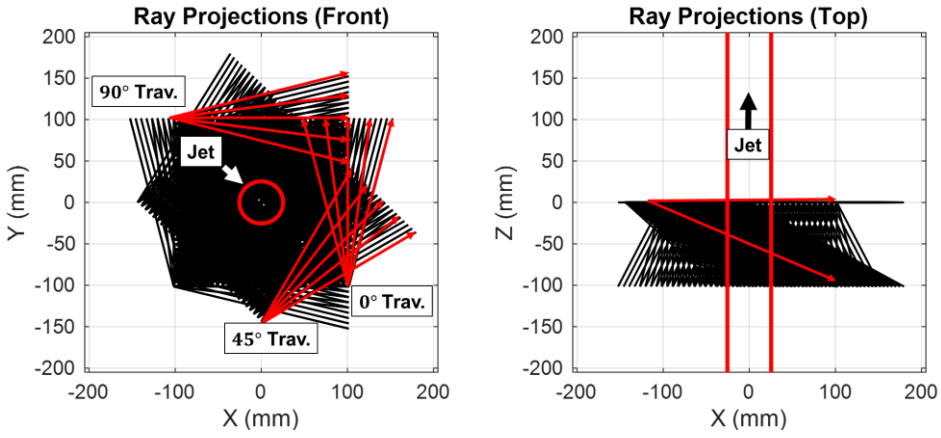

Figure 6.8. *Acoustic paths at all traversed locations and orientations relative to the jet*

Once all the acoustic measurements were collected, the cross correlation technique described by Otero et al.[10] was used to determine the propagation TOF for each path.

To validate the CVTT results, a set of intrusive probe measurements were used. First, total pressure and total temperature measurements were collected at the 4 D_{jet} streamwise position. A Pitot probe and K-type thermocouple probe were traversed a span of 4 D_{jet} in steps of 1/16th D_{jet}. At each traversed location, data was measured for 30 seconds. Using the known static pressure of the room, the isentropic equations were used to determine jet velocity and static temperature at different spatial positions for comparison with CVTT results. The setup used to collect this data is shown in Figure 6.6b.

4. Experimental Results & Discussion

Using the acoustic and probe configurations described above, measurements were collected for Mach 0.48 and 0.72 jet flows with a total temperature of 675 K. In the following subsections, both sets of measurement results are described and compared to assess CVTT system performance.

4.1. Probe Measurement Results

The traversed Pitot-probe and K-type thermocouple measurements of total temperature and total pressure for both test conditions are shown in Figure 6.9 (static pressure was known).

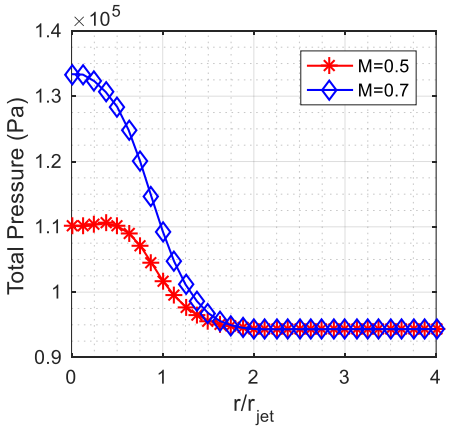

(a)

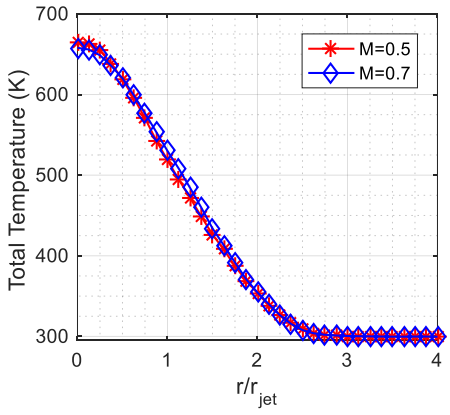

(b)

Figure 6.9. *Traversed probe measurements of jet plume at 4 D_{jet} streamwise position. (a) Total Pressure. (b) Total Temperature.*

From Figure 6.9, it is evident that the jet total temperature was consistent for both test cases, as expected, but the pressure profile transitioned from a flat top behavior at Mach 0.48 to a smooth curve at Mach 0.72. Using the known nozzle pressure ratio, total temperature, and the specific heat ratio of air, the facility Mach number, static temperature, speed of sound, and velocity were identified using equations (15-18).

$$M = \sqrt{\frac{2}{\gamma - 1}\left(\left(\frac{P_t}{P_s}\right)^{\frac{\gamma-1}{\gamma}} - 1\right)} \tag{15}$$

$$T_s = T_t\left(\frac{P_s}{P_t}\right)^{\frac{\gamma-1}{\gamma}} \tag{16}$$

$$c = \sqrt{\gamma \bar{R} T_s / MW_{air}} \tag{17}$$

$$v = Mc \tag{18}$$

Figure 6.10 shows the radial distribution of jet velocity and static temperature, deduced from the intrusive probe measurements.

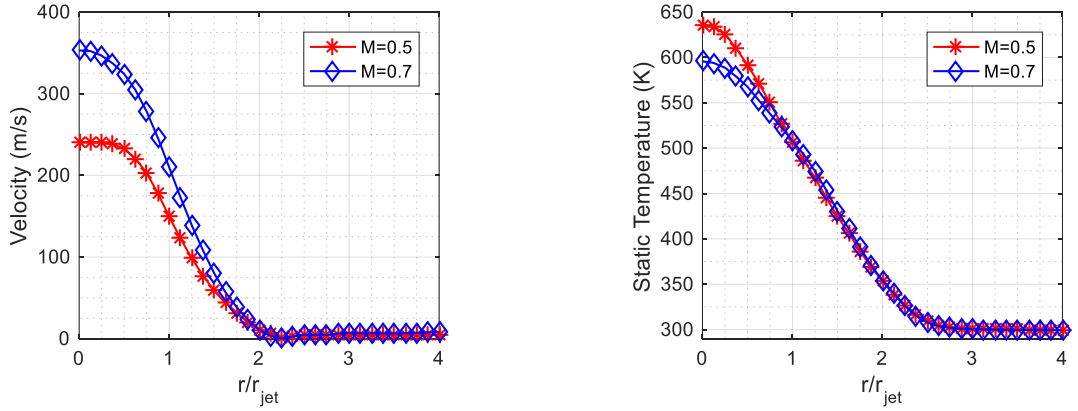

(a) (b)

Figure 6.10. *Radial distribution of jet velocity and static temperature at the 4 D_{jet} streamwise position. (a) Velocity. (b) Static temperature.*

For the current work, the data presented in Figure 6.10 was used to assess tomography performance. Since a raster scan of the jet plume was not available, only the data along the y=0 line is considered.

4.2. CVTT Measurement Results

Using the procedure outlined in Section 2, a tomographic reconstruction of the jet plume velocity and static temperature distribution was performed. The tomography algorithm inputs are described in Table 6.1 below.

Table 6.1. *Tomography algorithm inputs*

λ_c	1
λ_M	1
δx_j	8.5 mm
δy_j	8.5 mm
convergence criteria	$\left\|\frac{c_j^q - c_j^{q-1}}{c_{j_{max}}}\right\| < 0.005$ $\left\|\frac{v_j^q - v_j^{q-1}}{v_{j_{max}}}\right\| < 0.005$

The Mach 0.48 and 0.72 tomographic reconstructions of jet velocity and static temperature are shown in Figures 6.11 and 6.12 respectively.

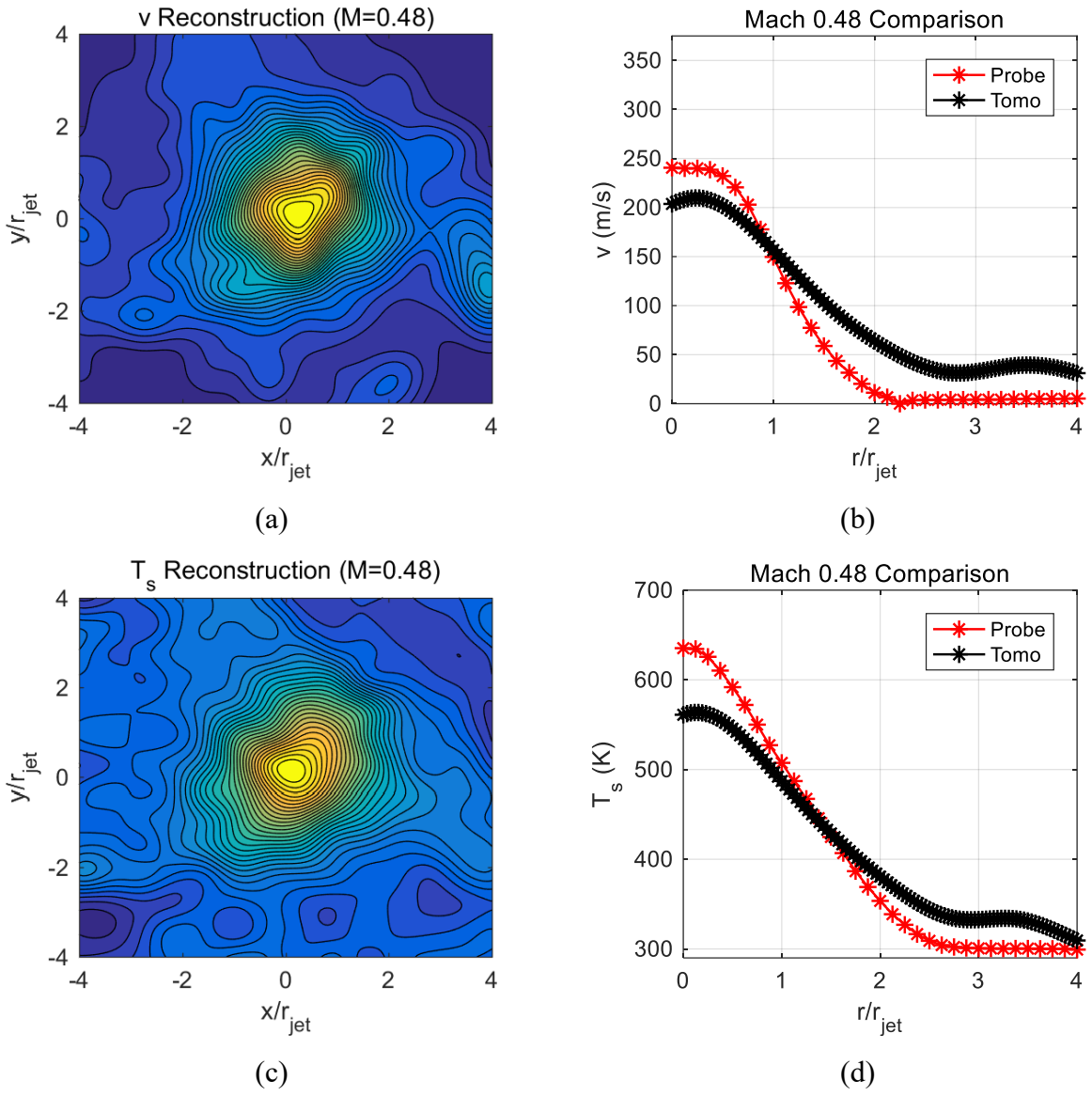

Figure 6.11. *Tomographic reconstruction of Mach 0.48 jet velocity and static temperature. (a) Velocity contour. (b) Velocity profile at* $y/r_{jet} = 0$. *(c) Static temperature contour. (d) Static temperature profile at* $y/r_{jet} = 0$.

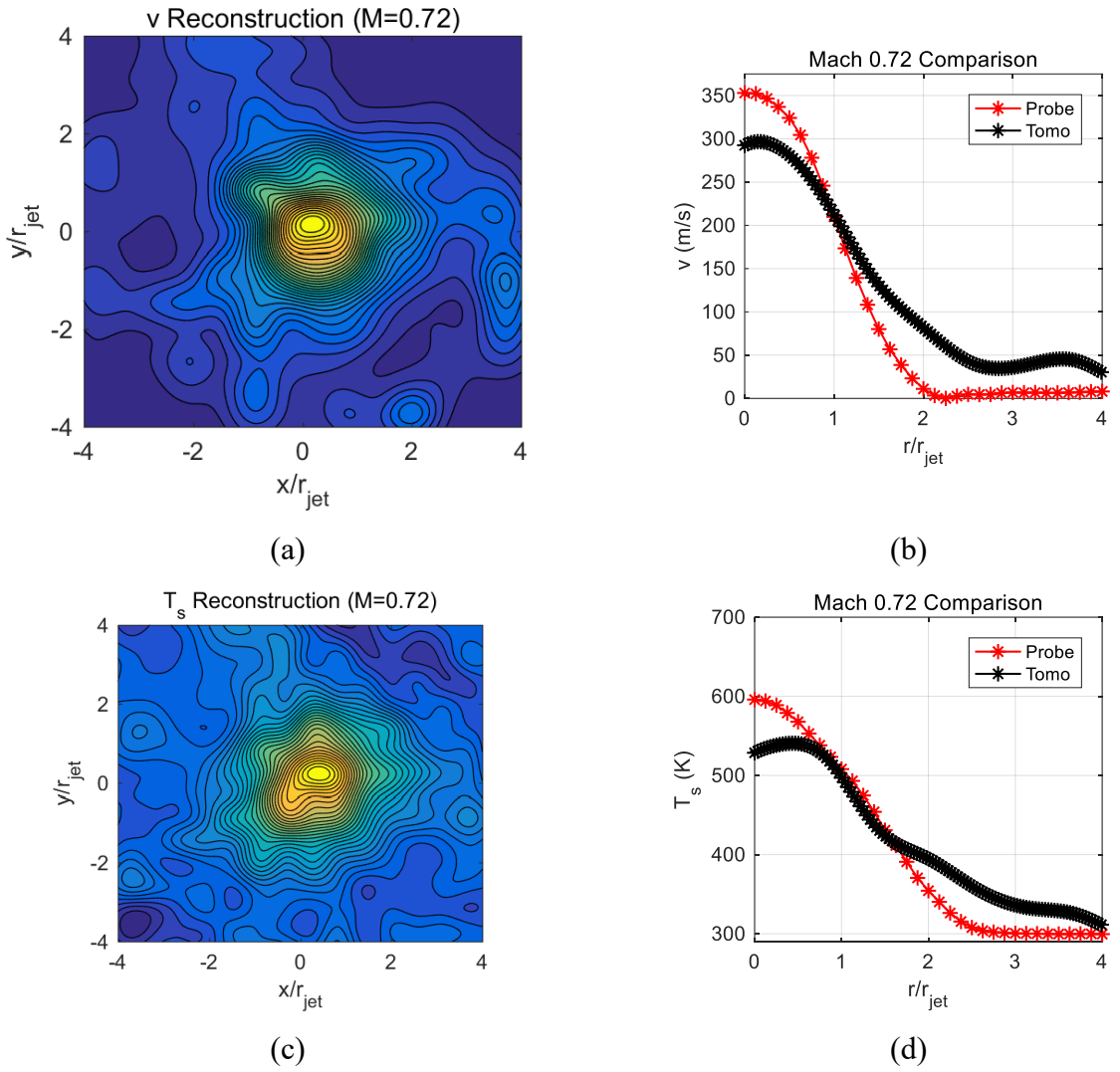

Figure 6.12. *Tomographic reconstruction of Mach 0.72 jet velocity and static temperature. (a) Velocity contour. (b) Velocity profile at* $y/r_{jet} = 0$. *(c) Static temperature contour. (d) Static temperature profile at* $y/r_{jet} = 0$.

In general, the technique does a great job of identifying the jet's location and size for both sets of test conditions. Although there is some error in the magnitudes of velocity and static temperatures when compared to the probe measured values, the results were better than expected for only using 3 orientations and reconstructing such a small jet.

In the Figure 6.11 and 6.12 reconstruction contours, the effects of only using 3 orientations can be seen through the elongation of fluid characteristics along the 0°, 45°, and 90° axes. Notably, the tomography algorithm also over-predicts the ambient section and under-predicts the jet conditions as can be seen in the profile plots. These behaviors are a clear sign that additional

orientations are necessary to improve system accuracy. To justify this claim, the author's explored the impact of projecting TOF measurements (horizontal traverse data) onto 8 other azimuthal orientations as shown in Figure 6.13. If the jet was properly centered and axisymmetric, the reconstruction results should approach the probe measured velocity and static temperatures.

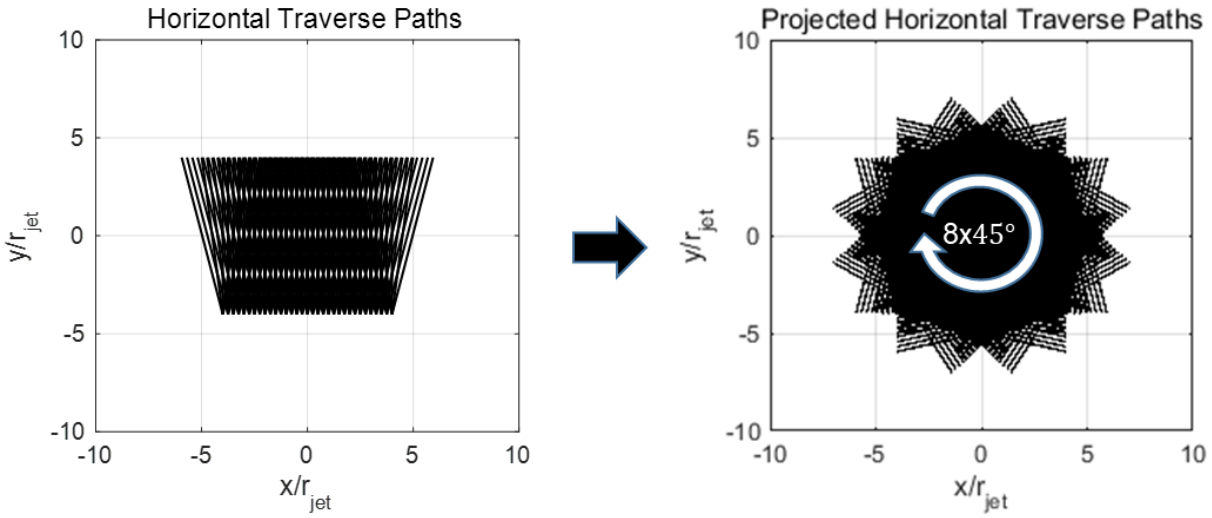

Figure 6.13. *Projection of horizontal traverse data onto 8 evenly distributed azimuthal orientations.*

The results of the tomographic reconstruction using the projected data are shown in Figures 6.14 and 6.15.

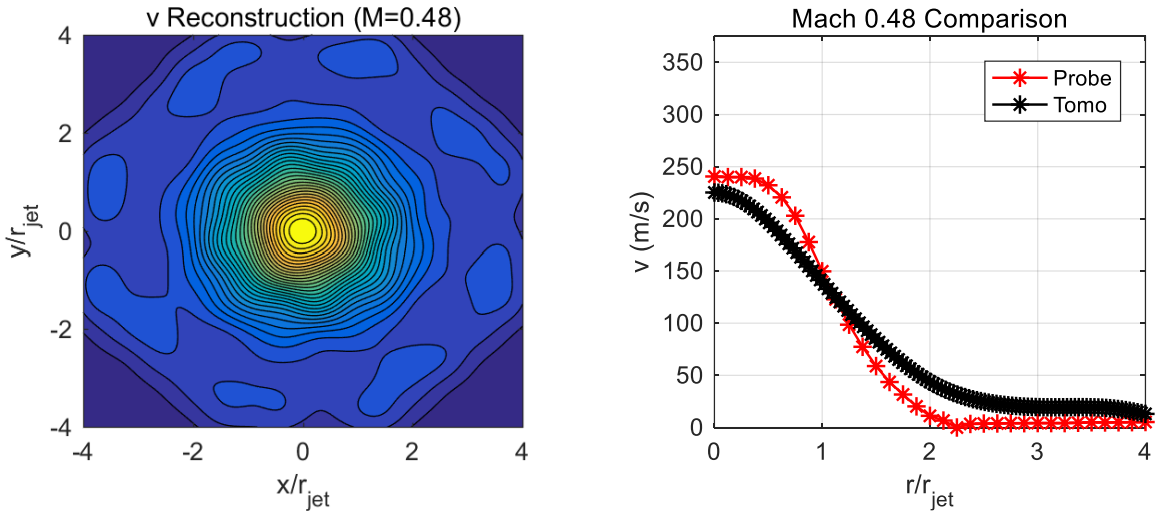

(a) (b)

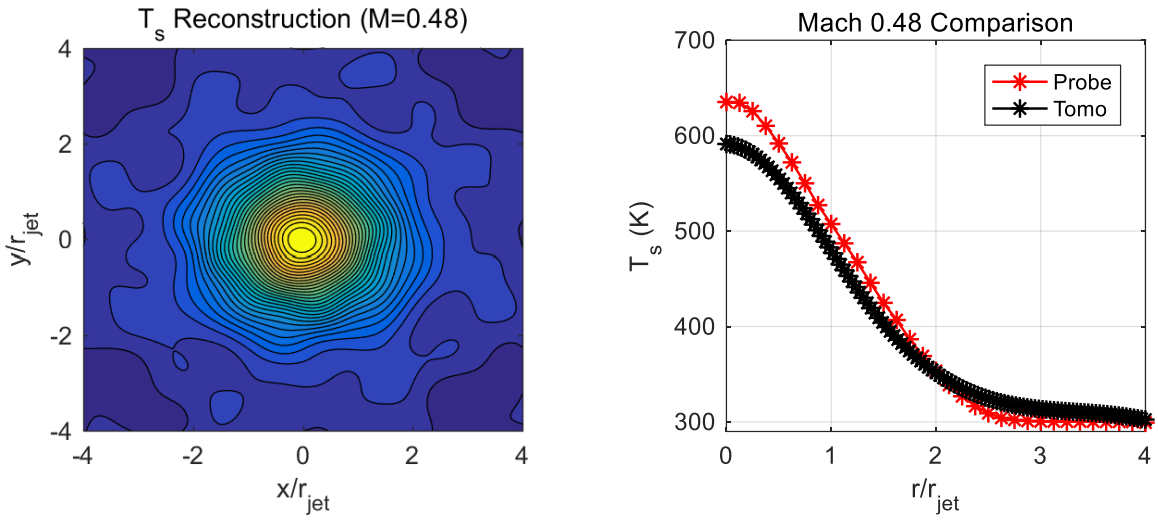

(c) (d)

Figure 6.14. *Tomographic reconstruction of Mach 0.48 jet velocity and static temperature. (a) Velocity contour. (b) Velocity profile at* $y/r_{jet} = 0$. *(c) Static temperature contour. (d) Static temperature profile at* $y/r_{jet} = 0$.

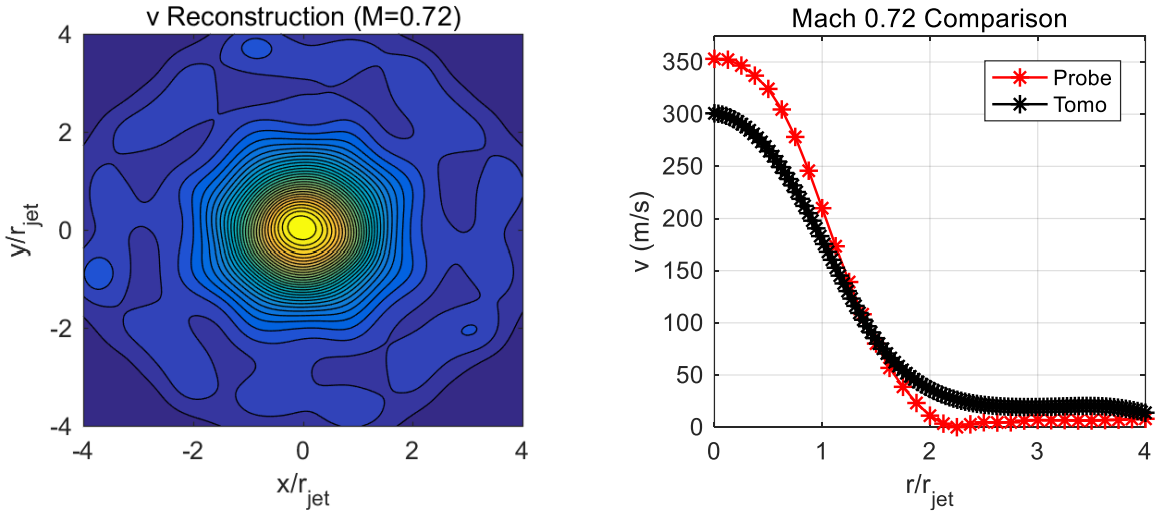

(a) (b)

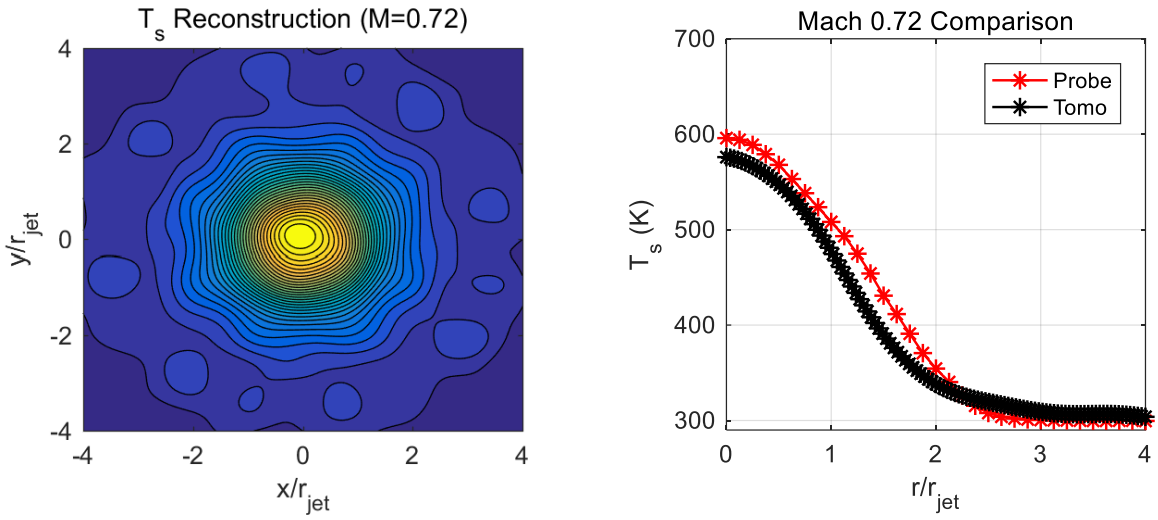

(c) (d)

Figure 6.15. *Tomographic reconstruction of Mach 0.72 jet velocity and static temperature. (a) Velocity contour. (b) Velocity profile at* $y/r_{jet} = 0$. *(c) Static temperature contour. (d) Static temperature profile at* $y/r_{jet} = 0$.

As expected, the results shown in Figures 6.14 and 6.15 more closely resemble the probe measured data. A comparison of RMS errors (calculated using profile data for respective Figure) is presented in Table 6.2.

Table 6.2. *Tomography algorithm inputs*

Mach Number	Case	$RMSE_v(m/s)$	$\frac{RMSE_v}{v_{max}}(\%)$	$RMSE_{T_s}(K)$	$\frac{RMSE_v}{T_{s_{max}}}(\%)$
0.5	3 Orientation	35.1	14.6	34.6	5.3
0.5	Axisymmetric Projection	22.7	9.4	23.1	3.6
0.7	3 Orientation	43.8	12.4	34.8	5.8
0.7	Axisymmetric Projection	30.1	8.5	22.0	3.7

Overall, the tomographic results presented in Figures 6.11-6.14 are very promising! In the final section of this manuscript, several sets of numerical simulations are used to characterize some of

the technique's limitations. In particular, the effects of orientation count, voxel resolution, and plane displacement uncertainty on velocity and static temperature estimation error are explored.

5. Sensitivity Studies

Throughout this series of sensitivity studies, a method of manufactured solutions approach was used to explore the impact of various tomography inputs on system accuracy. First, a Mach 0.72 Gaussian distribution of jet characteristics mesh was created to simulate experimental measurement results. This Gaussian distribution is defined in Figure 6.16.

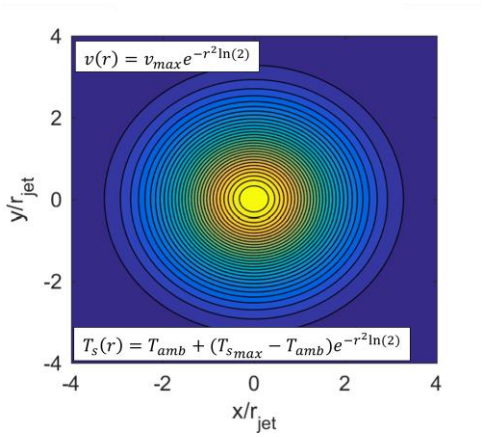

Figure 6.16. *Gaussian profile used to perform sensitivity studies.* $T_{s_{max}} = 595.9\ K$, $T_{amb} = 300\ K$, $v_{max} = 353.0\ m/s$

Using a set of study-defined start and end positions, the simulated TOF values for the respective study are first obtained using the eigenray detection procedure outlined in section 2.1. The TOF values obtained during this step ultimately serve as inputs to the tomography algorithm. Since the exact profile of the jet is known, the effects of varying algorithm inputs and equipment configurations can be explored by comparing the reconstructed results with the known distribution of jet velocity and temperature.

To quantify reconstruction accuracy, an image error and correlation coefficient defined by equations (19) and (20) are used [17].

$$\Delta(\%) = 100 * \frac{\sqrt{\sum\left[\zeta_{phantom}(x,y) - \zeta_{tomo}(x,y)\right]^2}}{\sqrt{\sum[\zeta_{tomo}(x,y)]^2}} \tag{19}$$

$$\Gamma = \frac{\sum[(\zeta_{phantom}(x,y) - \overline{\zeta_{phantom}})(\zeta_{tomo}(x,y) - \overline{\zeta_{tomo}})]}{\sqrt{\sum[\zeta_{tomo}(x,y) - \overline{\zeta_{tomo}}]^2 \sum\left[\zeta_{phantom}(x,y) - \overline{\zeta_{phantom}}\right]^2}} \tag{20}$$

In the following subsections, three sensitivity studies are explored. The first study looks at the impact of orientation count on measurement accuracy, the second explores the effects of varying voxel resolution, and the last study focuses on plane displacement uncertainty effects for the current configuration. The objective of these sensitivity studies is to identify the factors that most contribute to accuracy improvement.

5.1. Number of Orientations Study

One of the most difficult questions to answer in Tomography is; "how many projections do I need for an accurate reconstruction?" If not enough projections are used, the accuracy of the system will suffer, while too many projections may result in wasted resources and time. Ultimately, the answer to this question depends on the size and shape of the gradients being resolved, the object function spatial resolution (voxel size), and the relative spacing of the measurement equipment. In the current work, a sensitivity study is conducted to explore the impact of orientation count on velocity and temperature estimation error. To perform this study, the same traversing arrangement described in the Section 3 is modeled, but a varying number of orientation angles are used to reconstruct the velocity and temperature profiles. This arrangement is illustrated in Figure 6.17.

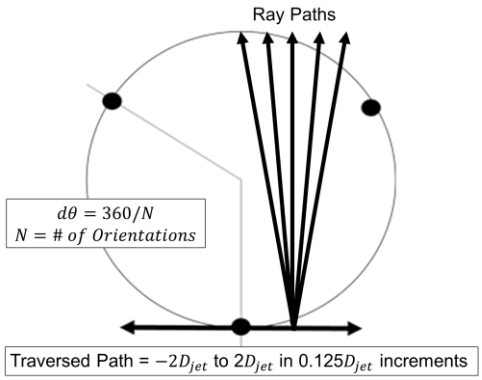

Figure 6.17. *Arrangement used to carry out orientation sensitivity study*

Throughout this study, 6 different orientation test cases were explored. The image error and correlation coefficient for these test cases are presented in Figure 6.18.

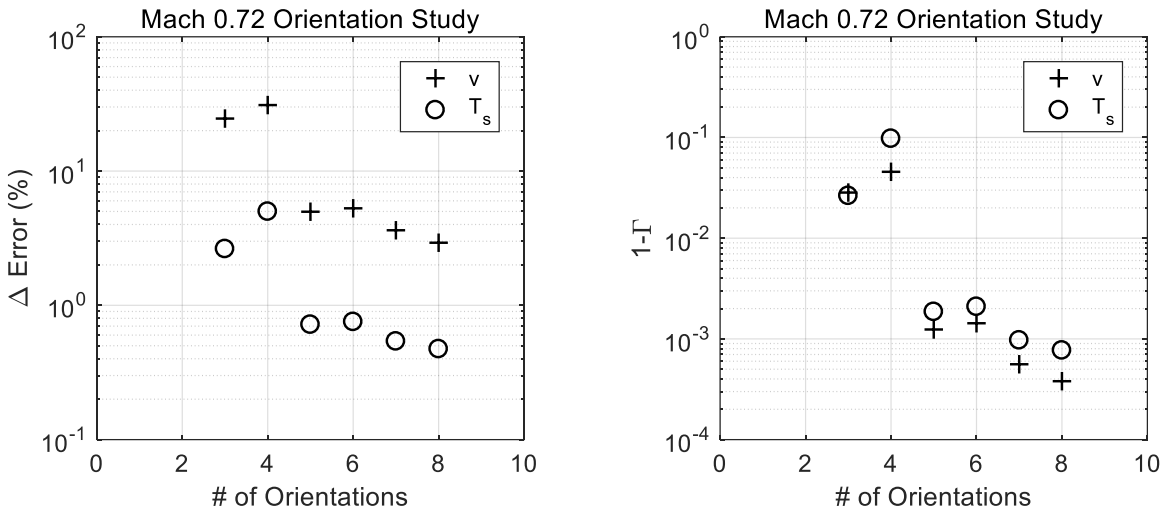

Figure 6.18. *Orientation sensitivity study results. (a) Image error. (b) 1 - Correlation Coefficient*

In the Figure 6.18 results, it is evident that increasing the number of orientations undoubtedly improves system accuracy. Additionally, there is a noticeable reduction in reconstruction error when more than 5 orientations are used. Finally, a comparison of odd and even orientation counts reveal a slight improvement in accuracy when an odd number of orientations is

used versus the next even number. This behavior is largely associated with the existance of diametrically opposed propagation paths (redundent data) in the even configurations.

5.2. Voxel Resolution Study

In the second sensitivity study, the effect of varying voxel dimensions was investigated. Voxel resolution is important because it limits the flow feature size that can be resolved during tomographic reconstruction. While a small voxel size enables the resolution of small flow features, multiple paths must still traverse the voxel in order to properly estimate fluid characteristics. Generally, this signifies that more propagation paths are necessary and convergence time increases.

To perform this investigation, the 8 orientation case described in Section 5.1 was used to estimate the fluid characteristics. This case was selected because it resulted in the smallest image error and best correlation in the previous study. In total, 6 different voxel sizes were used to tomographically reconstruct the jet velocity and static temperature profile. The image error and correlation coefficient for these test cases are presented in Figure 6.19.

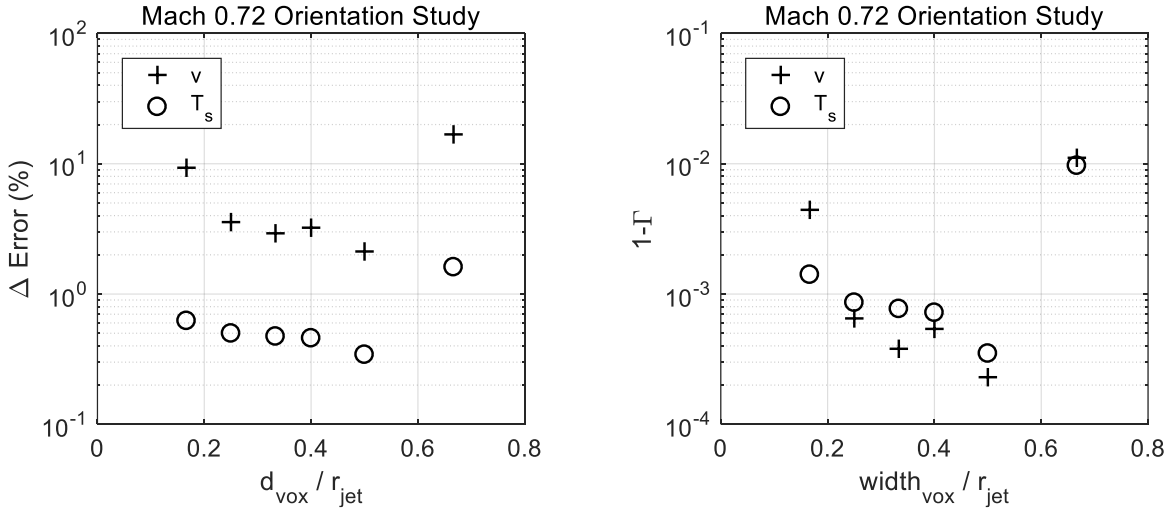

Figure 6.19. *Voxel sensitivity study results. (a) Image error. (b) 1 - Correlation Coefficient*

In Figure 6.19, it is evident that a voxel width greater than half of the jet radius results in significant error. This behavior is expected because the basis function does not have sufficient points to approximate gradient behavior. Conversely, Figure 6.19 also shows that too small of a voxel width

also produces increased error. Since fewer ray paths traverse any given voxel (compared to larger voxel widths), the algorithm must use less information to approximate the voxel characteristics. Additionally, the weighting function in equations (12) and (13) becomes smaller since the ratio of distance travelled in the voxel over the path length decreases in size.

In the current work, a voxel width of 1/3rd r_{jet} was used to resolve fluid behavior. Although a slightly smaller or larger voxel width could have been used according to the Figure 6.19 results, this selection was made as a compromise between reconstruction resolution and algorithm convergence time.

5.3. Plane Displacement Study

In the final sensitivity study, the effects of plane displacement uncertainty were explored to better understand its effects on technique accuracy. Although many other distance related uncertainties could have been explored, Otero et al.'s [8] velocity uncertainty analysis revealed that the technique is highly sensitive to plane two microphone placement for the current configuration.

In the current study, the microphone 2 position was perturbed in the upstream and downstream directions to evaluate its impact on technique accuracy. Figure 6.20 portrays the arrangement used to carry out this investigation.

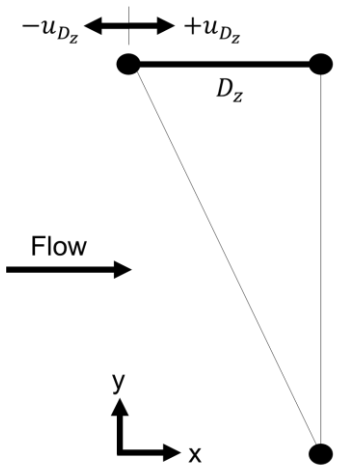

Figure 6.20. *Arrangement used to carry out plane displacement error sensitivity study*

Throughout the study, 7 cases were used to explore plane displacement sensitivity. Once again, the 8 orientation arrangement described in section 5.1 was used, and the voxel width remained 1/3rd r_{jet}. The image error and correlation coefficient for these test cases are presented in Figure 6.21.

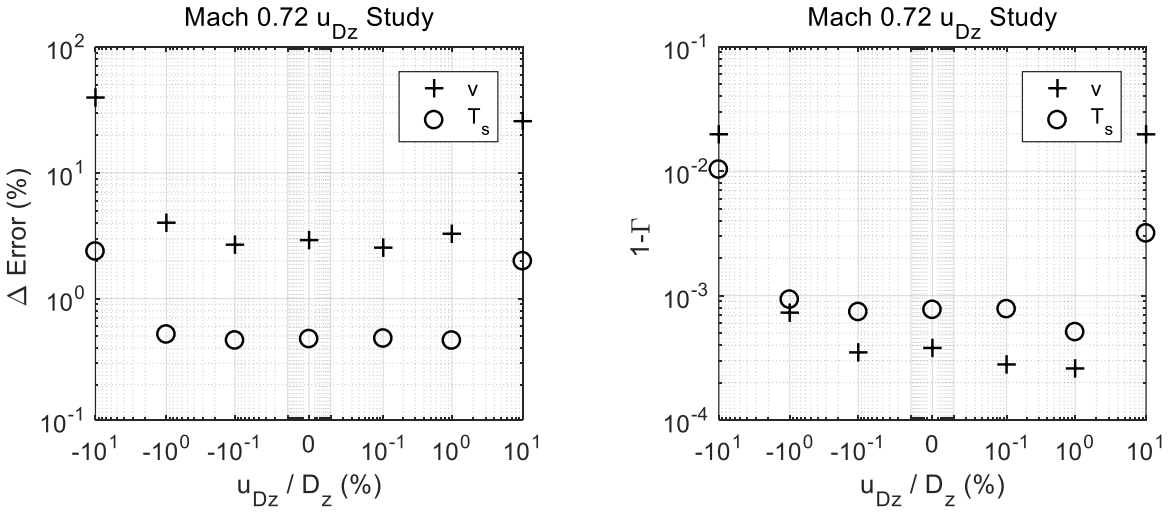

(a) (b)

Figure 6.21. *Plane displacement error sensitivity study results. (a) Image error. (b) 1 - Correlation Coefficient*

In Figure 6.21, the accuracy of the tomographic reconstruction does not appear to change significantly between -1% and 1% u_{Dz}/D_z. Additionally, the magnitude of the perturbed reconstruction errors are approximately the same as the case with no streamwise displacement error. The relative insensitivity to streamwise displacement error is thought to be a function of the numerical methods used to identify eigenrays. It is likely that the eigenray exit criteria could account for a 1% distance uncertainty in the reconstruction results. Unfortunately, the effect of improving eigenray detection accuracy was not explored because smaller exit criterias result in significantly greater computational times. Errors above 10% were also not explored because the accuracy of the algorithm would be significantly compromized for such a high plane displacement error.

6. Future Work and Conclusion

In the current work, an acoustic tomography reconstruction approach for high subsonic Mach number flows was developed and later tested in a single stream jet facility operating at Mach 0.48 and 0.72 with total temperatures of 675 K. Using only three traverse orientations, RMS errors in velocity and static temperature estimation of 35.1 m/s (14.6% of max jet velocity) and 34.6 K (5.3% of max static temperature) were observed at the Mach 0.48 test condition, while 43.8 m/s (12.5% of max jet velocity) and 34.8 K (5.8% of max jet static temperature) RMS errors were observed at Mach 0.72. In general, the reconstruction contours were effective in determining the jet geometry and location. However, the effects of using a small number of traversed orientations were evident in the tomographic reconstruction via elongations along the orthogonal direction relative to each traversed path. The authors used a projection of the horizontally traversed data onto other azimuthal orientations to illustrate the effects of using additional orientations in the tomographic reconstruction. Although this set of results required several assumptions (centered symmetric jet), the tomographic reconstruction results were better able to predict plume characteristics that were measured with a probe. RMS errors of 22.6552 m/s (9.4% of max jet velocity) and 23.0996 K (3.6% of max jet static temperature) were observed for the Mach 0.48 test condition, while RMS errors of 30.0778 m/s (8.5% of max jet velocity) and 22.0054 K (3.7% of max jet static temperature) were observed at Mach 0.72.

Using several sensitivity studies, the effects of various tomography design and input variables were explored to better understand technique limitations. In particular, the authors explored the relationship between orientation count, voxel resolution, and plane displacement uncertainty on tomographic reconstruction accuracy. In the orientation count study, it was evident that more traverse orientations result in an improved accuracy. Since additional traverse orientations may require additional resources and measurement time, the authors recommend using at least 5 azimuthal positions due to a noticeable improvement in system accuracy. In the second study, the effects of varying voxel resolution were explored. This study revealed that there are limitations to using too large or small of a voxel dimension. If the voxel size is too large, the flow features cannot be adequately estimated because there is aren’t enough data points for basis function interpolation. Additionally, if the voxel dimensions are too small, there is less information per voxel because fewer rays travel through each one. Convergence time is also severely affected

because more data points must be iteratively resolved. Finally, the third sensitivity study revealed that plane displacement errors less than 1% did not significantly influence reconstruction error because other numerical errors were more influential.

Although the results of these studies are problem specific, the outlined procedure for assessing system accuracy can easily be implemented to explore reconstruction accuracy in other scenarios. In the future, additional work is necessary to explore the impact of TOF uncertainty and other displacement measurement errors on reconstruction accuracy. Since this method could ultimately be implemented on aero-gas turbine engines, co-flow jet geometries should be explored to assess system performance. Overall, the experimental results and studies performed in the current work are very promising. This is the first time an acoustic tomography technique has been implemented in a high subsonic Mach number jet! Although there is plenty of room for improvement, the authors are generally optimistic about the future of this technology.

Acknowledgments

The authors are grateful for the support of Rolls Royce and would like to give a special thanks to Edward Hodge, Vic Oechsle and Fred Smith for their ongoing support of this work.

References

[1] Johnson S A, Greenleaf J F, Hansen C R, Samoya W F, Tanaka M, Lent A, Christensen D A and Woolley R L 1977 Reconstructing Three-Dimensional Fluid Velocity Fields From Acoustic Transmission Measurments *Acoustical Holography* ed L W Kessler (Springer US) pp 307–26

[2] Komiya K-I and Teerawatanachai S 1993 Ultrasonic tomography for visualizing the velocity profile of air flow *Flow Meas. Instrum.* **4** 61–5

[3] Beckord P, Hofelmann G, Luck H O and Franken D 1998 Temperature and velocity flow fields measurements using ultrasonic computer tomography *Heat Mass Transf.* **33** 395–403

[4] Jovanovic I, Sbaiz L and Vetterli M 2006 Acoustic Tomography Method for Measuring Temperature and Wind Velocity *IEEE International Conference on Acoustics, Speech, and Signal Processing* p 4

[5] Li Y-Q and Zhou H-C 2006 Experimental study on acoustic vector tomography of 2-D flow field in an experiment-scale furnace *Flow Meas. Instrum.* **17** 113–22

[6] Ostashev, V E, Vecherin, S N, Wilson, D K, Ziemann A and Goedecke G H 2008 Recent progress in acoustic tomography of the atmosphere *IOP Conf. Ser. Earth Environ. Sci.* **1** 12008

[7] Keith Wilson D, Thomson D W, Wilson D K and Thomson D W 1994 Acoustic Tomographic Monitoring of the Atmospheric Surface Layer *J. Atmos. Ocean. Technol.* **11** 751–69

[8] Otero Jr. R, Lowe K T and Ng W F 2017 Extension of sonic anemometry to high subsonic mach number flows *Meas. Sci. Technol* **28** 1–12

[9] Otero Jr. R, Lowe K T, Ng W F, Ma L and Kim C-Y 2016 Non-Intrusive Gas Turbine Engine Exhaust Characterization using Acoustic Measurements *32nd AIAA Aerodynamic Measurement Technology and Ground Testing Conference* (Washington D.C.: AIAA) pp 2016–4160

[10] Otero Jr R, Lowe K T and Ng W F 2017 Non-Intrusive Acoustic Measurement of Flow Velocity and Temperature in a High Subsonic Mach Number Jet (Submitted) *Meas. Sci. Technol.*

[11] Herman G T and Lent A 1976 Iterative reconstruction algorithms *Comput. Biol. Med.* **6** 273–94

[12] Verhoeven D 1993 Limited-data computed tomography algorithms for the physical sciences. *Appl. Opt.* **32** 3736–54

[13] Subbarao P M V, Munshi P and Muralidhar K 1997 Performance of iterative tomographic algorithms applied to non-destructive evaluation with limited data *NDT E Int.* **30** 359–70

[14] Ugincius P 1970 Ray acoustics and Fermat's principle in a moving inhomogeneous medium *J. Acoust. Soc. Am.* **51** 1759–63

[15] Ostashev V E and Wilson D K 2015 *Acoustics in moving inhomogeneous media* (CRC Press)

[16] Hsieh Hou and Andrews H 1978 Cubic splines for image interpolation and digital filtering *IEEE Trans. Acoust.* **26** 508–17

[17] Liu J-N, Wang B-X, Cui Y-Y and Wang H-Y 2015 Ultrasonic tomographic velocimeter for visualization of axial flow fields in pipes *Flow Meas. Instrum.* **41** 57–66

Part VII. Conclusions and Outlook

The primary objective of this dissertation was to determine if acoustics could be used for non-intrusive velocity and temperature measurements in compressible flows. An extensive review of the literature revealed that existing acoustic techniques have been restricted to low Mach number applications (Mach < 0.3). In Part II, the existing technique literature was described in detail and several key limitations were highlighted. Among these key limitations were the inability to account for acoustic refraction and sound level sensitivity to flow direction. These limitations, however, did not indicate that compressible flow sensing was impossible. The author hypothesized that acoustic signals could be used to identify fluid velocity and temperature in compressible flows if the SNR and acoustic refraction obstacles could be overcome.

In the first manuscript, the theoretical groundwork for this investigation was established. In this study, a novel approach was developed for measuring fluid velocity and temperature simultaneously. Much like the existing sonic anemometry and thermometry technique, the new approach relies on propagation time and displacement measurements to estimate flow conditions, but a unique configuration and solution procedure was used to avoid the upstream and downstream propagation requirements. This characteristics enables design for improved SNR systems and measurements in higher Mach number conditions as well. Throughout this investigation, an analytical expression for velocity and temperature was derived for uniform flows, and an iterative method was described for single-stream non-uniform flows. Using a Snell's law for convected flows propagation model, and Amiet's lip-line assumption for shear layer refraction, the iterative method was used to measure flow velocity and temperatures up to Mach 0.83 in an unheated laboratory jet facility. Further analysis of measurement results ultimately revealed that the difference in time-of-flight for two stream-wise displaced acoustic paths was more sensitive to fluid velocity than temperature. This observation was instrumental for the work described in the fourth manuscript. Overall, the findings of this work verified that acoustic measurements could be used to non-intrusively measure fluid conditions in compressible flows!

The next two manuscripts were largely focused on exploring the capabilities and limitations of the acoustic instrument. The second manuscript was a follow-up to the first manuscript. In the unheated jet experiment, the effects of temperature were not investigated because the fluid was unheated. The second manuscript explored total temperature flows up to 700 K and a Mach number

of 0.7. The technique performed well at higher temperatures and tracked both velocity and temperature increases in the flow. Velocity and temperature RMS errors up to 8.5 m/s (2.4% of max velocity) and 23.3 K (3.3% of total temperature) were observed which further verified the usefulness of the acoustic technique. Throughout this experiment, the effect of using a two-zone model for determining jet characteristics was noticed. As the temperature of the fluid increased, the temperature error appeared to grow as well. Ultimately, it was hypothesized that the algorithm inputs of ambient conditions did not properly account for ambient temperature heating by the jet. The major takeaway from this experiment was that the acoustic technique was able to track temperature changes effectively, but additional work was necessary to capture the effects of non-uniform flow conditions.

The third manuscript was concerned with the applicability of this new technique in an engine environment. Using a similar configuration to the one described in the unheated jet experiment, acoustic measurements were used to measure flow conditions in a JT15D-1A turbofan engine. Given the non-uniform flow associated with the engine exhaust, it was not possible to deduce fluid velocity and temperature distributions, but a critical observation was made regarding the engine's exhaust profiles. The normalized exhaust profiles did not change significantly at the measurement plane, indicating that exhaust shape information could be used to approximate other engine performance metrics. Intrusive measurements at engine idle conditions were used to identify two calibration constants which were used to estimate engine mass flow rate and thrust at higher engine speeds. Although additional research is necessary to assess technique feasibility at higher Mach number conditions, these observations were very encouraging.

Manuscripts two and three largely underscored the need for a non-intrusive, non-uniform flow handling technique. Although acoustic tomography has been used in the past to estimate fluid velocity and temperature non-uniformities, an incompressible flow requirement makes existing techniques ineffective at higher Mach number flow conditions. The final stage of this research was focused on the development of a compressible flow tomography technique. Such a technique could enable the non-intrusive detection of mass flow and thrust in aero gas turbine engine environments, which is of significant interest to the aviation community. Using temperature and velocity sensitivity observations made in manuscripts one and three, a novel acoustic tomography technique was developed for compressible flow applications. This method, along with the results of a proof of concept experiment were described in the fourth manuscript. Overall, the technique did a great

job of tracking the shape and location of the fluid non-uniformities. The reconstruction results also alluded to a potential source of measurement error. Using a numerical sensitivity study, the impact of various system design and input variables on estimation accuracy were explored. This investigation revealed the major source of measurement error was associated with a limited number of tomography measurement orientations. To verify this finding, the measurements along a single tomography orientation were projected onto other azimuthal positions, and used to estimate the velocity and temperature distribution of the experimental flow field. The results of this axisymmetric projection demonstrated a considerable improvement in measurement accuracy when compared to the three orientation reconstruction results. Although additional sources of compressible flow tomography error are yet to be explored, the findings of this research were very promising!

1. Summary of Findings

A new non-intrusive acoustic measurement system for use in measuring flow velocity and temperature in propulsion related flows was successfully constructed and tested. The research confirmed that:

- Limited signal-to-noise ratio and acoustic refraction limited previous research to incompressible flow applications
- Non-intrusive acoustic measurements can be used to measure compressible (Mach>0.3) flow velocity and temperature.
- An acoustic instrument can be used to estimate gas turbine engine mass-flow rate and thrust in a non-intrusive manner.
- A tomographic arrangement of sonic anemometry and thermometry equipment can be used to measure compressible flow velocity and temperature non-uniformities.

2. Outlook

As with any research, there are always opportunities to build on current work. Several key research questions that remain are outlined below:

- **Can the methods described in the current work be implemented in supersonic flows?**

  The author hypothesizes that two stream-wise displaced measurements of transverse acoustic propagation could be used to estimate supersonic flow conditions as long as the measuring equipment is positioned within the Mach cone of the sound source (mics are downstream of the source) and the relative position vector to each microphone are not parallel.

- **How accurately can this technique estimate gas turbine engine mass flow rate and thrust?**

  The sponsor of this research is primarily interested in the use of this technique for non-intrusive mass flow and thrust detection. Since the tomographic reconstruction accuracy is strongly dependent on the magnitude of velocity and temperature gradients, the shape of non-uniformity distributions, algorithm inputs, and measurement accuracy, the answer to this question will require additional research.

- **What is the relationship between turbulence characteristics (eddy convection velocities and length scales) and the scattering of acoustic waves in compressible flows?**

  In the literature, several investigations have been performed in wind tunnel facilities to explore this phenomena, but applications have generally been restricted to low Mach number applications (Mach<0.3). Knowledge of this relationship in compressible flows could be used to identify sound source requirements for specific operating conditions (e.g. large engines, higher Mach numbers, etc.).

- **Can eddy convection velocities and length scales be resolved using two stream-wise displaced spectral broadening measurements?**

  Previous work has associated the spectral broadening “humps” in the frequency domain with turbulence time scales. Could two streamwise displaced measurements of acoustic propagation be used to determine eddy convection velocities, and consequently, length scales non-intrusively? This could have tremendous implications on the field of turbulence research.

Appendix G. Compressible Flow Tomography Algorithm

The compressible flow tomography algorithm uses the procedures outlined in Figure G.1. See description below figure for additional information.

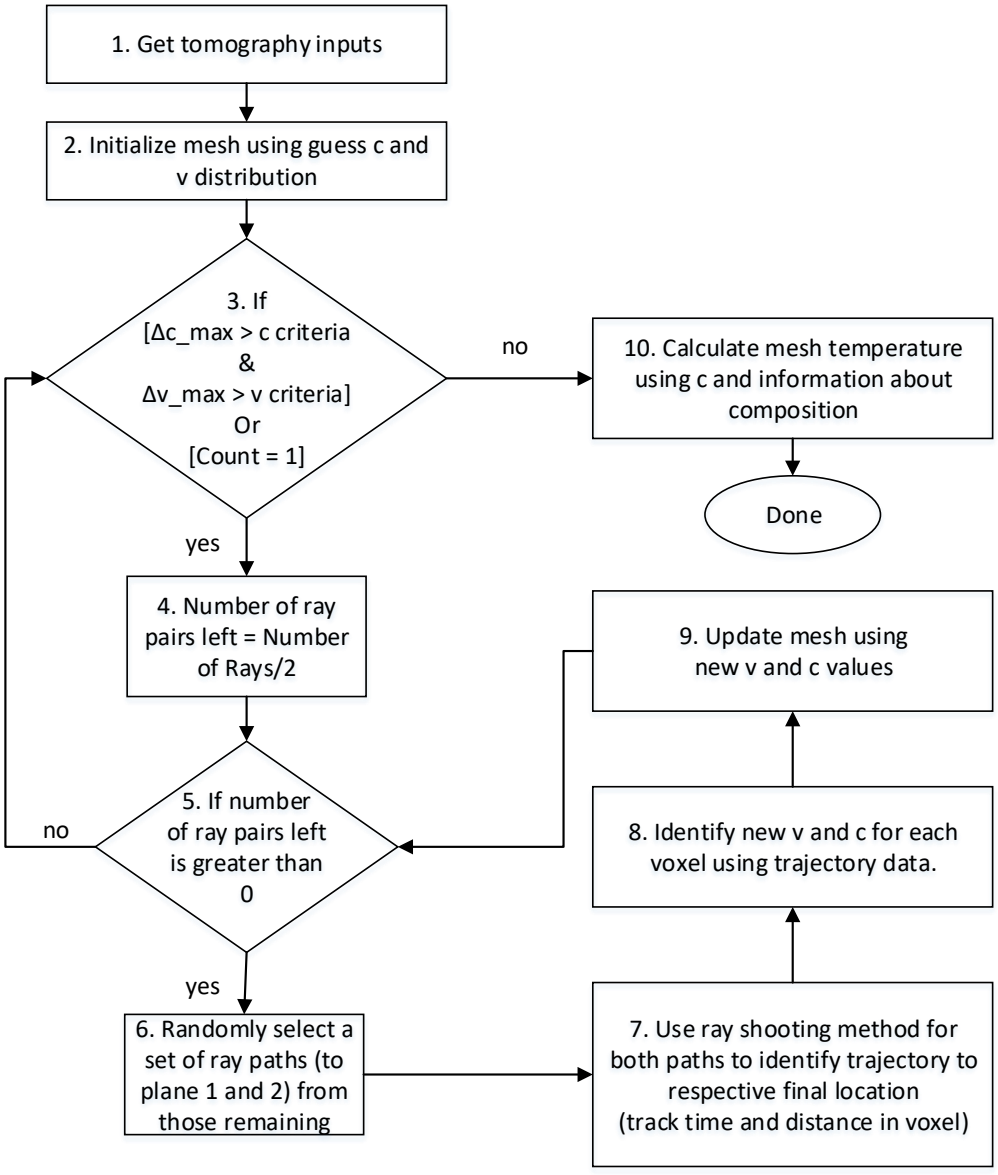

Figure G.1. *General compressible flow acoustic tomography flow diagram*

In Figure G.1, there are 11 steps. Each step is more clearly defined below.

1. The tomography inputs include:

a. Mesh domain boundaries
b. Voxel definition
c. Initial guess of mesh v and c values
d. Ray start and end positions
e. v and c convergence criteria
f. Ray tracing convergence criteria
g. v and c relaxation parameters

2. In the mesh definition, the velocity and speed of sound is assumed not to vary in the stream-wise direction. This is a requirement for using the novel sonic anemometry and thermometry configuration. This step is required for acoustic ray tracing
3. Step number 3 marks to beginning of one cycle. If the loop is on cycle number one, or the v and c convergence criteria have been met, the algorithm will exit the loop. The time it takes to converge is strongly dependent on the number of voxels, mesh discretization, number of acoustic rays, and relaxation parameters. The algorithm is not guaranteed to converge so an additional loop count criteria may be added to terminate the algorithm.
4. Step number 4 is necessary to define the number of ray path sets that will be used to update the mesh. It is a simple calculation
5. Step number 5 is used to count down the number of ray paths that have been used to update the mesh in a given cycle. Once all ray path sets have been used, the algorithm escapes the internal loop to check for convergence
6. Step number 6 is used to select a ray path set at random. Verhoeven recommended this approach because it significantly accelerates (*Verhoeven D 1993 Limited-data computed tomography algorithms for the physical sciences. Appl. Opt. 32 3736–54*).
7. Step number 7 is used to identify the eigenray between start and end positions for a specific ray. There are two approaches that may be used to solve this problem. The first step involves emitting multiple rays using different initial angles of propagation and identifying their respective distances to the end position. Using the closest path, a smaller range of initial angles is used and the process is repeated until an exit criteria is met. The second approach is to emit a single acoustic ray and measure its distance to the end location. The azimuthal and elevation angles are subsequently changed and the ray is emitted again. This procedure is repeated until the ray reaches a final position. In our work, we used the second

approach for its simplicity and relatively faster convergence speed. If many computer cores are available for computation. The former may be a better option for solving the eigenray problem.

8. Once the eigenray sets are determined in step number 7, the path length and travel time in each voxel are stored. Using the old information about the voxel, and path information, the equations defined in Part VI are used to identify new velocity and speed of sound values.
9. Once the updated v and c values have been determined for each voxel, the mesh is redefined for future eigenray detection.
10. After the algorithm has converged, the user has velocity and speed of sound distributions defined for the mesh. The static temperature distribution is then approximated using the equation of state. For ideal gases, for example, the gas composition molecular weight and specific heat ratio can be used to identify temperature. The step has been outlined in Parts III through VI.

Appendix H. Note on Pressure Measurements

1. Obtaining Static Pressure

Throughout all 4 experiments, upstream total pressure and total temperature measurements were used to obtain the jet's velocity and static temperature with the help of the isentropic relations. In each experiment, the static pressure of the exhausting subsonic jet was obtained using weather station measurements collected by the Virginia Montgomery Executive Airport. The instrumentation used by the airport is National Institute of Standards and Technology (NIST) traceable and Federal Aviation Administration (FAA) certified to provide accurate atmospheric data. This data was collected using historical tables provided by the National Weather Service (NWS) upon completion of each experiment. Since the NWS pressure data was corrected to atmospheric pressure, equation H1 below was used to identify the local static pressure (This equation is provided by the National Oceanic and Atmospheric Administration, (NOAA) and h is defined as the station altitude in meters).

$$\mathrm{P_s} = P_{corr}\left(\frac{288 - 0.0065h}{288}\right)^{5.2561} \tag{H1}$$

2. Total Pressure Calibration

A ZOC pressure transducer was used to collect total pressure measurements in the laboratory jet facility. This device was calibrated using a deadweight pressure calibration device. The calibration slope and offsets for each port are shown below. These calibration constants were used to relate transducer output voltage to flow pressure.

Table H.3. *ZOC Transducer Port Calibration Constants*

Port Calibration		
Port	**Slope**	**Offset**
1	18.3869	0.2391
2	Damaged	Damaged
3	17.9250	0.2868
4	18.5150	0.3258
5	18.5580	0.3390
6	18.4710	0.2754
7	18.2770	0.2582
8	18.8080	0.2898